Dynamic changes of subtropical western boundary currents under global warming

DISSERTATION

zur Erlangung des akademischen Grades eines

Doktor der Naturwissenschaften

— Dr. rer. nat. —

Vom Fachbereich für Physik und Elektrotechnik,
Universität Bremen

von

Hu Yang

- Supervisor: Prof. Dr. Gerrit Lohmann

Eingereicht am: January 24, 2017

Erklärung

Hiermit versichere ich, dass ich die vorliegende Arbeit selbstständig verfasst und keine anderen als die angegebenen Quellen und Hilfsmittel benutzt habe, dass alle Stellen der Arbeit, die wörtlich oder sinngemäß aus anderen Quellen übernommen wurden, als solche kenntlich gemacht sind und dass die Arbeit in gleicher oder ähnlicher Form noch keiner Prüfungsbehörde vorgelegt wurde.

Bremerhaven, den January 24, 2017 .....

Abstract

The subtropical western boundary currents (WBCs) carry a large amount of heat from the low latitudes to the mid- and high-latitudes, which contribute to the Earth's energy balance and have a broad impact on the weather and climate over the adjacent mainland. Based on the analysis of ocean surface turbulent heat fluxes (THF) trends, we recognize a prominent increase of ocean heat loss over all the mid-latitude expansions of WBCs during the past half century, suggesting significant dynamic changes of these currents.

To understand the background mechanism, several coupled parameters are analyzed, including the SST, net surface heat flux, ocean velocity, near-surface wind and sea level pressure. These data are collected from three types of independent data resources, i.e., reanalysis products, satellite-blended observations and climate model outputs from the third and fifth phase of the Climate Model Intercomparison Project (CMIP3/CMIP5). Based on these broad ranges of data sets, we find that the WBCs (except the Gulf Stream) are intensifying and shifting toward the poles as long-term effects of global warming. An intensification and poleward shift of near-surface ocean winds are proposed to be the forcing of such dynamic changes over both hemispheres. In contrast to the other WBCs, the Gulf Stream is expected to be weaker under global warming, which is most likely related to a weakening of the Atlantic Meridional Overturning Circulation (AMOC).

The systemic intensification and poleward shift of ocean surface wind are proposed to be attributed to the positive trends of annular modes. Over the Northern Hemisphere, strong natural variations of Northern Annular Mode (NAM) are observed, which conceal the long-term effect of global warming. While both observations and climate models record a robust positive trend of Southern Annular Mode (SAM) under global warming. The mechanism for this phenomenon is still under debate. Here, we find that the major feature of global warming induced SST pattern over the Southern Hemisphere is characterized by a stronger equator-to-pole gradient. Model sensitivity study demonstrates that such meridional gradient in SST is potential to drive a stronger Southern Annular Mode in a warming climate.

Contents

1 Introduction

The subtropical western boundary currents (WBCs), including the Kuroshio Current, the Gulf Stream, the Brazil Current, the East Australian Current and the Agulhas Current, are the western branches of the subtropical gyres. They are characterized by fast ocean velocities, sharp sea surface temperature (SST) fronts and intensive ocean heat loss. The strength and routes of WBCs have a broad impact on the weather and climate over the adjacent mainland. For instance, WBCs regions favor the formation of severe storms [*Kelly et al.*, 1996; *Inatsu et al.*, 2002; *Taguchi et al.*, 2009; *Cronin et al.*, 2010], while the poleward ocean heat transport by the WBCs contributes to the global heat balance [*Colling*, 2001].

In recent years, there has been an increasing interest in the variability of WBCs under global warming. *Deser et al.* [1999] suggested that there has been a decadal intensification of Kuroshio Current during the 1970-1980 period due to a decadal variation in wind stress curl, whereas *Sato et al.* [2006] and *Sakamoto et al.* [2005] projected a stronger Kuroshio Current in response to global warming according to a high-resolution coupled atmosphere-ocean climate model. *Curry and McCartney* [2001] found that the transport of the Gulf Stream has intensified after the 1960s, which is attributed to a stronger North Atlantic Oscillation. In agreement with *Curry and McCartney* [2001], an increase in the storm frequency has also been recorded in extreme turbulent heat fluxes events over the Gulf Stream [*Shaman et al.*, 2010]. For the South Pacific Ocean, *Qiu and Chen* [2006] and *Roemmich et al.* [2007] suggested that the 1990s decadal increase in sea surface height over the subtropical western basin of the South Pacific is related

to a spin-up of the local subtropical ocean gyres. Based on long-term temperature and salinity observations from an ocean station off eastern Tasmania, *Ridgway* [2007] demonstrated that the East Australian Current has increased over the past 60 years. Based on repeated high-density XBT transects, CTD survey and satellite altimetry, *Ridgway et al.* [2008] also found a strengthening of the East Australian Current in the 1990s. Regarding the South Atlantic Ocean, *Goni et al.* [2011] observed a southward shift of the Brazil Current during 1993-2008 using satellite-derived sea height anomaly and sea surface temperature (SST). Over the Indian Ocean, the Agulhas leakage was reported to have increased due to latitudinal shifts in the Southern Hemisphere Westerlies [*Biastoch et al.*, 2009]. In addition, modelling studies indicate ocean circulation changes over the Southern Hemisphere in response to a positive trend of the Southern Annular Mode [*Hall and Visbeck*, 2002; *Cai et al.*, 2005; *Sen Gupta and England*, 2006; *Cai*, 2006; *Fyfe and Saenko*, 2006; *Sen Gupta et al.*, 2009]. These studies consistently show that the Southern Hemisphere subtropical gyres do shift southward as a consequence of a positive Southern Annular Mode.

Besides these studies focusing on individual branches of the WBCs, recent work suggests that the change over the WBCs is likely to be a global phenomenon over all ocean basins [*Wu et al.*, 2012]. Based on multiple SST data sets, *Wu et al.* [2012] reported that a stronger warming trend occurred over the WBCs during the past century. However, the mechanism for this phenomenon is still not clear, mostly due to the uncertainties and limitations of the data sets [*Brunke et al.*, 2002; *L'Ecuyer and Stephens*, 2003; *Van de Poll et al.*, 2006; *Gulev et al.*, 2007a; *Krueger et al.*, 2013; *Dee et al.*, 2014].

By investigating the prominent ocean surface turbulent heat fluxes (THF) trends in Chapter 2, a significant increase of ocean surface heat loss over the WBCs is identified during 1958-2013, indicating that the heat transportation by the WBCs has intensified. To understand the mechanism, in Chapter 3, the dynamic changes of WBCs are explored by applying a large range of data sources. We find a systematic intensification and poleward movement of WBCs, which are related to the positive trends of annular modes over both hemispheres. In Chapter 4, the mechanism for the Southern Annular Mode (SAM) is examined, pointing out that the global warming induced meridional sea surface temperature gradient plays a vital role for the upward trend of SAM.

Content of the thesis

Besides the general introduction (chapter 1), The rest of the thesis is organized as follows. Chapter 2 introduces the motivation of investigating the western boundary currents dynamic changes as a finding from the ocean surface turbulent heat flux trends. Chapter 3 investigates the dynamic changes of western boundary currents and the mechanism, i.e., a positive trend of annular mode over both hemispheres. Chapter 4 explore the mechanism for a stronger Southern Annular Mode under global warming. Conclusions and future perspectives are given in 5.

2

Prominent trends in ocean surface turbulent heat fluxes during 1958-2013

Turbulent heat fluxes (THF) consist of two components: latent heat flux (LHF) and sensible heat flux (SHF). LHF is the flux of heat from the ocean to the atmosphere that is associated with evaporation. SHF is the conductive heat flux from the ocean to the atmosphere. As the main form of air-sea heat exchange, THF are of particular interest for the comprehensive understanding of the coupled ocean-atmosphere interactions.

Several studies have addressed the THF trends and their associated mechanisms in different regions and for varying periods. As reported by *Tomita and Kubota* [2005], the THF have increased during the 1990s over the Kuroshio-Oyashio extension region and reached their maximum during the past half century due to a pronounced warming in sea surface temperature (SST). By examining the variability of the LHF during 1989-2000, *Liu and Curry* [2006] found an increasing LHF associated with a positive trend of near-surface wind speed over the tropical and subtropical regions. *Zhang et al.* [2010a] showed that the LHF dampens the increase in SST caused by oceanic advection in the coastal China Seas during 1948-2006. *Iwasaki and Kubota* [2011] demonstrated that the LHF and freshwater flux were strengthened over the north-eastern subtropical Pacific during 1988-2005. Based on the National Centers for Environmental Prediction/National Center for Atmospheric Research (NCEP/NCAR) reanalysis, *Shaman et al.* [2010] pointed out that THF have increased over the Gulf Stream during 1948-2008 mainly due to higher storm frequency. The extreme THF events over the subtropical western boundary currents (WBCs), as described by *Gulev and Belyaev* [2012], have

increased significantly during the same period. By analyzing the Goddard Satellite-based Surface Turbulent Fluxes (GSSTF), *Gao et al.* [2013] also found an increase in the LHF over the Kuroshio Current and Gulf Stream during 1988-2008. On the basis of investigating the relationship between SST and THF on different time scales, *Gulev et al.* [2013] emphasized that on multi-decadal time scales, the ocean drives the atmosphere variability, whereas the opposite case is true for shorter timescales over the North Atlantic region (35^o-50^oN). Given all above results, investigating the THF variability is of crucial importance for understanding and evaluating the climate feedbacks and changes.

This study aims to assess the long-term changes of the coupled ocean-atmosphere dynamics by examining the prominent sea surface THF trends. The International Comprehensive Ocean-Atmosphere Data Set (ICOADS) is the longest and most extensive collection of surface marine meteorological data mainly from ships and buoys since 1662 [*Woodruff et al.*, 2011]. However, the ICOADS suffers serious spatial/temporal sampling problems and measurement uncertainties [*Da Silva et al.*, 1994; *Chou et al.*, 2004; *Gulev et al.*, 2007a]. Regions with continuous ship observations are sparse. As in *Gulev et al.* [2013], they only evaluated the North Atlantic region, where a large number of ship observations are available over a long period of time. Recent satellite-based data products could overcome the shortcoming of spatial/temporal sampling problems, but are insufficient to study the long-term climate variability due to a lack of temporal coverage, as the data sets only cover relatively short period from 1987 to today. These products include the GSSTF v3 [*Chou et al.*, 2003], the Hamburg Ocean Atmosphere Parameters and Fluxes from Satellite data (HOAPS) [*Andersson et al.*, 2010], the Japanese Ocean Flux Data Sets with Use of Remote Sensing Observations (J-OFURO) [*Kubota et al.*, 2002] and the Ocean Surface Turbulent Flux (SeaFlux) [*Liu et al.*, 2011; *Clayson and Bogdanoff*, 2013]. The Objectively Analyzed air-sea Fluxes (OAFlux) are constructed from an optimal blending of surface meteorological variables from satellite retrievals and atmospheric reanalysis since 1958 [*Yu and Weller*, 2007; *Yu et al.*, 2008]. Compared with ICOADS and satellite data sets, OAFlux fulfill the requirement of both acceptable accuracy and spatial/temporal coverage for this study.

The data sets used here, together with the method employed to identify the dominant factors for the THF trends are introduced in the next section. In Section 2.2.1, the

prominent THF trends and their dominant factors are examined. We try to explore the physical mechanisms behind the THF trends in Section 2.2.2. Finally, discussion and conclusions are presented in Section 2.3 and 2.4, respectively.

2.1 Data and Method

2.1.1 Data

The OAFlux use the objective analysis to obtain optimal estimates of flux-related surface meteorology and then computes the global fluxes by applying the state-of-the-art COARE bulk flux algorithm 3.0 [*Fairall et al.*, 2003]. The surface meteorological fields used in OAFlux are derived from satellite remote sensing and reanalysis outputs. OAFlux have several versions of THF products with different spatial and temporal resolutions, i.e., monthly 1-degree resolution (1958 onward), daily 1-degree resolution (1985 onward), and daily 0.25-degree resolution (1987 onward). Different input data sources are blended in different versions of OAFlux. In this work, the monthly 1-degree resolution of OAFlux, spanning 1958-2013, is used to study the prominent THF trends. This version of OAFlux blends three atmosphere reanalysis (i.e., NCEP/NCAR, NCEP/DOE and ERA-40) and four satellite products (i.e., OISST, SSM/I, AMSR-E and QuikSCAT). Furthermore, it has been validated against in situ flux measurements. Note that, before 1985, only atmosphere reanalysis data sets are blended in this version. After 1985, both satellite data and atmosphere reanalysis are synthesized [*Yu and Weller*, 2007; *Yu et al.*, 2008].

Another set of data used in this work is the NCEP/NCAR reanalysis, which is a long-term data set based on a frozen global data assimilation and observational data from a variety of sources i.e., weather stations, ships, buoys, aircrafts, radiosondes and satellites [*Kalnay et al.*, 1996]. The NCEP/NCAR spans from 1948 to 2013 with a spatial resolution of T62 (approximately 210 km at the equator).

The monthly mean THF (positive-upward) along with flux-related input state parameters from the OAFlux data set, and the monthly mean atmosphere parameters (i.e., near-surface wind, sea level pressure, SST, surface air temperature, surface specific humidity) from the NCEP/NCAR data set are used in our study. The OAFlux

are used to investigate the prominent THF trends, and the NCEP/NCAR is utilized to interpret the associated ocean-atmosphere dynamic changes. Besides, NCEP/NCAR data set also serves as a cross validation of the THF trends from the perspective of climate dynamics.

2.1.2 Method

The THF depend primarily on near-surface wind speed, air-sea humidity and temperature differences, as described in the COARE bulk flux algorithm 3.0 [*Fairall et al.*, 2003]:

$$LHF = \rho_a L C_E U_a (q_s - q_a) \tag{2.1}$$

$$SHF = \rho_a c_p C_H U_a (T_s - T_a) \tag{2.2}$$

where ρ_a is the surface air density, L is the latent heat of vaporization for water, c_p is the specific heat of air at constant pressure, C_E and C_H represent the bulk transfer coefficients for humidity and temperature, respectively. U_a stands for the near-surface wind speed. q_s and q_a are the surface saturation humidity and surface specific humidity, T_s and T_a are the SST and surface air temperature, respectively. Taking into account the effect of salinity, q_s is usually computed as $0.98 q_{sat}(T_s)$, where q_{sat} represents the saturation humidity for pure water at T_s. In addition, T_a includes a correction from the measured surface air temperature T_z at the height z, using the adiabatic lapse rate γ, as $T_a = T_z + \gamma z$.

In order to identify the dominant factors that are responsible for the THF variability, we divide U_a, q_s, q_a, T_s and T_a into the climatological means and the anomaly terms ($U_a = \overline{U_a} + U_a{}'$, $q_s = \overline{q_s} + q_s{}'$, $q_a = \overline{q_a} + q_a{}'$, $T_s = \overline{T_s} + T_s{}'$, $T_a = \overline{T_a} + T_a{}'$). The overbar denotes the climatological mean and the prime denotes anomaly. Since the anomaly terms of each variable are much smaller than the climatological means (mostly less than 10%), Equation. 2.1 and 2.2 can be linearized by the same method as in *Tanimoto et al.* [2003]:

$$LHF' \approx \rho_a L C_E (L_{q_s} + L_{q_a} + L_{U_a}) \tag{2.3}$$

$$SHF' \approx \rho_a c_p C_H (S_{T_s} + S_{T_a} + S_{U_a}) \tag{2.4}$$

Here, LHF' and SHF' represent the anomalies of LHF and SHF, L_{q_s}, L_{q_a}, L_{U_a}, S_{T_s}, S_{T_a} and S_{U_a} refer to $\overline{U_a} q_s{}'$, $-\overline{U_a} q_a{}'$, $(\overline{q_s} - \overline{q_a}) U_a{}'$, $\overline{U_a} T_s{}'$, $-\overline{U_a} T_a{}'$, $(\overline{T_s} - \overline{T_a}) U_a{}'$, in Equation. (6) and (7) in *Tanimoto et al.* [2003], respectively. L_{q_s}, L_{q_a} and L_{U_a} can be treated as the respective contributions from $q_s{}'$, $q_a{}'$ and $U_a{}'$ to the total LHF anomaly. S_{T_s}, S_{T_a} and S_{U_a} represent the respective contributions from the $T_s{}'$, $T_a{}'$ and $U_a{}'$ to the total SHF anomaly.

Finally, we introduce two indices CL_X and CS_X to quantify the relative importance of the terms in Equation. 2.3 and 2.4 :

$$CL_X = \frac{|L_X|}{|L_{q_s}| + |L_{q_a}| + |L_U|} \tag{2.5}$$

$$CS_X = \frac{|S_X|}{|S_{T_s}| + |S_{T_a}| + |S_U|} \tag{2.6}$$

For Equation. 2.5, CL_X represents the relative importance of either the surface saturation humidity (in this case $X = q_s$), surface specific humidity (i.e., $X = q_a$)) or the near-surface wind speed (i.e., $X = U_a$). The denominator of the right side ($|L_{q_s}| + |L_{q_a}| + |L_U|$) stands for the total contribution of the three influencing factors to the LHF anomaly. By such definition, CL_X ranges from 0 to 1, and a larger CL_X indicates a more dominated contribution by the variable X to the LHF anomaly. If CL_X exceeds 0.5, the term X basically dominates the LHF anomaly. Therefore, we define the X with $CL_X > 0.5$ as the dominant factor causing the LHF anomaly. A similar definition applies to the SHF in Equation. 2.6 as well, and X in Equation. 2.6 represents the SST (T_s), surface air temperature (T_a), or the near-surface wind speed (U_a).

To interpret the long-term trends, all our analysis is based on annual mean values. However, we note that both the THF and the flux-related parameters have a seasonal variability. Finally, as the linearization of the bulk flux formulae no longer applies over high latitude [*Liu et al.*, 1979; *Bourassa et al.*, 2013], we only present the results between $50°S - 50°N$ in this work.

2.2 Results

2.2.1 Identification of prominent THF trends and associated dominant factors

The linear trends of THF from OAFlux, as depicted in Fig. 2.1a, exhibit three prominent features: 1) a significant increase in the THF occurs over the mid-latitude expansions of the primary subtropical WBCs (i.e., the Kuroshio Current, the Gulf Stream, the Agulhas Current, the Eastern Australian Current and the Brazil Current) with a magnitude of ∼8-12 W/m^2 per decade; 2) a pronounced decrease in the THF happens over the tropical eastern Pacific Ocean at the rate of ∼6-10 W/m^2 per decade; and 3) over the northern tropical Atlantic Ocean the THF reduce at a speed of ∼4-6 W/m^2 per decade. These three prominent features of THF' are also observed in the LHF and SHF trends (Figs. 2.1b, 2.1c), with almost equivalent magnitudes for the former, and however, a less pronounced pattern for the latter, indicating an overwhelming contribution of LHF' to the THF trends.

To identify the dominant factors which are responsible for the prominent THF trends, we compute the trends of the q_s, q_a, T_s, T_a and U_a, respectively (Figs. 2.2 and 2.3). The CL_X and CS_X are further calculated based on the climatology mean and linear trends of each parameter (see Equations. 2.5 and 2.6). The areas with $CL_X > 0.5$ and $CS_X > 0.5$ are marked with black crosses in Figs. 2.2 and 2.3.

The paths of the primary WBCs experienced a significant increase in SST (Figs. 2.2a and 2.3a), which constitutes the dominating cause of LHF' and SHF' over the same regions. Meanwhile, the surface winds over these regions have accelerated, contributing to enhancing the ocean heat loss over there. Over the tropical eastern Pacific Ocean, we observe a significant decrease in SST (q_s and T_s) and U_a, both of which together contribute to the decreasing LHF and SHF over the tropical eastern Pacific Ocean. Furthermore, the reduced LHF and SHF over the northern tropical Atlantic Ocean is primarily associated with an increases in surface specific humidity (q_a) and surface air temperature (T_a) (Figs. 2.2b and 2.3b).

Having described the patterns of THF trends and their contributors, we turn to examine the time evolution of these factors. Since the surface specific humidity (q_a) is physically linked to the surface saturation humidity (q_s), their contributions to the LHF

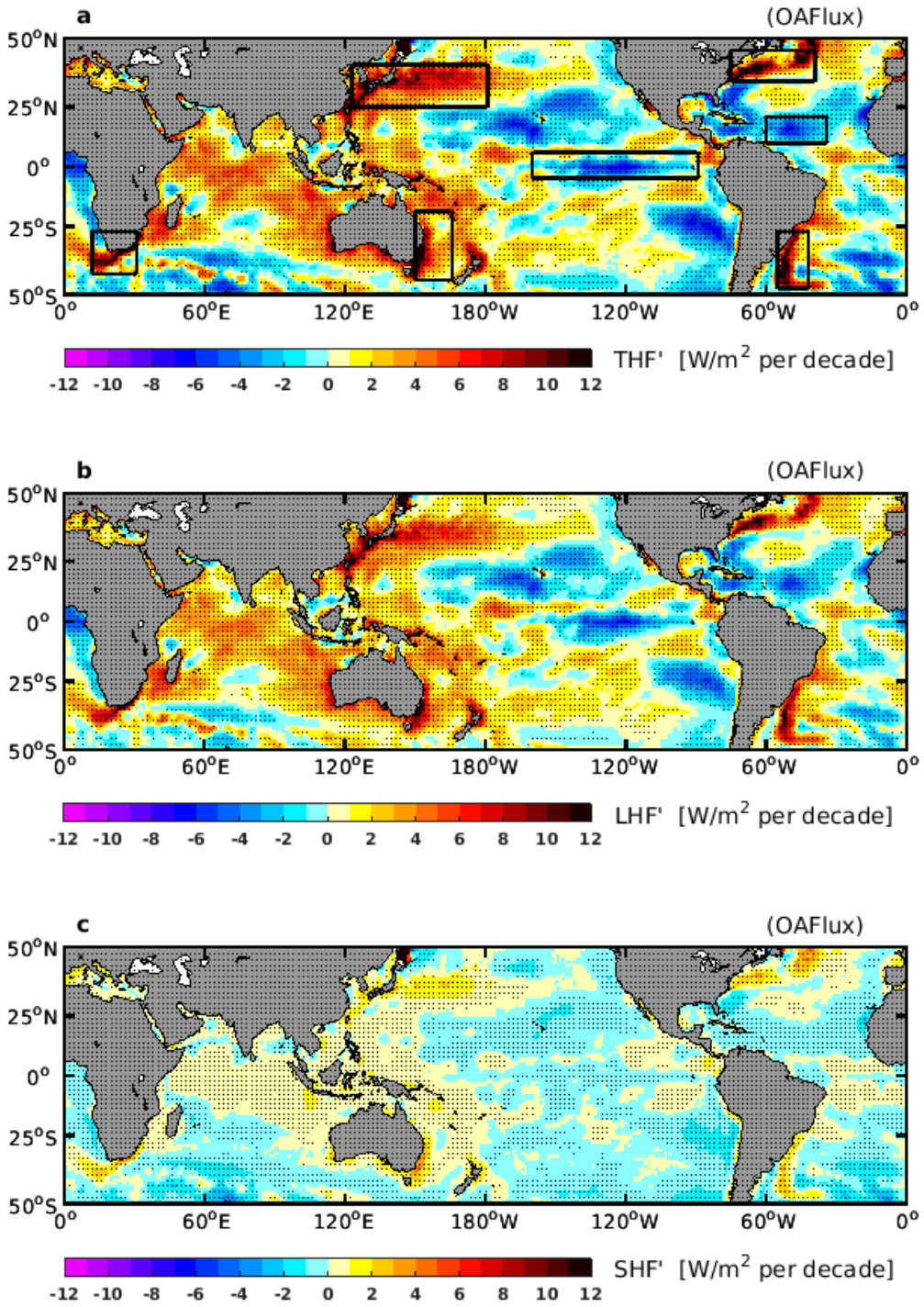

Fig. 2.1: *Spatial distributions of trends in turbulent heat fluxes (THF'), latent heat flux (LHF') and sensible heat flux (SHF') in OAFlux data set. Stippling indicates regions where the trends pass the 90% confidence level (Student's t-test).*

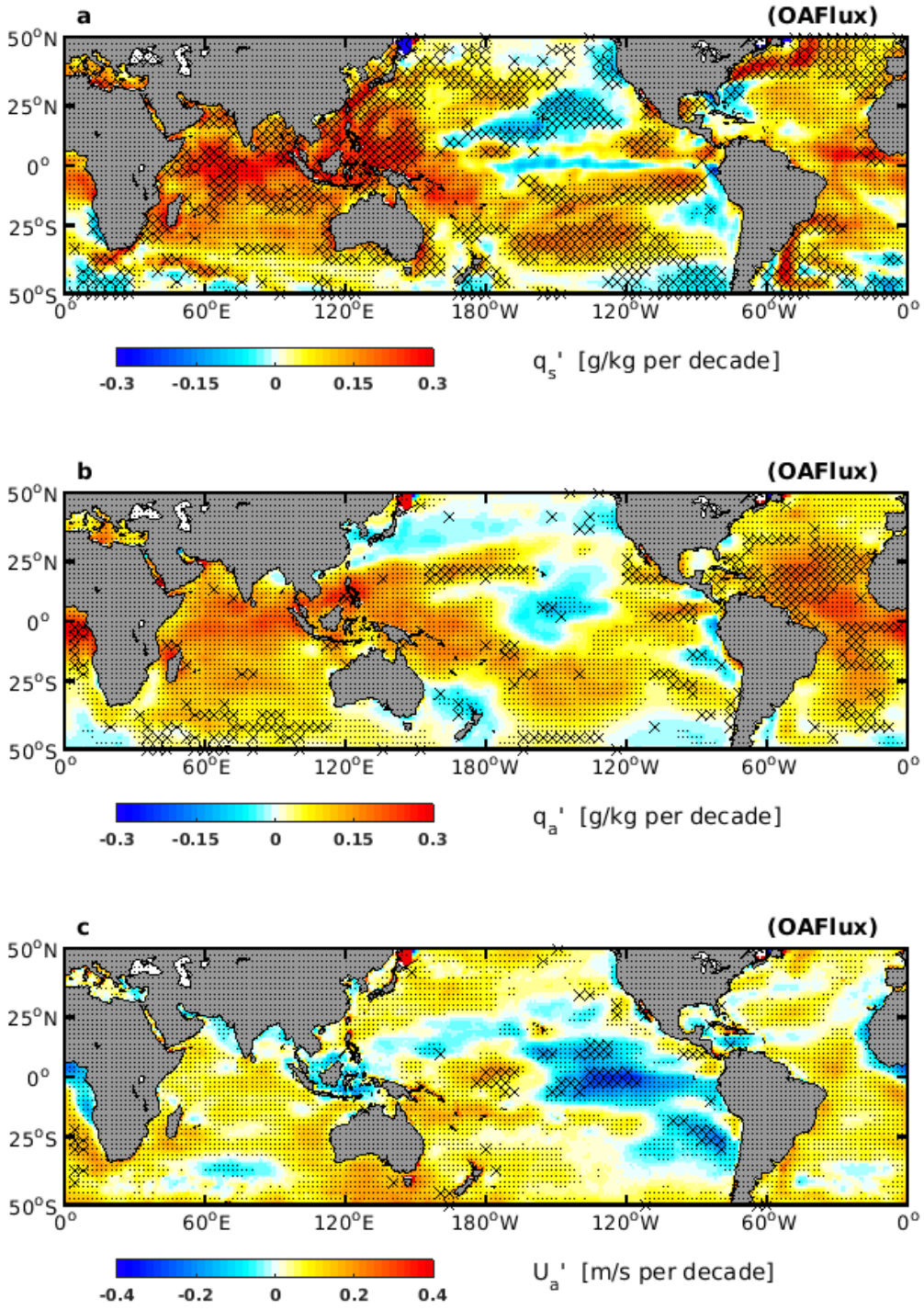

Fig. 2.2: *As Fig. 2.1, spatial distributions of the trends in surface saturation humidity (q_s'), specific humidity (q_a') and wind speed (U_a'). The area with $CL_X > 0.5$ (see Equation. 2.5) are marked with black cross.*

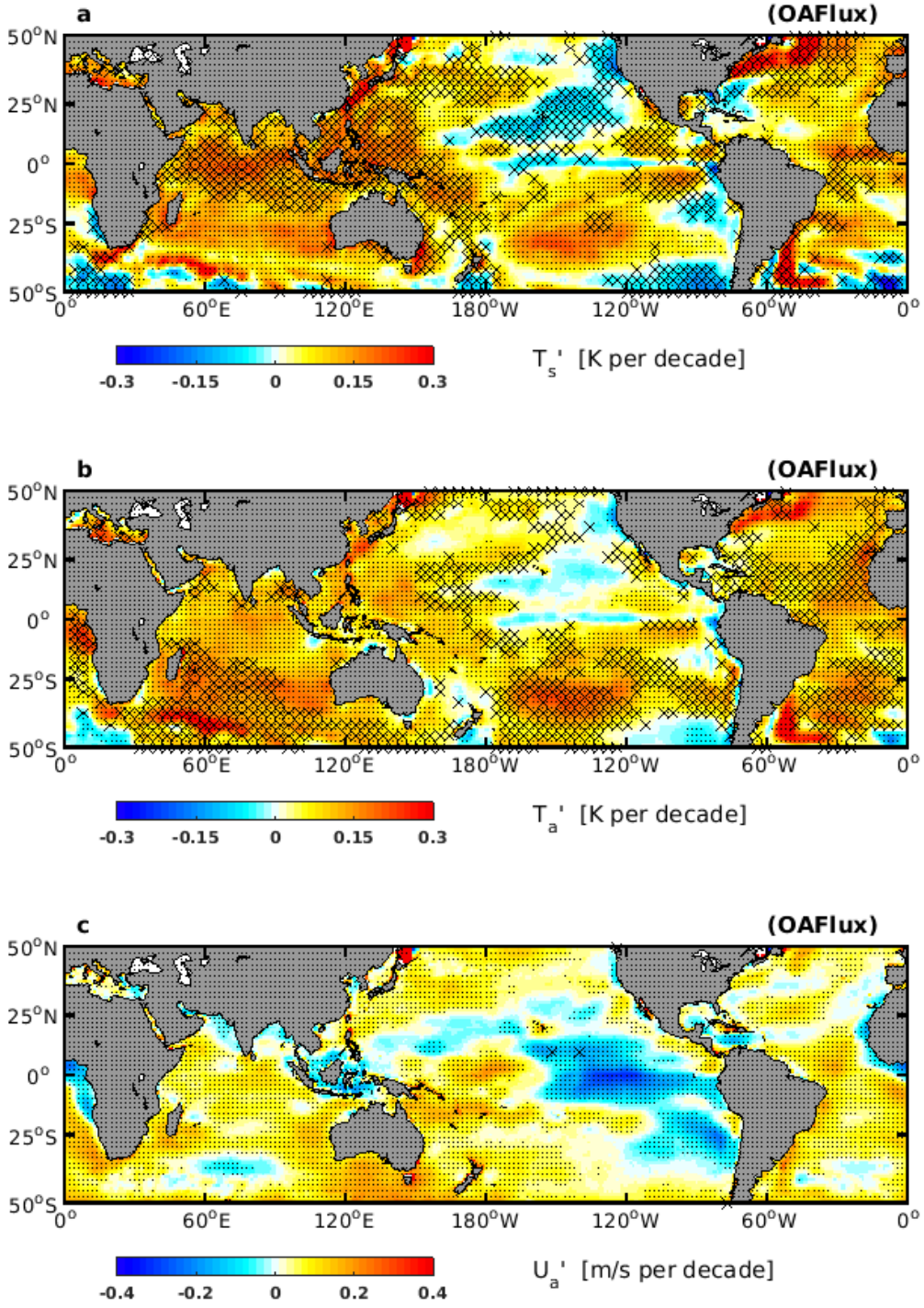

Fig. 2.3: *As Fig. 2.1, spatial distributions of the trends in sea surface temperature (T_s'), surface air temperature (T_a') and wind speed (U_a'). The area with $CS_X > 0.5$ (see Equation. 2.6) are marked with black cross.*

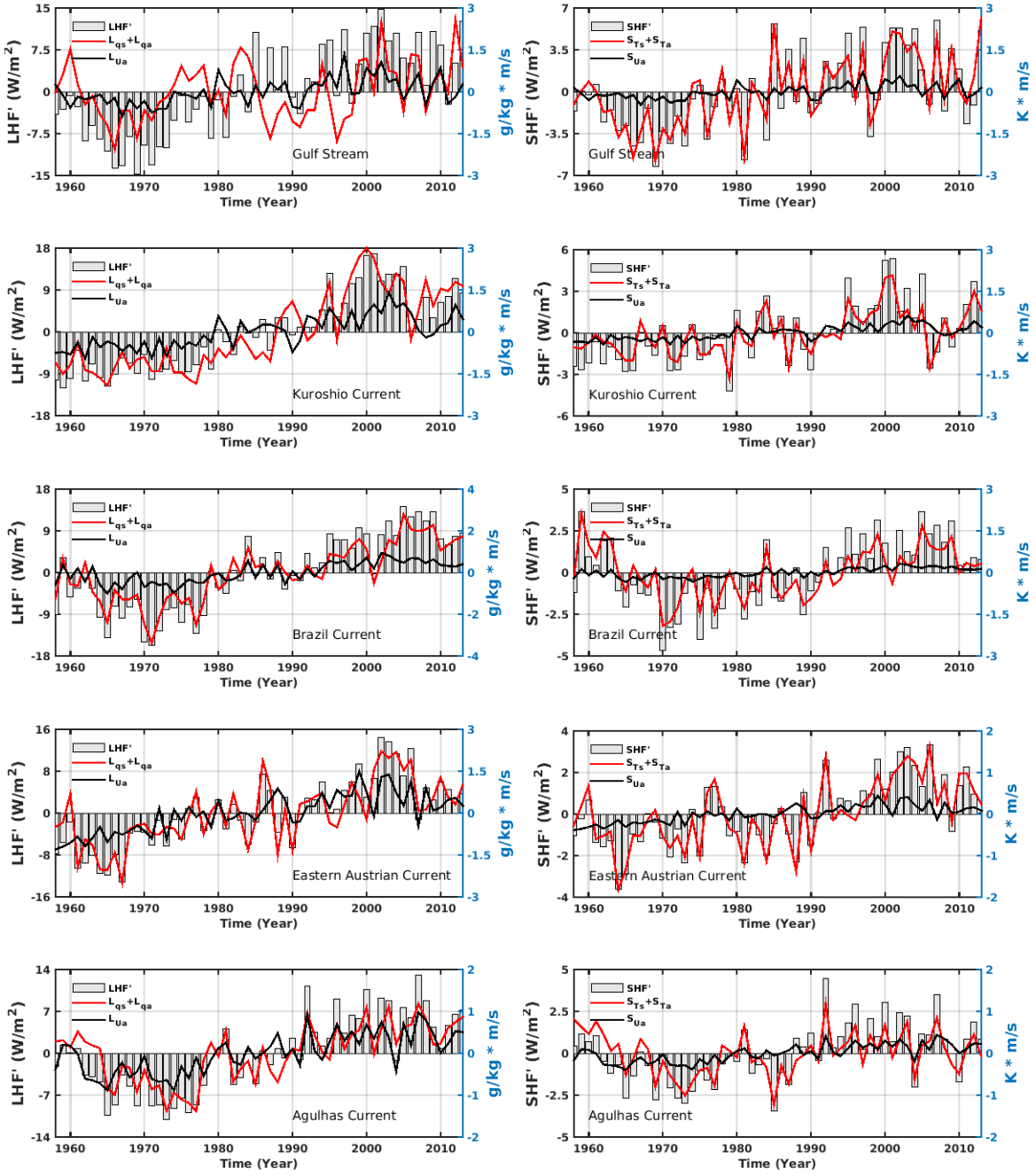

Fig. 2.4: *Time series of area-averaged LHF and SHF anomalies (grey bar) and their corresponding contributors (red and black lines) over the identified regions (as shown in Figs. 2.1a). The left axis is for the heat flux anomaly, and the right axis is for the THF's contribution terms.*

anomaly are treated together as a contribution by air-sea humidity difference ($L_{q_s}+L_{q_a}$). A similar assumption applies to the air-sea temperature difference (as $S_{T_s}+S_{T_a}$) in Fig. 2.4. We find that the increases in LHF and SHF over the WBCs mainly occur during 1970-2000. The air-sea humidity and temperature differences are the main drivers for the increases. For the tropical eastern Pacific Ocean, strong interannual variations of LHF and SHF are observed, which resemble the signal of the El Nino-Southern Oscillation (ENSO). While, on long time scales, the weakening surface wind plays an equivalent role as the reduced air-sea humidity and temperature differences in the decreasing THF. Regarding the northern tropical Atlantic, a continuous decline of air-sea humidity difference depresses the ocean THF loss there.

2.2.2 Possible mechanisms for the THF trends

Increasing THF over the WBCs

WBCs transport a large amount of heat from the low latitudes to the mid and high latitudes, which contribute to the Earth's energy balance. The heat release from the WBCs is primarily in the form of THF. Fig. 2.3a describes the spatial distribution of SST trends during 1958-2013. It appears that there is an enhanced warming of the main WBCs, on a magnitude of ~0.2-0.3 K per decade consistent with *Wu et al.* [2012]. This is remarkably stronger than the SST increase at the same latitudes during the same period. As demonstrated in section 2.2.1, the enhanced SST warming greatly strengthens the THF loss over the WBCs, indicating an ocean controlled climate trend. The THF in turn has a damping effect on the SST [*Cayan*, 1992; *Zhang and Mcphaden*, 1995; *Frankignoul and Kestenare*, 2002]. Moreover, from the perspective of ocean and atmosphere heat balance, increasing SST associated with enhanced THF loss implies that the heat transport by the WBCs has strengthened.

Fig. 2.5 presents the trend and climatology of near-surface zonal wind stress. On one hand, the westerly winds over the mid and high latitudes are stronger in intensity. On the other hand, over most of the tropical regions, the easterly winds are also accelerated, except for the tropical eastern Pacific Ocean. The pattern correlation coefficient between the trend and climatology zonal wind is 0.54, with a 95% confidence level (Student t-test), illustrating that the background surface wind circulation has strengthened

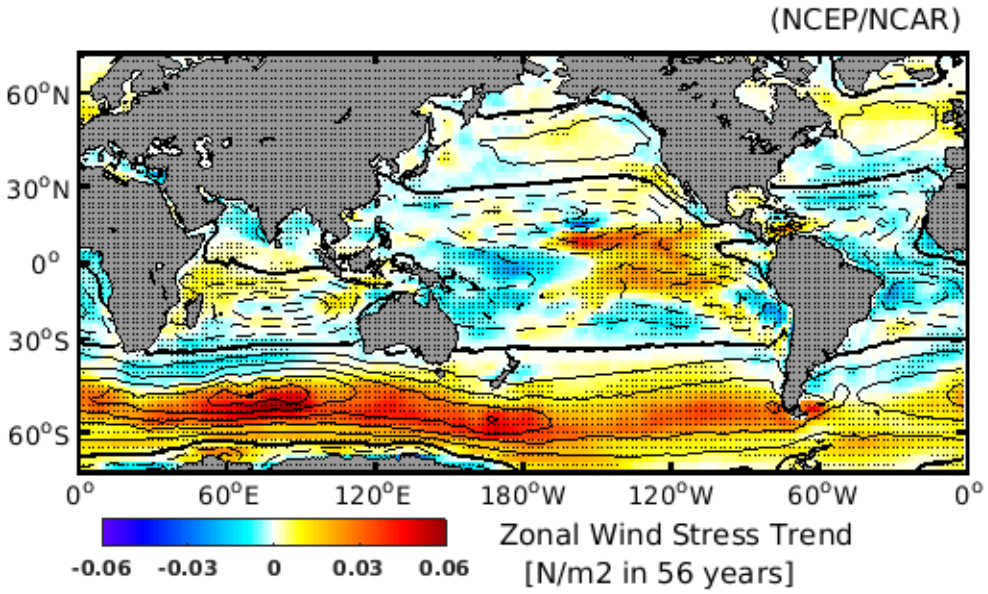

Fig. 2.5: *Spatial distributions of the trend (shading, westerly-positive) and climatology (contours) of zonal wind stress. Easterly wind stress is in dash lines; westerly wind stress is in solid lines; zero zonal wind stress is bold.*

in the latitude belts approximately between 10° to 65° in both hemispheres. Note that the stronger westerly winds are more pronounced over the Southern Hemisphere than that over the Northern Hemisphere.

According to the Sverdrup's theory of oceanic circulation, wind stress curl between the low latitudes and mid-latitudes is the main driver of the subtropical gyres. We compute the averaged wind stress curl over the corresponding subtropical gyres (as shown in Fig. 2.6a). It comes out that the magnitude of wind stress curl has increased over all the five subtropical gyres (Fig. 2.6b). The intensification of both the low latitude easterly and mid-latitude westerly (Fig. 2.5) would strengthen the subtropical wind stress curl, which forces stronger WBCs. Even though the intensification of zonal wind stress (or subtropical wind stress curl) over the Northern Hemisphere is not significant, it could have an amplifying effect over the WBCs through the ocean dynamic feedback. The WBCs in turn transport more heat and accelerate the THF loss over the mid-latitude expansions of these currents. It is worth noting that further analyses based on the European Centre for Medium-Range Weather Forecasts 40-year Reanalysis (ERA40, covering 1958-2001) [*Uppala et al.*, 2005] reveal similar patterns as the NCEP/NCAR (not shown), indicating that the results found here are not dataset-dependent.

Decreasing THF over the tropical eastern Pacific Ocean

The decreased SST over the eastern tropical Pacific Ocean, as depicted in Fig. 2.7a, shows good agreement with the OAFlux (Fig. 2.3a). Such cooling limits the heat loss from ocean surface. Meanwhile, the cooling SST is coupled with a sinking air flow, accompanied by a positive SLP trend (shading in Fig. 2.7b) and a divergence tendency of near-surface winds (vectors in Fig. 2.7a and 2.7b). The divergence of near-surface winds over the eastern Pacific weakens the background easterly trade winds and reduces the wind speed there. The combined effects of both the decreased SST and the weakened wind speed suppress the ocean surface THF loss.

Decreasing THF over the northern tropical Atlantic Ocean

To investigate the negative THF trend over the northern tropical Atlantic Ocean, we present the trends of near-surface wind, and air-sea humidity and temperature differences in Fig. 2.8. During 1958-2013, there is a strengthening of easterly winds over the

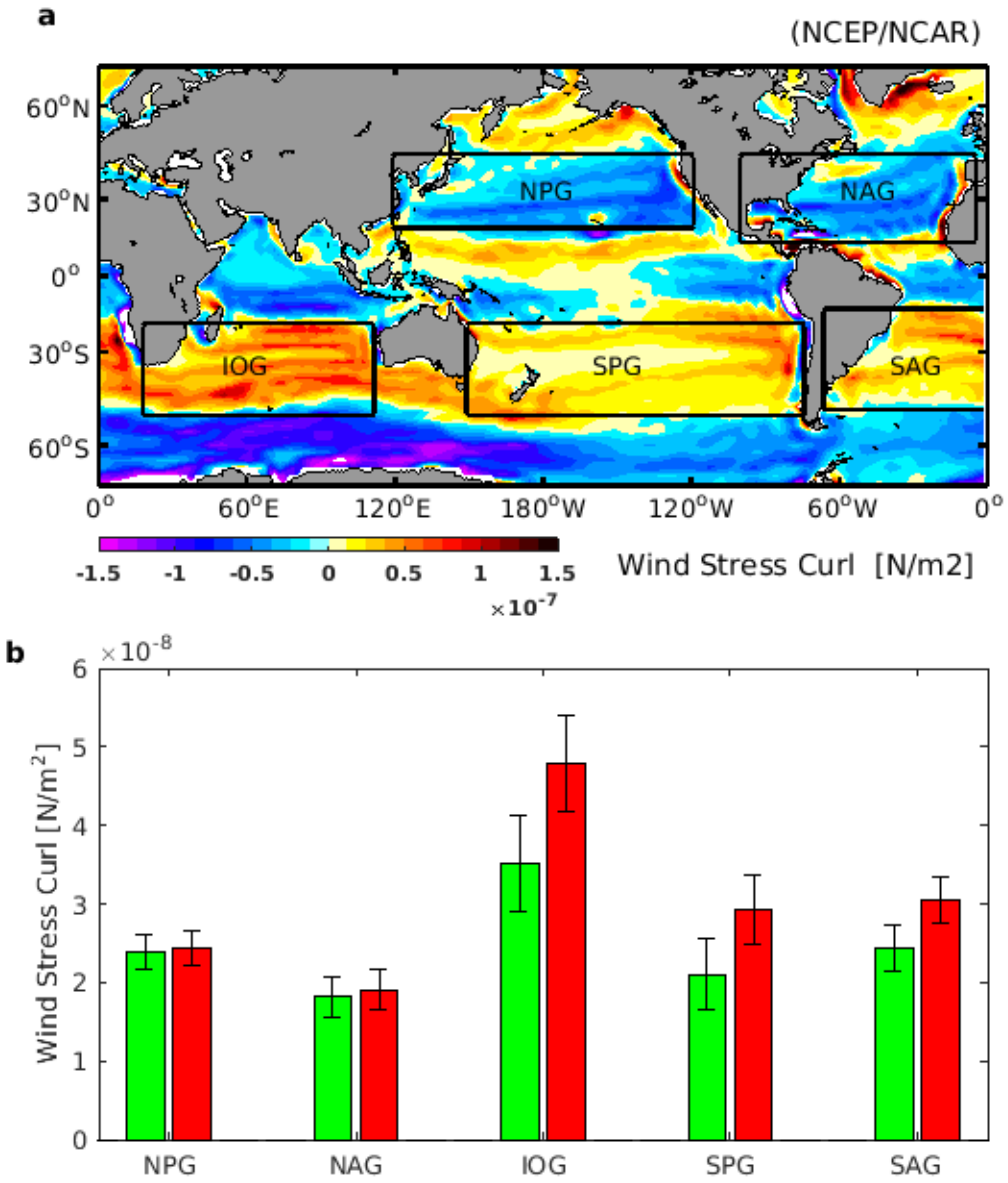

Fig. 2.6: *a. Spatial distribution of the climatological ocean surface wind stress curl. The black rectangles locate the area where we compute the area-mean wind stress curl. b. Absolute values of area-mean wind stress curl over the corresponding subtropical gyres shown in the upper panel. Red and green bars denote mean±trend/2, with error bars indicating their corresponding standard deviations. NPG stands for North Pacific Gyre, NAG stands for North Atlantic Gyre, IOG stands for India Ocean Gyre, SPG stands for South Pacific Gyre, SAG stands for South Atlantic Gyre.*

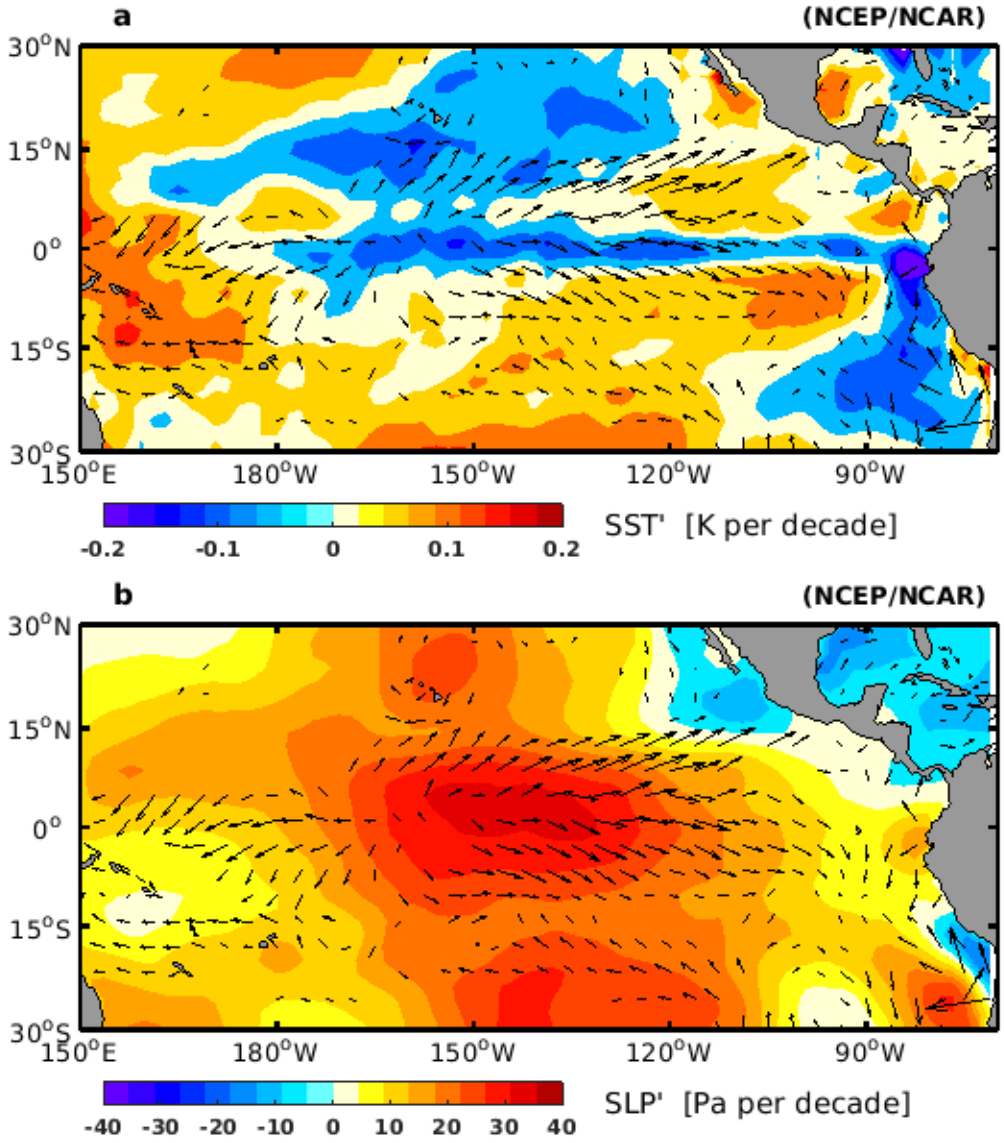

Fig. 2.7: *Trends in surface wind (vectors), SST (a, shading) and SLP (b, shading) over the Pacific Ocean. We only show the wind trend above 90% confidence level (Student's t-test).*

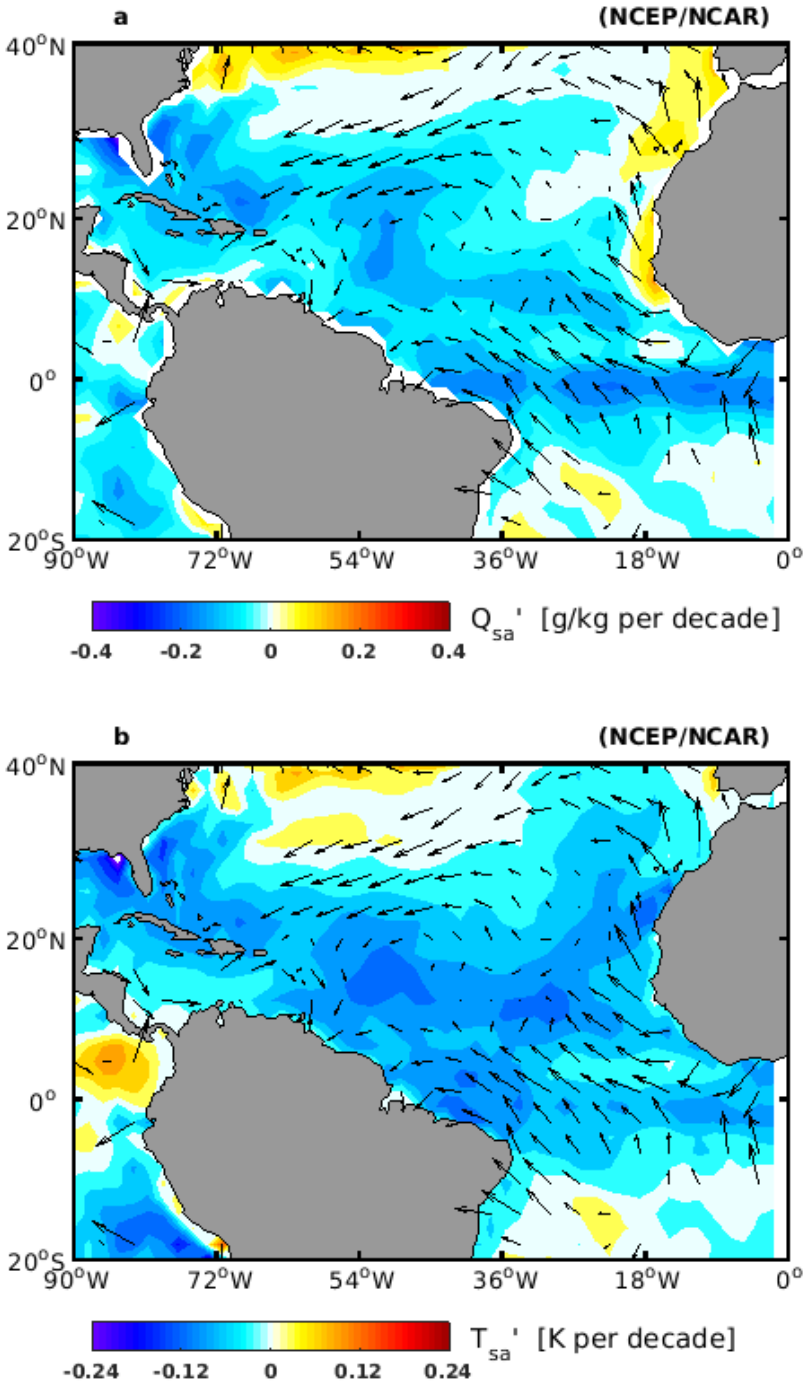

Fig. 2.8: *Trends in surface wind (vectors), air-sea humidity difference (a, shading) and air-sea temperature difference (b, shading) over the Atlantic Ocean.*

northern subtropical Atlantic and south-easterly winds near the equatorial Atlantic. Such wind anomalies tend to induce an Ekman divergence of the ocean current (upwelling) over the northern tropical Atlantic Ocean, which cools the ocean surface. By contrast, such pattern of wind trend results in a convergence of near-surface air at the same region, which provides a source of heat and water vapor from the adjacent area, contributing to the increases in the q_a (Fig. 2.2) and T_a (Fig. 2.3) there. Therefore, both the strengthening of easterly winds over the northern subtropical Atlantic and the intensified south-easterly winds near the equatorial Atlantic constitute the cause of the reduced air-sea humidity and temperature differences, which together suppress the ocean heat loss there.

2.3 Discussion

Due to the differences in the source of input variables, the formulation of bulk algorithms, and the changes in the observing system, uncertainties still remain in the THF data sets [*Kalnay et al.*, 1996; *Zeng et al.*, 1998; *Moore and Renfrew*, 2002; *Curry et al.*, 2004; *Yu et al.*, 2008; *Santorelli et al.*, 2011; *Brunke et al.*, 2011]. Considering the existing uncertainties in the heat flux data sets, we only focus on the prominent THF trends in this work. The THF trends we have identified are consistent with other studies. For example, *Yu et al.* [2008] showed that the increased LHF over the WBCs primarily occurs after the 1970s. Based on GSSTF data set, *Gao et al.* [2013] reported that the maximum LHF increases occur over the WBCs regions during 1988-2008. Additionally, their pattern of LHF trends also suggests that the LHF increases over the tropical Eastern Pacific and northern tropical Atlantic are relatively small compared to the overwhelming increase LHF over the tropical ocean surface (see *Gao et al.* [2013] Figure 2).

In this study we interpolate the THF trends based on annual mean values. However, THF have seasonal variations, particularly over the mid and high latitudes. In different seasons, the THF trends may vary depending on the flux-related state variables and different physical mechanism [*Gulev et al.*, 2007b; *Gulev and Belyaev*, 2012]. *Yu et al.* [2008] pointed out that the THF over the WBCs increased mainly during wintertime, associated with increasing storm frequency [*Shaman et al.*, 2010; *Gulev and Belyaev*,

2012]. In our analysis, we also find that the near-surface wind speed over the WBCs has accelerated, which is likely linked to higher storm activities. In the future, a comprehensive study on the seasonal THF trends and their contributors are essential to further understand the mechanism and the climate consequence.

Due to natural variability, trend estimates are sensitive to the analyzed time periods, especially when the period is short. To assess the long-term changes of the coupled ocean atmosphere dynamics, we choose a relatively long period (56 years, 1958-2013) to carry out this work. However, the presented trends could also reflect climate variations on multi-decadal time scales. For example, the THF over the Kuroshio Current and the Gulf Stream increase primarily during 1970-2000 (as in Fig. 2.4). The variations seem to be associated with an increase of the Arctic Oscillation starting from the late 1960s to the 1990s, which manifests in stronger westerly winds over the North Hemisphere [*Thompson and Wallace*, 2000]. But the Arctic Oscillation shifted towards a negative phase after the 1990s. Over the Southern Hemisphere, an increase of the Antarctic Oscillation is also observed, which explains the strengthening Southern Hemisphere westerly [*Thompson and Wallace*, 2000; *Marshall*, 2003]. However, we notice that the THF over the Brazil Current and the Agulhas Current also show strong decadal variations (see Fig. 2.4), which contribute to the increase THF at this certain period. To conclude whether the identified THF trends reflect long-term climate trends or multi-decadal variations, observations with a longer time interval are required.

The WBCs play a vital role in the climate over the adjacent mainland [*Minobe et al.*, 2008; *Kelly et al.*, 2010]. Previously, the strengthening WBCs has been documented individually, for example, the Gulf Stream [*Curry and McCartney*, 2001], the Kuroshio Current [*Qiu and Joyce*, 1992; *Deser et al.*, 1999; *Sato et al.*, 2006; *Sakamoto et al.*, 2005] and the Eastern Australia Current [*Cai et al.*, 2005; *Qiu and Chen*, 2006; *Ridgway*, 2007; *Roemmich et al.*, 2007; *Ridgway et al.*, 2008]. *Curry and McCartney* [2001] found that transport of the Gulf Stream has intensified after the 1960s. *Sato et al.* [2006] and *Sakamoto et al.* [2005] projected a stronger Kuroshio Current in response to global warming according to a high-resolution coupled atmosphere-ocean climate model. Based on long-term temperature and salinity observations from an ocean station off eastern Tasmania, *Ridgway* [2007] demonstrated that the East Australian Current had increased over the past 60 years. Beyond these studies on individual WBCs, our

study suggests that the climate change over the WBCs is likely to be a systematic phenomenon over all ocean basins. As *Wu et al.* [2012] also stressed, there was enhanced SST warming over all the WBCs. However, controversy still remains on the dynamic changes of WBCs due to the uncertainty of the data sets. According to a continuous observation from undersea telephone cables near 27° N in the Straits of Florida, *DiNezio et al.* [2009] constructed a time series of transport of the Florida Current (part of Gulf Stream) since 1982. The time series suggest no indication of positive trend during the covering period (1982-2007).

Considering the tropical eastern Pacific, *Cane et al.* [1997] and *Zhang et al.* [2010b] observed a cooling mode of the Pacific cold tongue under global warming associated with an increased upwelling [*Cane et al.*, 1997]. Model experiments show that the cooling over the tropical eastern Pacific leads the ocean to absorb more heat from the atmosphere, contributing to the global warming hiatus in recent decades [*Meehl et al.*, 2011; *Kosaka and Xie*, 2013]. However, the cooling mode is very likely to collapse in the future, as suggested by the coupled climate models [*Meehl et al.*, 2011]. Regarding the northern tropical Atlantic Ocean, the trend of wind speed is very likely to be a stronger regime of the Intertropical Convergence Zone (ITCZ) which is characterized by a convergence of surface air and divergence of ocean currents.

The THF are related to the energy and water vapor transport from the ocean to the atmosphere. Prominent THF trends can be an indicator for the remarkable changes in the ocean and atmosphere dynamics. Besides the three identified THF trends in this paper, there are some other regions where the THF trends are significant, i.e., the decreased THF over the northern subtropical central Pacific, the reduced THF over the southern subtropical eastern Pacific. These trends are also worth being investigated in the future. In addition, the seasonal dependence of THF trends and their corresponding impact factors are beyond the scope of this paper, which are of particular importance for understanding the mechanisms.

2.4 Conclusions for this chapter

Based on the OAFlux data set, we have recognized three prominent ocean surface THF trends during 1958-2013, i.e., the enhanced THF over the mid-latitude expansions of

subtropical WBCs, the reduced THF over the tropical eastern Pacific Ocean, and the reduced THF over the northern tropical Atlantic Ocean.

The dominant factors for these THF trends are identified by linearizing the bulk flux formulae. We find that over the WBCs, the THF are enhanced by the increasing SST. Such change is likely to be induced by intensified WBCs which are forced by a systemic stronger near-surface zonal wind stress in the latitude belts approximately between 10° to 65° in both hemispheres. Over the tropical eastern Pacific Ocean, the THF are reduced primarily through the decreasing near-surface wind speed and SST. The associated dynamic changes are found to be the divergence of near-surface wind coupled with a cooling ocean surface over the tropical Pacific Ocean. Over the northern tropical Atlantic Ocean, the reduced THF are primarily affected by the increasing surface specific humidity and air temperature, corresponding with a convergence of surface air and divergence of ocean currents.

This work proposes a novel way of exploring the changes of atmosphere-ocean dynamics by examining the trends of THF. As a next step, the associated dynamic changes will be investigated with more data sets and model scenarios.

3

Intensification and poleward shift of WBCs in a warming climate

In the previous chapter, a significant increase of THF is identified over the mid-latitude expansions of WBCs, indicating that the WBCs dynamics may have significant changes. However, the detection of ocean dynamic is challenging due to insufficient ocean observations, particularly over large spatial scale and over long period of time. WBCs transport large quantities of heat from the tropics to mid and high latitudes, and much of the heat is released along the routes of these currents. As shown in Fig. 3.1, the meandering of WBCs can be clearly captured by the upward ocean surface heat flux. Following this idea, ocean surface heat flux is used as the main metric to identify the dynamic changes of WBCs.

The available ocean surface heat fluxes data sets have several potential sources of uncertainty (e.g., uncertainty in the flux computation algorithms, sampling issues, instrument biases, changing observation systems) [*Brunke et al.*, 2002; *L'Ecuyer and Stephens*, 2003; *Van de Poll et al.*, 2006; *Gulev et al.*, 2007a]. Each data set has its own advantages and weaknesses. Satellite-blended records give observations with excellent spatial/temporal sampling, but they suffer from a lack of temporal coverage, which is insufficient to examine the long-term variability. Reconstructed and reanalysis products cover longer periods by synthesizing a variety of observations. However, the changing mix of observations can introduce spurious variability and trends into the output [*Dee et al.*, 2014]. The coupled general circulation models (CGCM) have the ability to simulate the Earth's climate over hundreds of years with consistent physical behaviors,

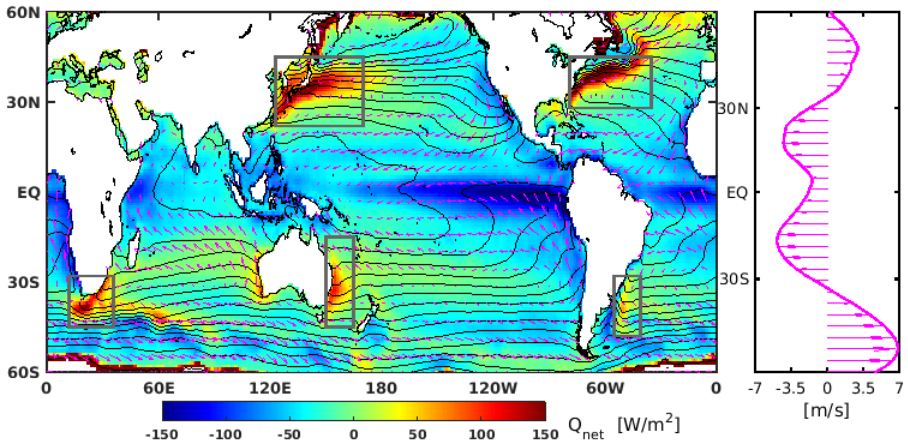

Fig. 3.1: *Left: Distribution of climatological Q_{net} (shaded, positive upward), SST (black contours, contour interval is 2 K) and near-surface ocean winds (pink arrows). Right: Zonally averaged near-surface ocean zonal wind speeds (positive westerly). Q_{net} is from the OAFlux/ISCCP data set; SST is from the HadISST1 data set; near-surface ocean winds are based on the NCEP/NCAR. The overlapping periods 1984-2009 are selected to derive the climatological conditions.*

but their performance on reproducing the climate variability is still under evaluation [*Refsgaard et al.*, 2014; *Bellucci et al.*, 2014]. For achieving reliable and comprehensive results, all three types of heat flux data sets mentioned above are included here. Moreover, the results based on sea surface heat flux will also be cross-validated by the ocean velocity fields and ocean surface winds. Since the reliability of the data sets before the 1950s is still a subject of controversy [*Krueger et al.*, 2013], we focus our analysis on the period after 1958. The paper is organized as follows. In section 3.1, the data sets and methods used are briefly introduced. Section 3.2 presents the observed and simulated dynamic changes of the WBCs. The physical mechanism responsible for these changes is investigated in section 3.3. Discussion and conclusions are given in sections 3.4 and 3.5, respectively.

3.1 Data and Methodology

All the data sets used in this paper are listed in Table 3.1. The reconstructed SST from the Hadley Centre Global Sea Ice and Sea Surface Temperature v1 (HadISST1, 1870-2013) [*Rayner et al.*, 2003] is used to compute the SST indices of individual WBCs. The time series of near surface temperature from the HadCRUT4 (1850-2013) [*Morice et al.*, 2012] is utilized to represent the signal of global warming.

Besides, two satellite-blended data sets are applied to identify the dynamic changes of WBCs. They are the SST from the Optimum Interpolation SST Analysis Version 2 (OISSTv2, 1982-2013) [*Reynolds et al.*, 2002], and the net surface heat flux (Q_{net}, sum of the radiative and turbulent heat fluxes) from the Objectively Analyzed Air-sea Fluxes and the International Satellite Cloud Climatology Project (OAFlux/ISCCP, 1983-2009) [*Rossow and Schiffer*, 1991; *Yu et al.*, 2008].

Moreover, four atmospheric reanalysis and four ocean reanalysis data sets are included, namely the National Centers for Environmental Prediction / National Center for Atmospheric Research reanalysis (NCEP/NCAR, 1948-2013) [*Kalnay et al.*, 1996], the European Centre for Medium-Range Weather Forecasts 40-year Reanalysis (ERA40, 1958-2001) [*Uppala et al.*, 2005], the Twentieth Century Reanalysis (20CRv2) [*Compo et al.*, 2006, 2011], the ECMWF's first atmospheric reanalysis of the 20th century (ERA-20C) [*Poli et al.*, 2016], the European Centre for Medium-Range Weather Fore-

Table 3.1: *List of data sets used in this study*

Data Type	Data Name	Periods	References
Reconstracted	HadISST	1870-2014	*Rayner et al.* [2003]
Reconstracted	HadCRUT4	1850-2014	*Morice et al.* [2012]
Satellite-blended	OISSTv2	1982-2014	*Reynolds et al.* [2002]
Satellite-blended	OAFlux/ISCCP	1983-2009	*Rossow and Schiffer* [1991]; *Yu et al.* [2008]
Atmospheric Reanalysis	NCEP/NCAR	1948-2014	*Kalnay et al.* [1996]
Atmospheric Reanalysis	ERA40	1958-2001	*Uppala et al.* [2005]
Atmospheric Reanalysis	20CRv2	1871-2012	*Compo et al.* [2006, 2011]
Atmospheric Reanalysis	ERA-20C	1900-2010	*Poli et al.* [2016]
Ocean Reanalysis	ORA-S4	1958-2009	*Balmaseda et al.* [2013]
Ocean Reanalysis	SODA2.2.0	1948-2008	*Carton and Giese* [2008]
Ocean Reanalysis	GECCO	1952-2001	*Köhl and Stammer* [2008]
Ocean Reanalysis	GECCO2	1948-2014	*Köhl* [2015]
Climate Model	CMIP5/historical	1850-2005	*Taylor et al.* [2012]
Climate Model	CMIP5/RCP4.5	2006-2300	*Taylor et al.* [2012]
Climate Model	CMIP3/20C3M	1850-2000	*Meehl et al.* [2007]
Climate Model	CMIP3/A1B	2001-2100	*Meehl et al.* [2007]
Climate Model	CMIP3/A2	2001-2100	*Meehl et al.* [2007]

casts ocean reanalysis system 4 (ORA-S4, 1958-2009) [*Balmaseda et al.*, 2013], the Simple Ocean Data Assimilation (SODA2.2.0, 1948-2008) [*Carton and Giese*, 2008], and the German partner of the consortium for Estimating the Circulation and Climate of the Ocean (GECCO, 1952-2001, and GECCO2, 1948-2014) [*Köhl and Stammer*, 2008; *Köhl*, 2015].

Additionally, the third and fifth phase of the Climate Model Intercomparison Project (CMIP3/5) [*Meehl et al.*, 2007; *Taylor et al.*, 2012] are used as well. As the CMIP3/5 models have different spatial resolutions and numbers of ensemble members, the trends in each CGCMs from the first ensemble member (named $r1i1p1$) [*Taylor et al.*, 2010] are computed first. Then the trends are re-gridded onto a regular $1^\circ \times 1^\circ$ latitude-longitude grid using bilinear interpolation. Finally, they are averaged over all the corresponding simulations to get the multi-model ensemble trends.

3.2 Dynamic changes of WBCs

3.2.1 Results from observations

Fig. 3.2 shows the SST indices of the five WBCs after removing the globally averaged SST anomaly. Positive trends are observed, indicating that the ocean surface warming over the WBCs is outpacing other regions. Moreover, the SST indices of WBCs share similarities with the global warming signal. These features raise the question as to whether the strength of WBCs is affected by the global warming. It is also noticed that the SST indices of WBCs have strong decadal variations, especially for the Kuroshio Current and the Gulf Stream.

The trends in SST and Q_{net} (positive-upward) are depicted in Figs. 3.3 and 3.4 (shading). The corresponding climatology values (contours) are also presented to locate the background routes of the WBCs.

The magnitudes and distributions of SST and Q_{net} trends reveal discrepancies among different data sets over different time periods. In a relative short period of time, the satellite-blended data sets (OISSTv2 and OAFlux/ISCPP) mainly capture the signal of decadal climate variability, i.e., a negative phase of Pacific Decadal Oscillation [*Mantua et al.*, 1997] over the Pacific Ocean, and a positive phase of Atlantic Multidecadal

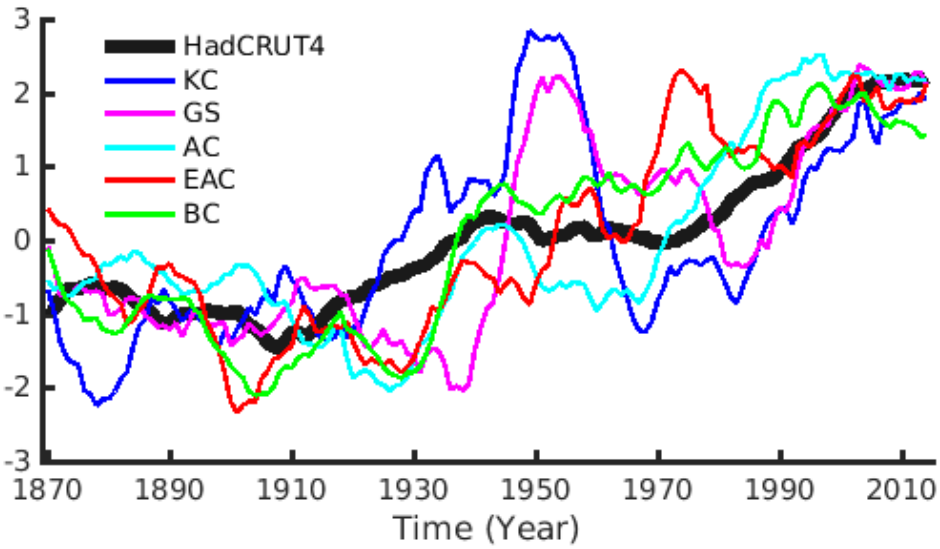

Fig. 3.2: *SST indices of WBCs (thin color line) and signal of global warming (HadCRUT4, thick black line). All indices are standardized after applying an 11-year running mean. SST indices of WBCs are extracted using the following approach: Firstly, regional mean SST indices are calculated over individual WBCs (as shown with grey rectangles in Fig. 3.1, i.e., Kuroshio current,* $123°E - 170°E$, $22°N - 45°N$; *Gulf Stream,* $79°W - 35°W$, $28°N - 45°N$; *Eastern Australian Current,* $150°E - 165°E$, $15°S - 45°S$; *Brazil Current,* $55°W - 41°W$, $48°S - 28°S$; *Agulhas Current,* $12°E - 36°E$, $45°S - 28°S$*). Then, the globally averaged SST anomaly is removed from the SST indices of individual WBCs.*

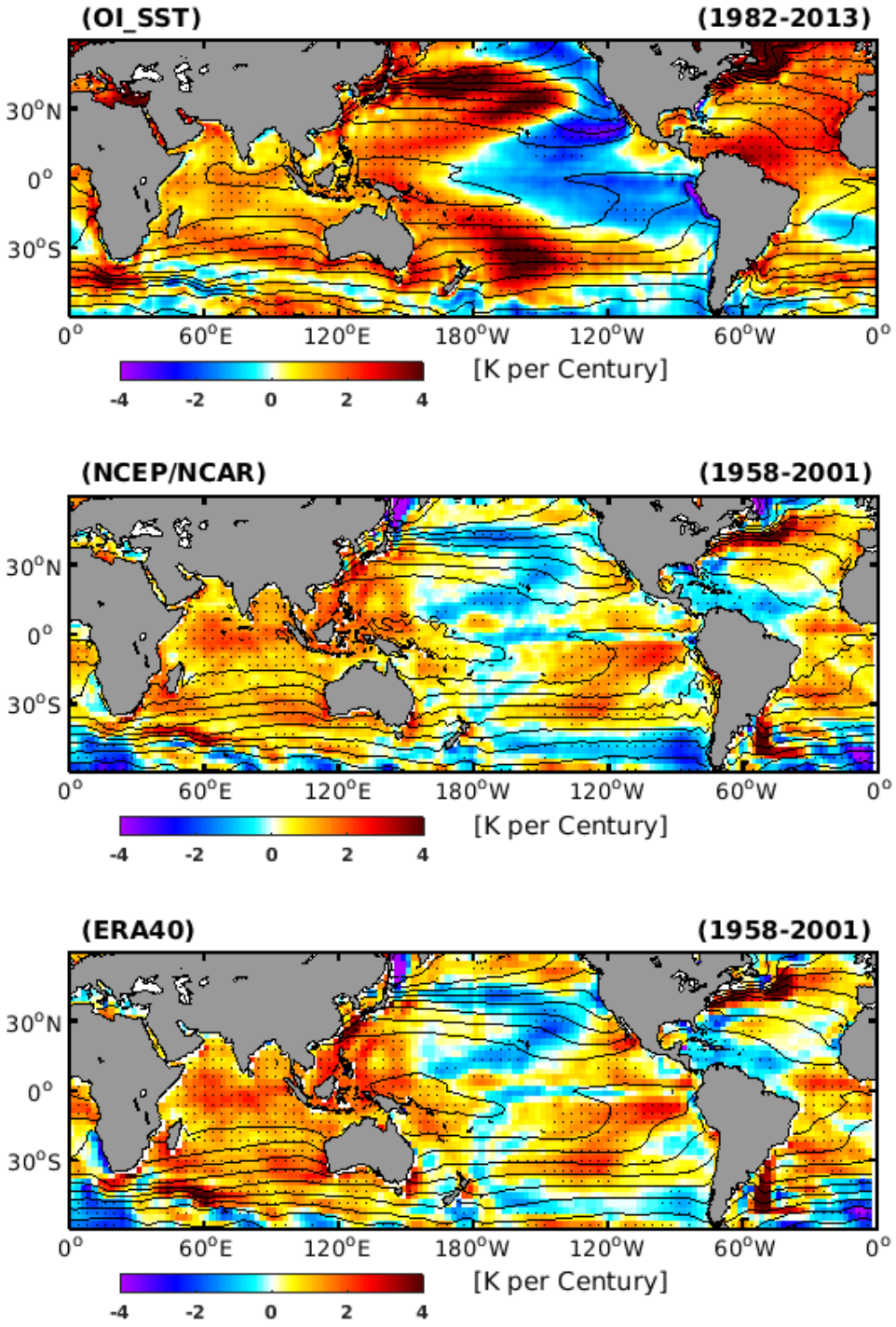

Fig. 3.3: *Observational trends in SST (shading). Black contours present climatological SST. Stippling indicates regions where the trends pass the 95% confidence level (Student's t-test).*

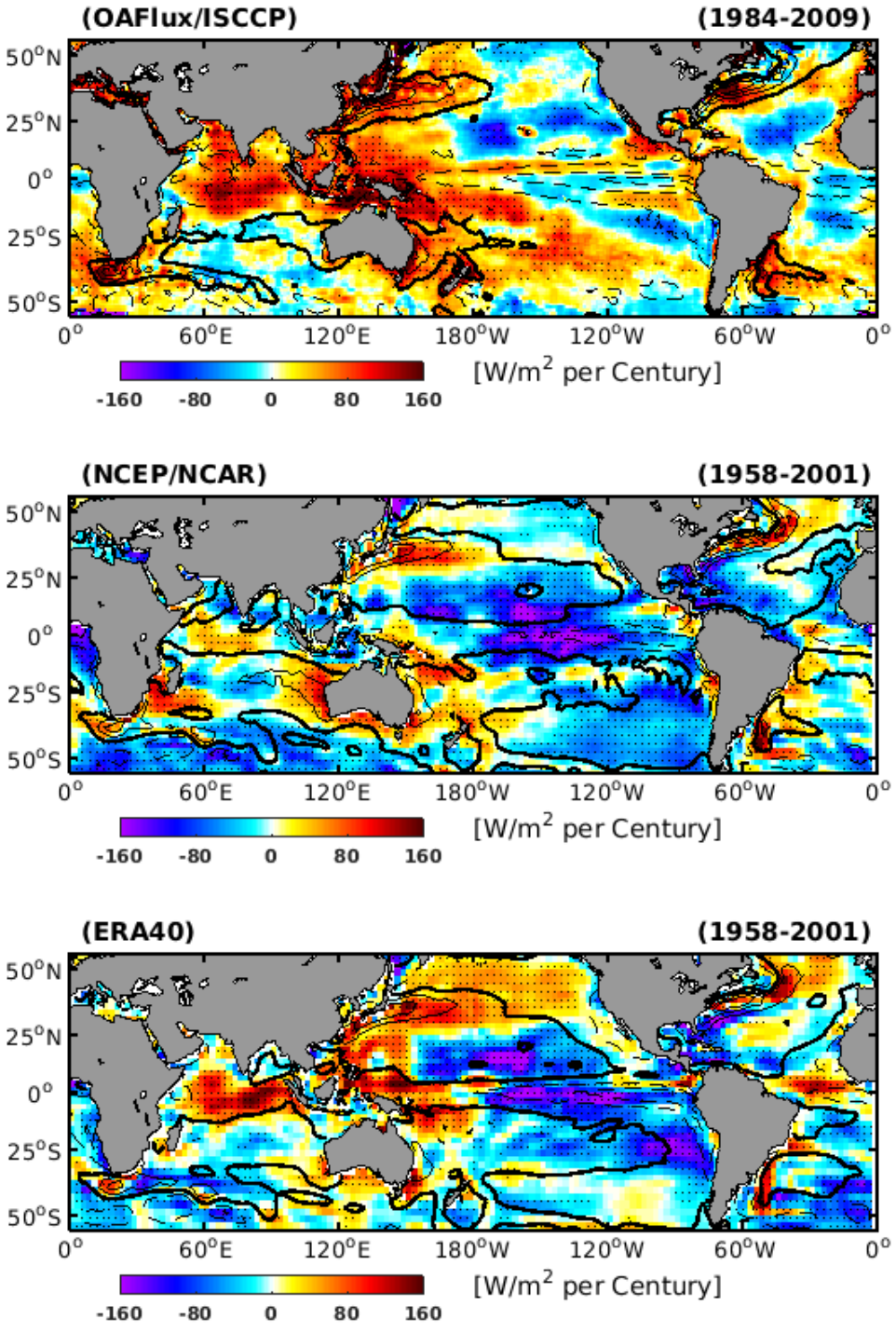

Fig. 3.4: *Observational trends in Q_{net} (shading, positive-upward). Black contours present climatological Q_{net}. Upward Q_{net} is in solid lines; downward Q_{net} is in dashed lines; zero Q_{net} is in bold lines. Stippling indicates regions where the trends pass the 95% confidence level (Student's t-test).*

Oscillation [*Schlesinger and Ramankutty*, 1994] over the Atlantic Ocean. Over a longer time scale, an overwhelming ocean surface warming is observed in the reanalysis data sets. Despite these discrepancies, consistent features emerge over the mid-latitude expansions of the WBSs with substantial increase in both SST and Q_{net}. Such trends occur not only over individual WBCs, but for WBCs within all ocean basins. From a perspective of ocean-atmosphere heat balance, increased SST accompanied by enhanced ocean surface heat loss indicates that the ocean surface warming is not caused by the atmospheric forcing, but by an intensified ocean heat transport though the WBCs.

With respect to the regional features, we find that the trends are asymmetrical over different flanks of the WBCs. Both NCEP and ERA40 show a stronger increase in SST and Q_{net} at the polar flanks of the Gulf Stream, the Brazil Current, the East Australian Current and the Agulhas Current. While, decreases or relative weaker increases in SST and Q_{net} present themselves over the equator flanks of the above currents. The asymmetrical pattern reveals that the positions of the SST gradients and the high Q_{net}, induced by WBCs, are shifting towards the polar regions. However, one clear exception is found over the North Pacific Ocean, i.e., the Kuroshio Current, which experiences a stronger positive trend in Q_{net} at the equatorial flank as illustrated by both reanalysis data sets, indicating an equatorward displacement of the Kuroshio Current over the period 1958-2001.

Comparing with the reanalysis data sets, the satellite-blended data sets also show stronger increases in Q_{net} and SST over the polar flank of the Agulhas Current (Figs. 3.3 and 3.4). While, due to their relatively short temporal period, the satellite-blended data sets are not able to identify signals of asymmetrical increases in the two elements over the other four WBCs.

In order to cross validate our results found from the ocean surface, we analyze the ocean velocity field. The imprint of the global warming on the ocean water velocity from four ocean reanalysis data sets is presented in the Figs. 3.5, 3.6, 3.7, 3.8. Since the WBCs are strong ocean currents, the background ocean velocity field (contour lines) indicates the climatological paths. The shading gives the changes in velocity speed. These ocean reanalyze show large discrepancies in terms of regional patterns of WBCs changes. Even the same model system (GECCO and GECCO2) does not produce consistent results, mostly likely, due to high nonlinearity of the WBCs and

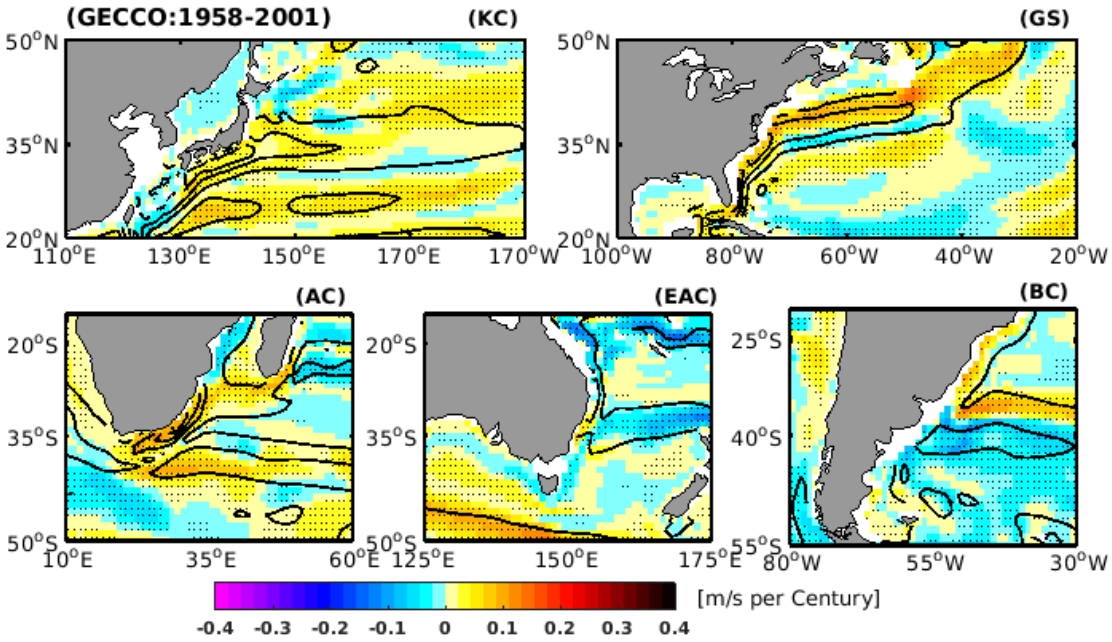

Fig. 3.5: *Trends of upper 100 m ocean velocity (shading) based on GECCO ocean reanalysis. Contours: climatological depth-averaged (upper 100 m) sea water velocity. Stippling indicates regions where the trends pass the 95% confidence level (Student's t-test).*

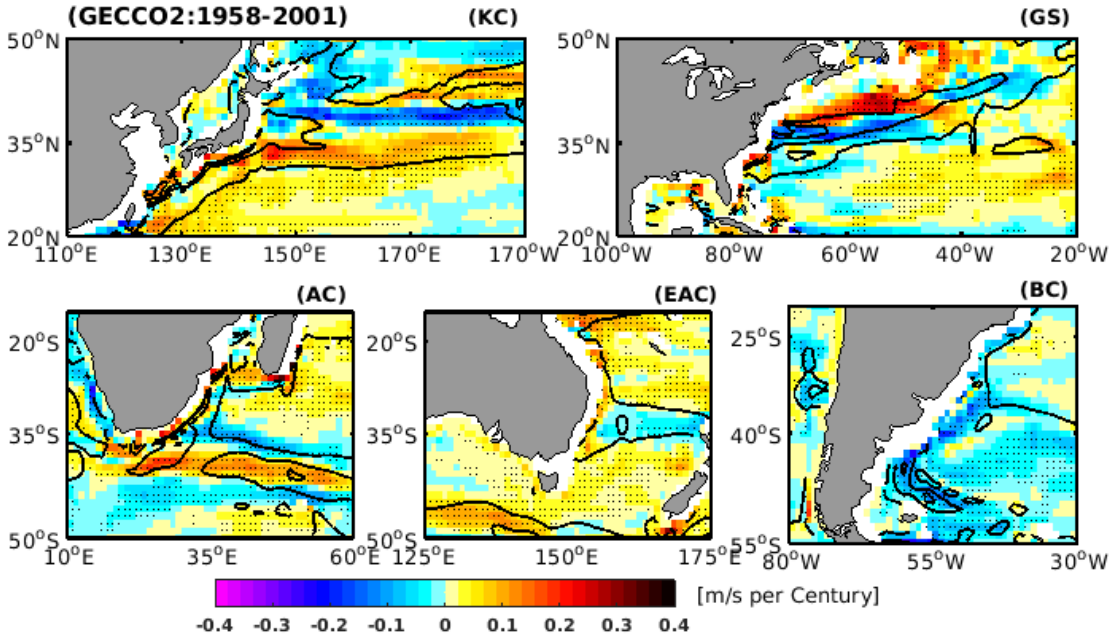

Fig. 3.6: *Trends of upper 100 m ocean velocity (shading) based on GECCO2 ocean reanalysis. Contours: climatological depth-averaged (upper 100 m) sea water velocity. Stippling indicates regions where the trends pass the 95% confidence level (Student's t-test).*

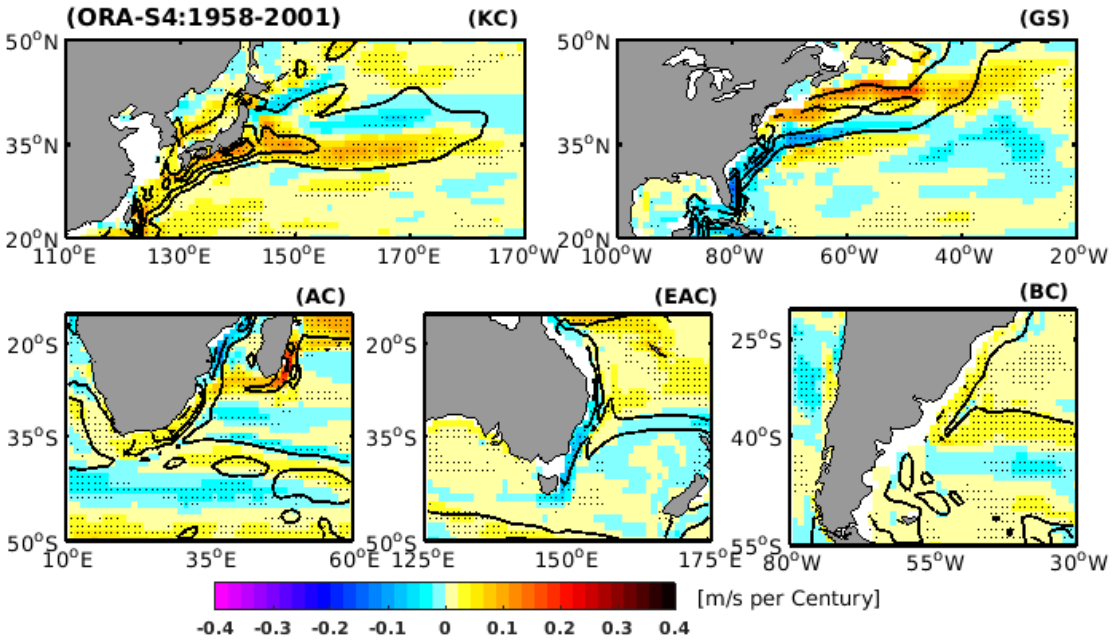

Fig. 3.7: *Trends of upper 100 m ocean velocity (shading) based on ORAS4 ocean reanalysis. Contours: climatological depth-averaged (upper 100 m) sea water velocity. Stippling indicates regions where the trends pass the 95% confidence level (Student's t-test).*

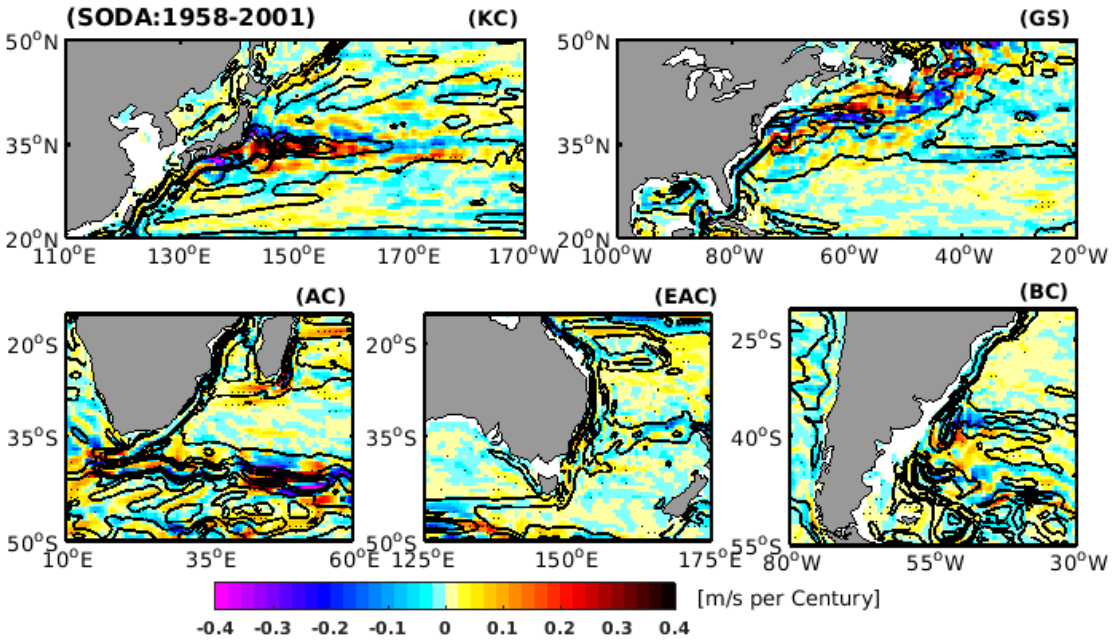

Fig. 3.8: *Trends of upper 100 m ocean velocity (shading) based on SODA ocean reanalysis. Contours: climatological depth-averaged (upper 100 m) sea water velocity. Stippling indicates regions where the trends pass the 95% confidence level (Student's t-test).*

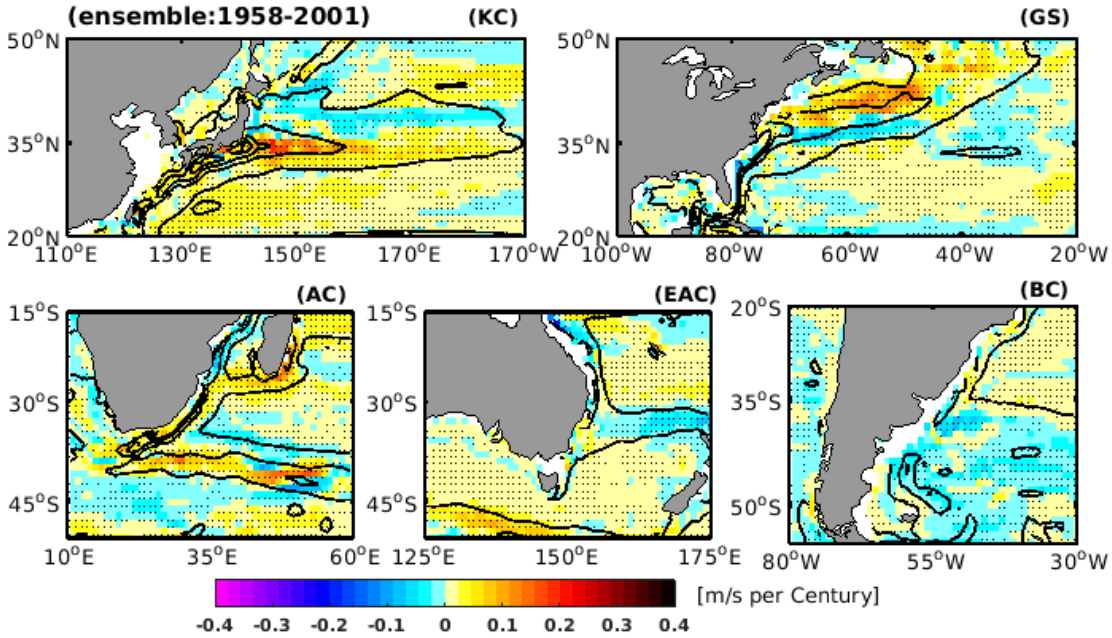

Fig. 3.9: *Ensemble trends in upper 100 m ocean velocity (shading) based on SODA, ORA-S4, GECCO and GECCO2 ocean reanalysis. Contours: climatological depth-averaged (upper 100 m) sea water velocity. Stippling indicates areas where at least 3 data sets agree on the sign of the trends.*

insufficient number of ocean observations assimilated in the ocean reanalysis data sets. We perform the ensemble changes of upper ocean water velocity in Fig. 3.9. Over the North Atlantic Ocean, a faster (slower) velocity over the polar (equator) flank of the Gulf Stream is observed, demonstrating a significant poleward shift of the Gulf Stream route. Over the south-western Indian Ocean, there is a prominent positive trend of the Agulhas Current along the continental shelf of south-eastern Africa. In contrast, a reduced velocity is found at the route of the Agulhas Current in the Mozambique Channel, demonstrating that the Agulhas Current is stronger and shifting southwards. For the Eastern Australian Current and the Brazil Current, the ensemble members (see 3.5, 3.6, 3.7, 3.8) show large differences, which makes the ensemble mean meaningless. Nevertheless, the SODA data set shows an intensified and southward shift of both the Brazil Current and the Eastern Australian Current.

Over the North Pacific Ocean, we find that the Kuroshio Current is stronger and shifting towards the equator, which is again different from the other four WBCs. However, the results in the velocity field are in agreement with the observational Q_{net} trends presented in the previous section (e.g., Fig. 3.4).

3.2.2 Results from climate models

In this section, the dynamic changes of the WBCs are assessed on the basis of CMIP3/5 archives (Figs. 3.10- 3.17, respectively). In order to suppress the internal fluctuations, we analyze the ensemble mean of more than 20 models. In general, the climate models present very similar patterns of WBCs climate changes over the Southern Hemisphere in comparison with observations. Over the Agulhas Current, the East Australian Current and the Brazil Current, the location of the maximum SST increase is found over the polar flanks of their mid-latitude expansions. Meanwhile, a relatively weak SST increase is found over their equatorial flanks. The corresponding Q_{net} trend exhibits dipole modes (positive values at the polar flank and negative values at the equator flank) over their mid-latitude expansions. Also, the ocean velocity trends over the above WBCs consistently illustrate increasing and poleward shifting of these currents.

Due to the large internal variability of the Northern Hemisphere WBCs (Fig. 3.2), there are strong discrepancies between the observations and climate models, e.g. the strengthening & poleward shift of the Kuroshio Current and a significant weakening

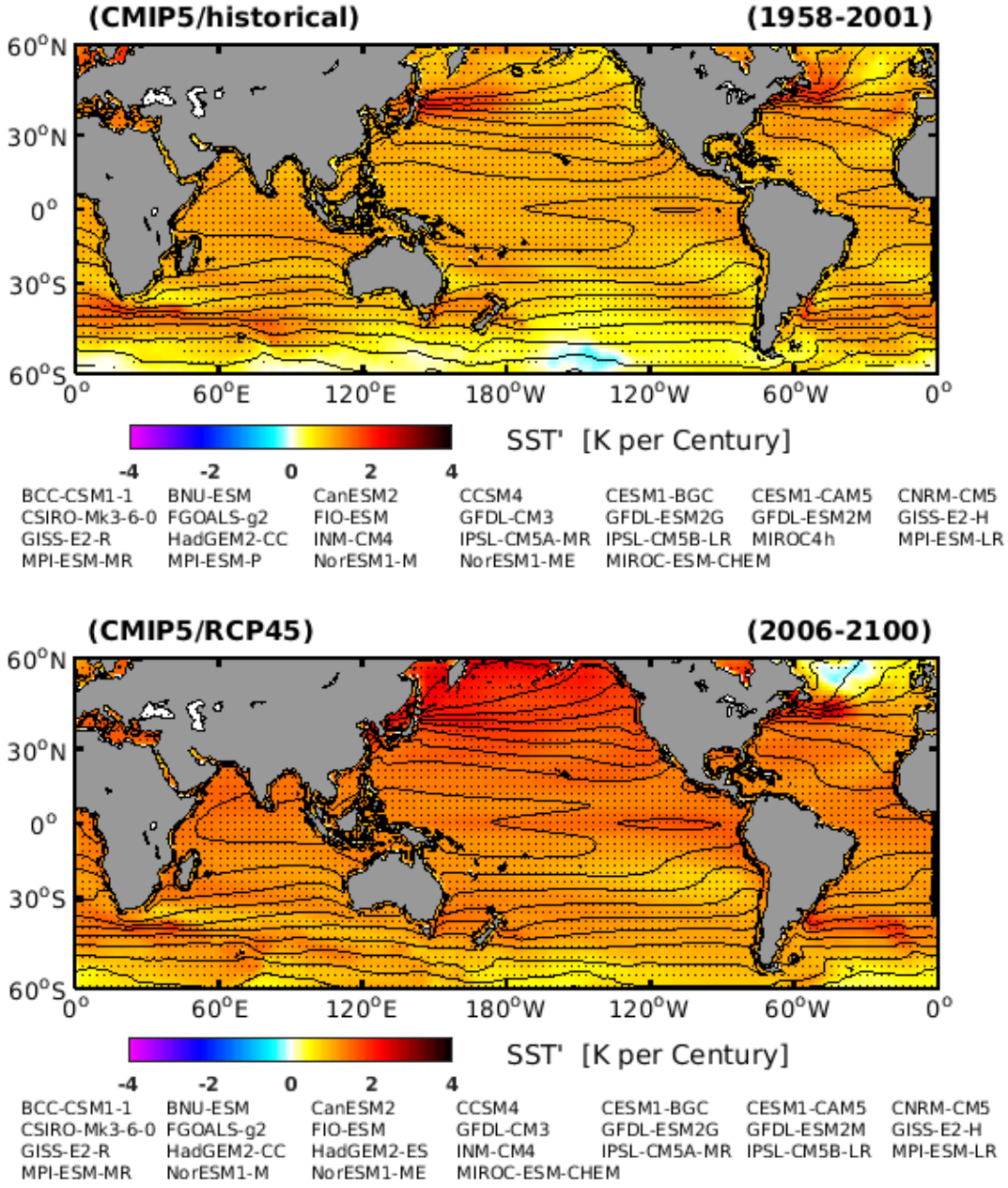

Fig. 3.10: *Multi-model ensemble trends in SST (shading) based on the CMIP5/historical and CMIP5/RCP4.5 simulations. Black contours present climatological SST. The models used to estimate the ensemble values are listed below each panel. Stippling indicates areas where at least 2/3 of the models agree on the sign of the trends.*

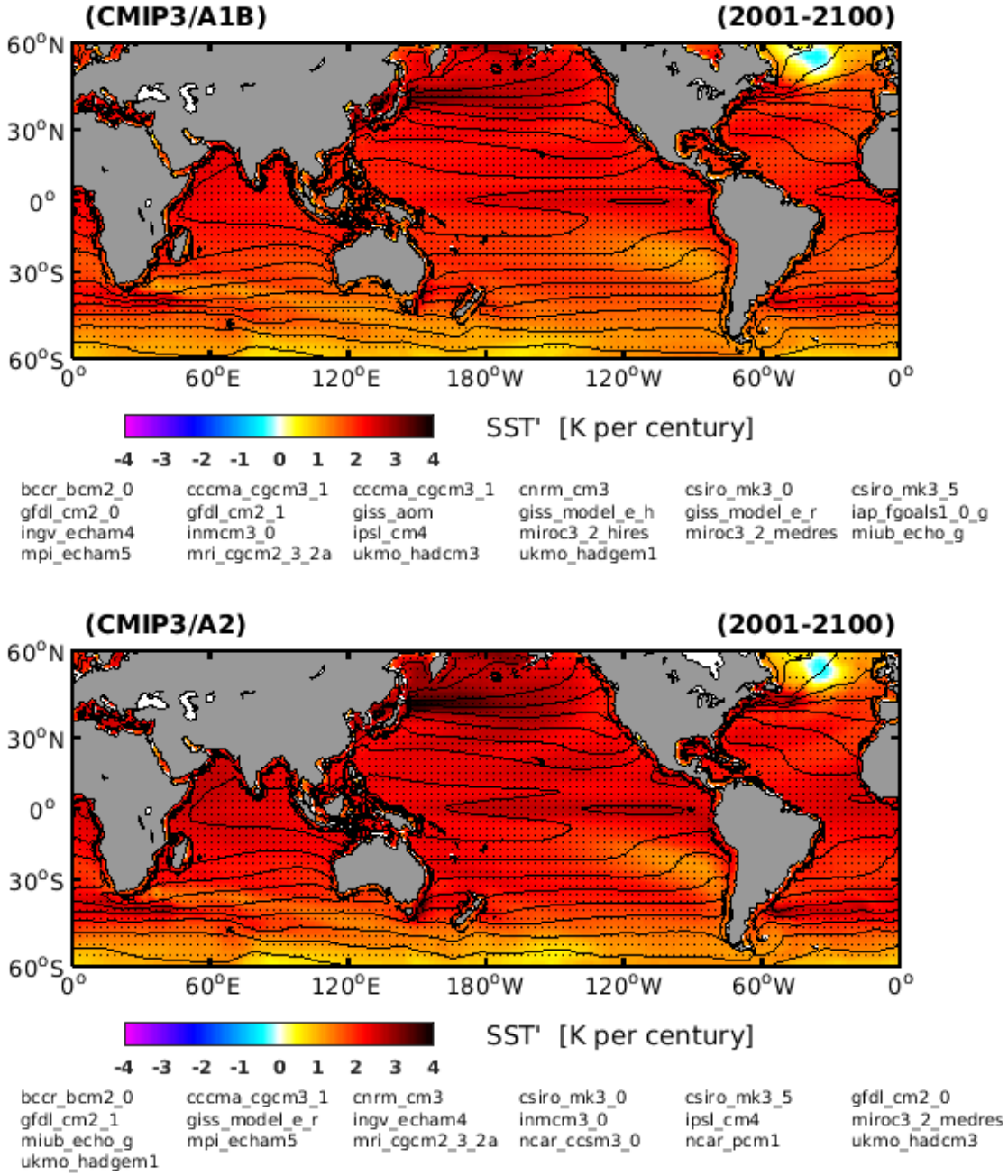

Fig. 3.11: *Multi-model ensemble trends in SST (shading) based on the CMIP3/A1B and CMIP3/A2 simulations. Black contours present climatological SST. The models used to estimate the ensemble values are listed below each panel. Stippling indicates areas where at least 2/3 of the models agree on the sign of the trends.*

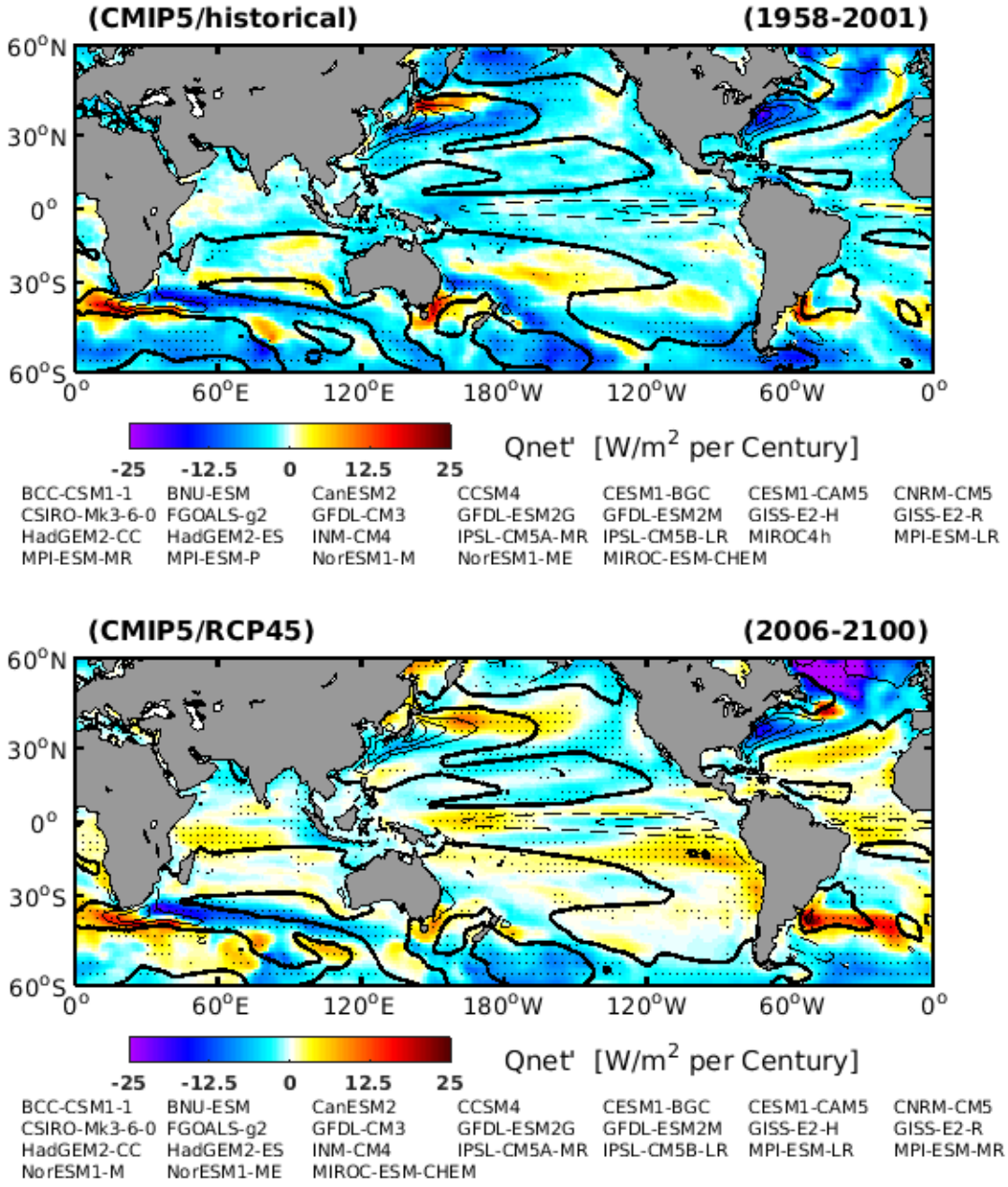

Fig. 3.12: *Multi-model ensemble trends in Q_{net} (shading) based on the $CMIP5/historical$ and $CMIP5/RCP4.5$ simulations. Black contours present climatological Q_{net}. Upward Q_{net} is in solid lines; downward Q_{net} is in dashed lines; zero Q_{net} is in bold lines. The models used to estimate the ensemble values are listed below each panel. Stippling indicates areas where at least 2/3 of the models agree on the sign of the trends.*

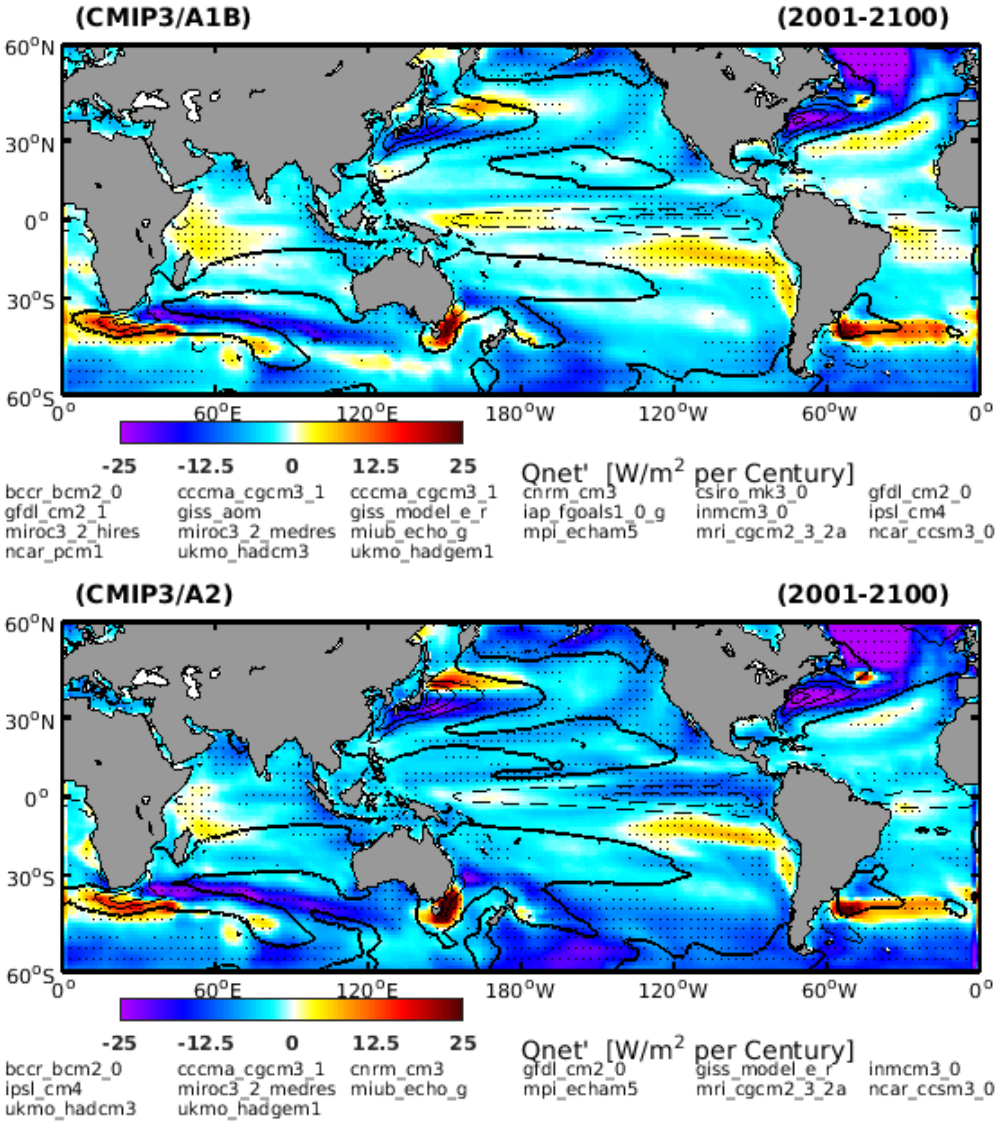

Fig. 3.13: *Multi-model ensemble trends in Q_{net} (shading) based on the CMIP3/A1B and CMIP3/A2 simulations. Black contours present climatological Q_{net}. Upward Q_{net} is in solid lines; downward Q_{net} is in dashed lines; zero Q_{net} is in bold lines. The models used to estimate the ensemble values are listed below each panel. Stippling indicates areas where at least 2/3 of the models agree on the sign of the trends.*

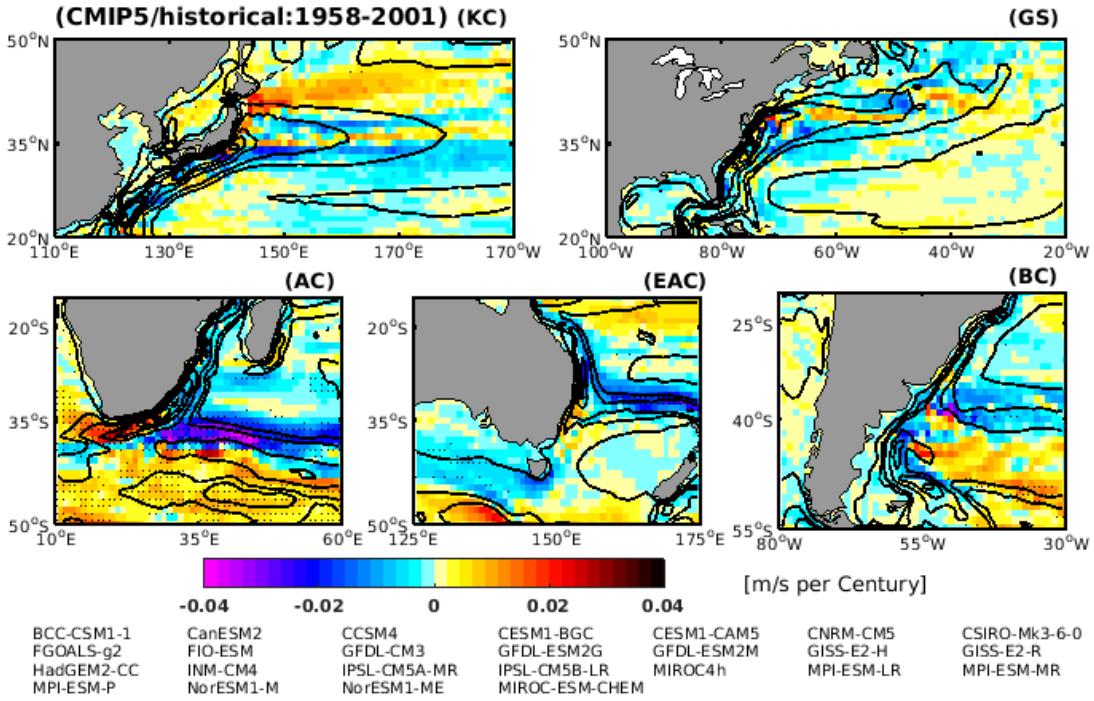

Fig. 3.14: *Multi-model ensemble trends in upper 100 m ocean velocity (shading) based on the CMIP5/historical simulations. Contours: climatological depth-averaged (upper 100 m) sea water velocity. The models used to estimate the ensemble values are listed in the low part of the corresponding panels. Stippling indicates areas where at least 2/3 of the models agree on the sign of the trends.*

Gulf Stream, with reducing Q_{net} and decreasing ocean velocity (Figs. 3.10- 3.17).

We notice that the ensemble results in the *historical* simulations are less pronounced compared to the future simulations, because the global warming signal in the *historical* simulations is not beyond the model internal variability.

To further validate how the WBCs response to global warming in the climate models, we perform the results from CMIP3. The ensemble results show similar patterns as that in the *RCP*4.5 projection, indicating that the results found here are not scenario dependent. Moreover, the consistency between ocean surface heat flux change and ocean velocity change in the climate models demonstrates that the method applied here (using Q_{net} to identify the WBCs dynamic change) is appropriate.

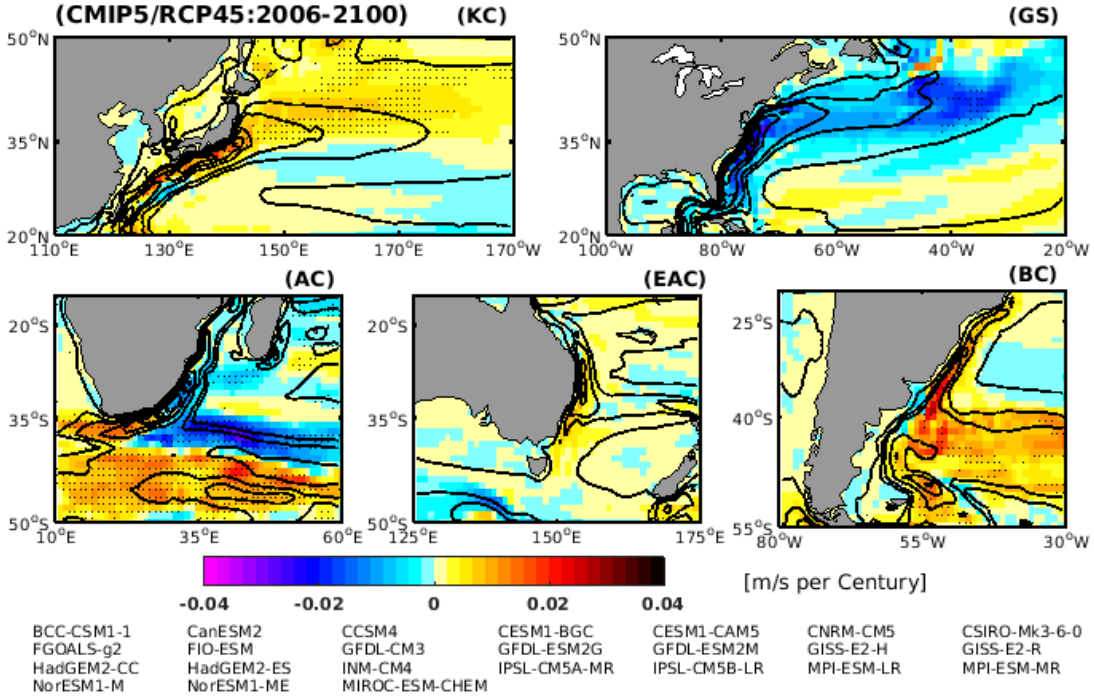

Fig. 3.15: *Multi-model ensemble trends in upper 100 m ocean velocity (shading) based on the CMIP5/RCP4.5 simulations. Contours: climatological depth-averaged (upper 100 m) sea water velocity. The models used to estimate the ensemble values are listed in the low part of the corresponding panels. Stippling indicates areas where at least 2/3 of the models agree on the sign of the trends.*

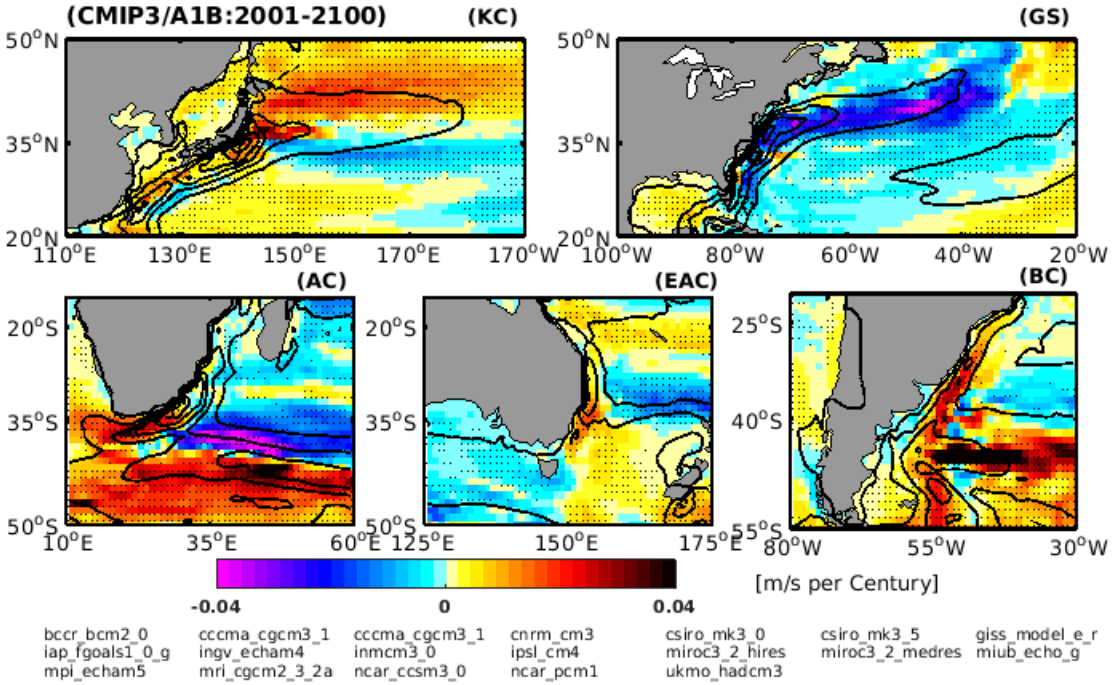

Fig. 3.16: *Multi-model ensemble trends in upper 100 m ocean velocity (shading) based on the CMIP3/A1B simulations. Contours: climatological depth-averaged (upper 100 m) sea water velocity. The models used to estimate the ensemble values are listed in the low part of the corresponding panels. Stippling indicates areas where at least 2/3 of the models agree on the sign of the trends.*

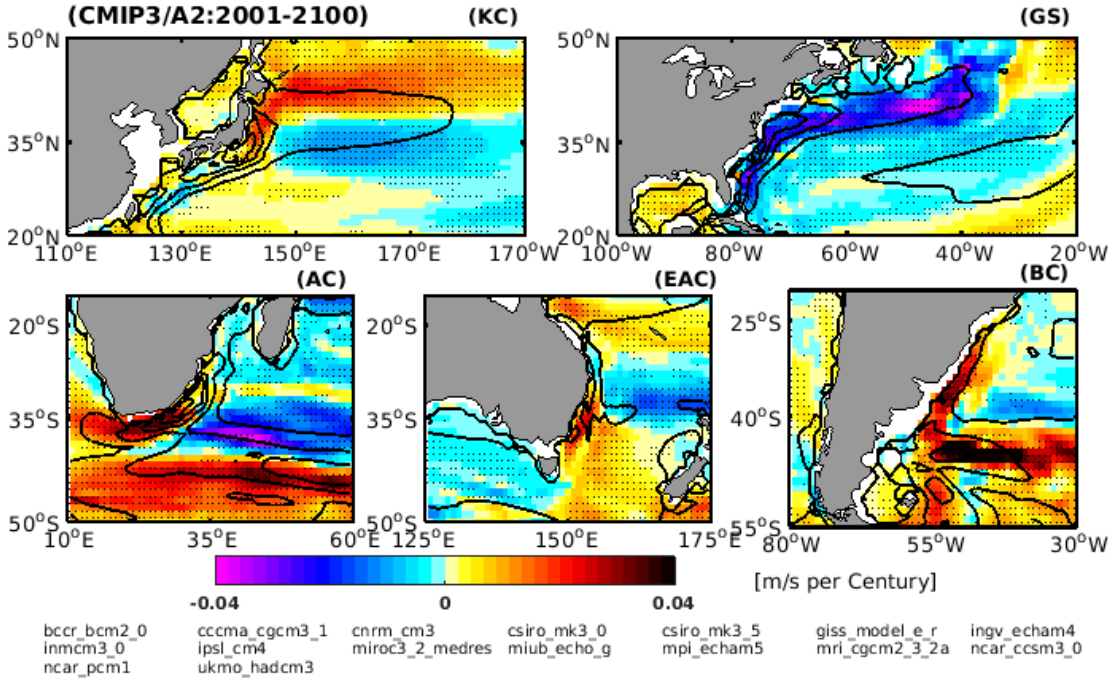

Fig. 3.17: *Multi-model ensemble trends in upper 100 m ocean velocity (shading) based on the CMIP3/A2 simulations. Contours: climatological depth-averaged (upper 100 m) sea water velocity. The models used to estimate the ensemble values are listed in the low part of the corresponding panels. Stippling indicates areas where at least 2/3 of the models agree on the sign of the trends.*

3.3 Possible mechanism

The easterly winds over low latitudes, associated with the westerly winds over high latitudes, largely drive the anti-cyclonic subtropical ocean gyres, which show an intensification over the western boundary (Fig. 3.1) [*Pedlosky*, 1996]. Significant dynamic changes of WBCs hint that the near-surface ocean zonal wind may have changed.

Figs. 3.18- 3.22 show the trends of the near-surface ocean zonal winds in the observational data sets and CMIP3/5 simulations, respectively. Over the Southern Hemisphere, the wind trends over the mid and high latitudes are dominated by stronger westerly winds. Meanwhile, stronger easterly winds are found over most of the subtropical regions. Such trends reinforce the background zonal winds. As a consequence, the wind shear between the low and the high latitudes (wind stress curl) becomes stronger, which can force stronger WBCs in a warming climate. Besides the intensification of the zonal wind, all data sets consistently show that the zonal mean winds are shifting towards the South Pole in comparison with their climatology profile (Figs. 3.18- 3.22, right-side). Such shifts show dynamic consistency with the poleward shift of the Southern Hemisphere WBCs.

Over the North Atlantic Ocean, all the data sets consistently show a stronger and poleward shift of zonal wind. However, over North Pacific Ocean, some discrepancies appear between the observations (1958-2001) and climate models. Both atmospheric reanalysis present a stronger and equatorward shift of the North Pacific westerlies during 1958-2001, which contribute to a stronger and equatorward shift of the Kuroshio Current, (section 3.2.1). In contrast, the CMIP3/5 models simulate stronger and poleward shift of the North Pacific westerlies, forcing a stronger and poleward shift of the Kuroshio Current, as identified in Section 3.2.2. To explore the reason for the differences over Northern Pacific, we present the long-term (1900-2010) trends of surface wind based on the century long reanalysis (Fig. 3.22). Both 20CRv2 and ERA-20C consistently presents a stronger and poleward shift of the Northern Pacific westerly, indicating the observed equatorward shift during 1958-2001 are attribute to internal variability, as also shown in Fig. 3.2. Associated with the near-surface wind, the SLP trends are displayed in Figs. 3.23- 3.27, respectively. Both the observations as well as the CMIP3/5 models consistently show a decreasing SLP over the Poles and increasing

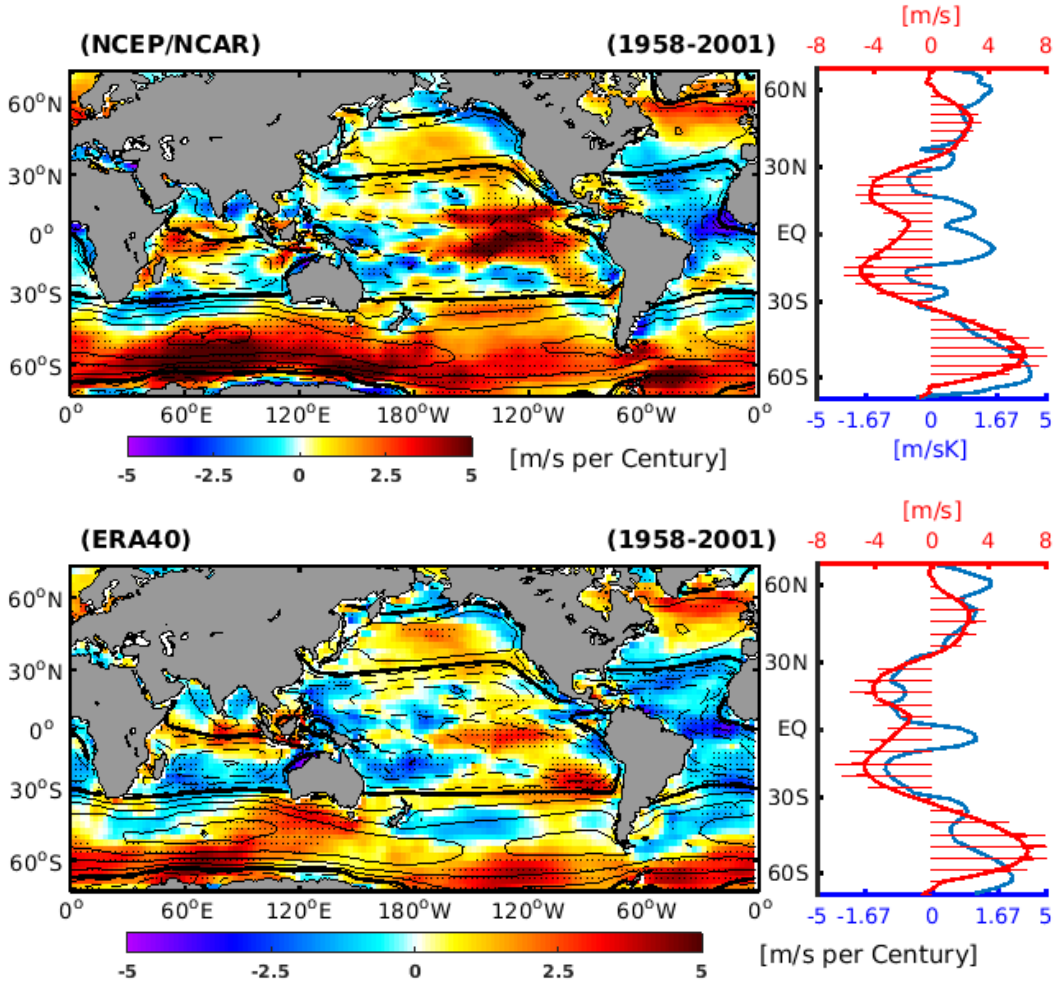

Fig. 3.18: *Left: Trends (shaded) and climatology (contours) near-surface ocean zonal wind. Easterly winds are in solid lines; westerly winds are in dashed lines; zero zonal winds are bold. Stippling indicates regions where the trends pass the 95% confidence level (Student's t-test). Right: Zonally averaged trend (blue) and climatology (red with arrow) of near-surface ocean zonal winds. Results are based on the NCEP/NCAP and ERA40 atmospheric reanalyses.*

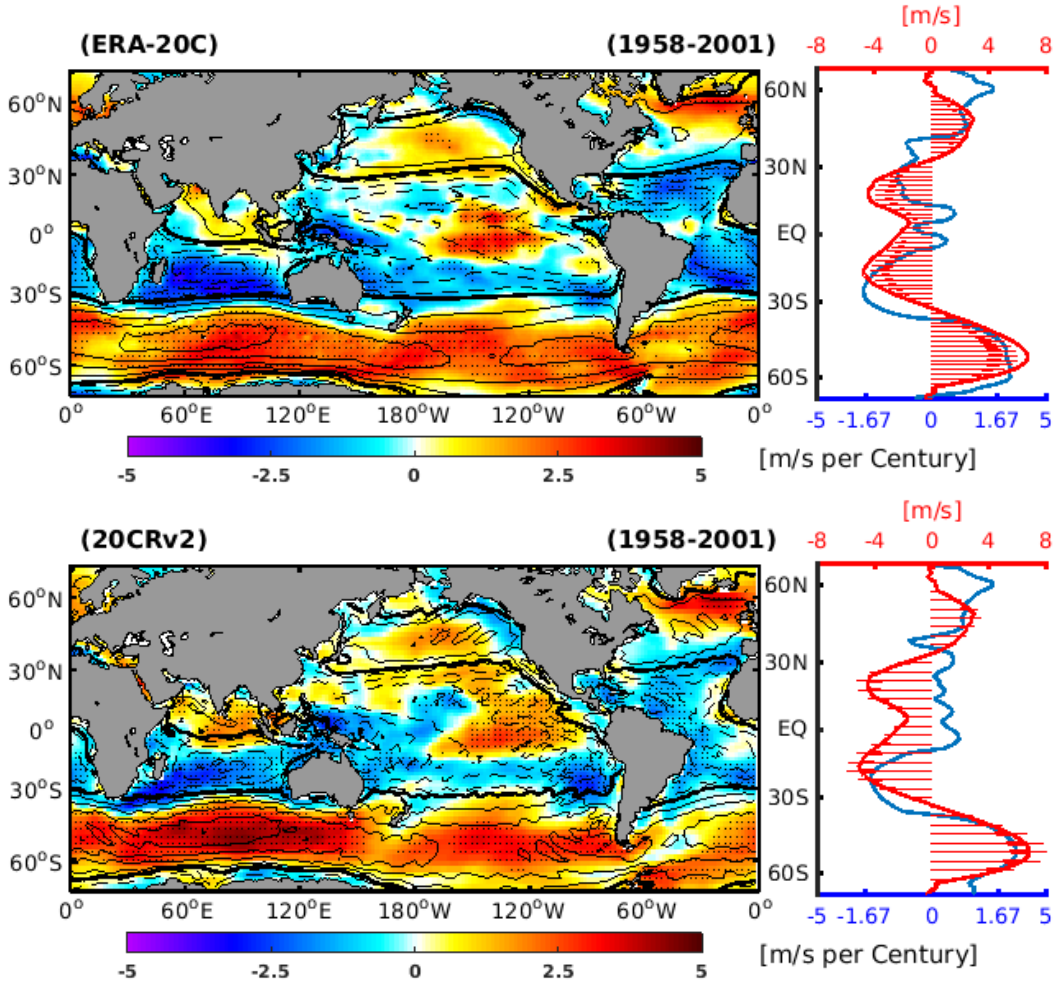

Fig. 3.19: *Left: Trends (shaded) and climatology (contours) near-surface ocean zonal wind. Easterly winds are in solid lines; westerly winds are in dashed lines; zero zonal winds are bold. Stippling indicates regions where the trends pass the 95% confidence level (Student's t-test). Right: Zonally averaged trend (blue) and climatology (red with arrow) of near-surface ocean zonal winds. Results are based on the ERA20c and 20CRv2 atmospheric reanalyses.*

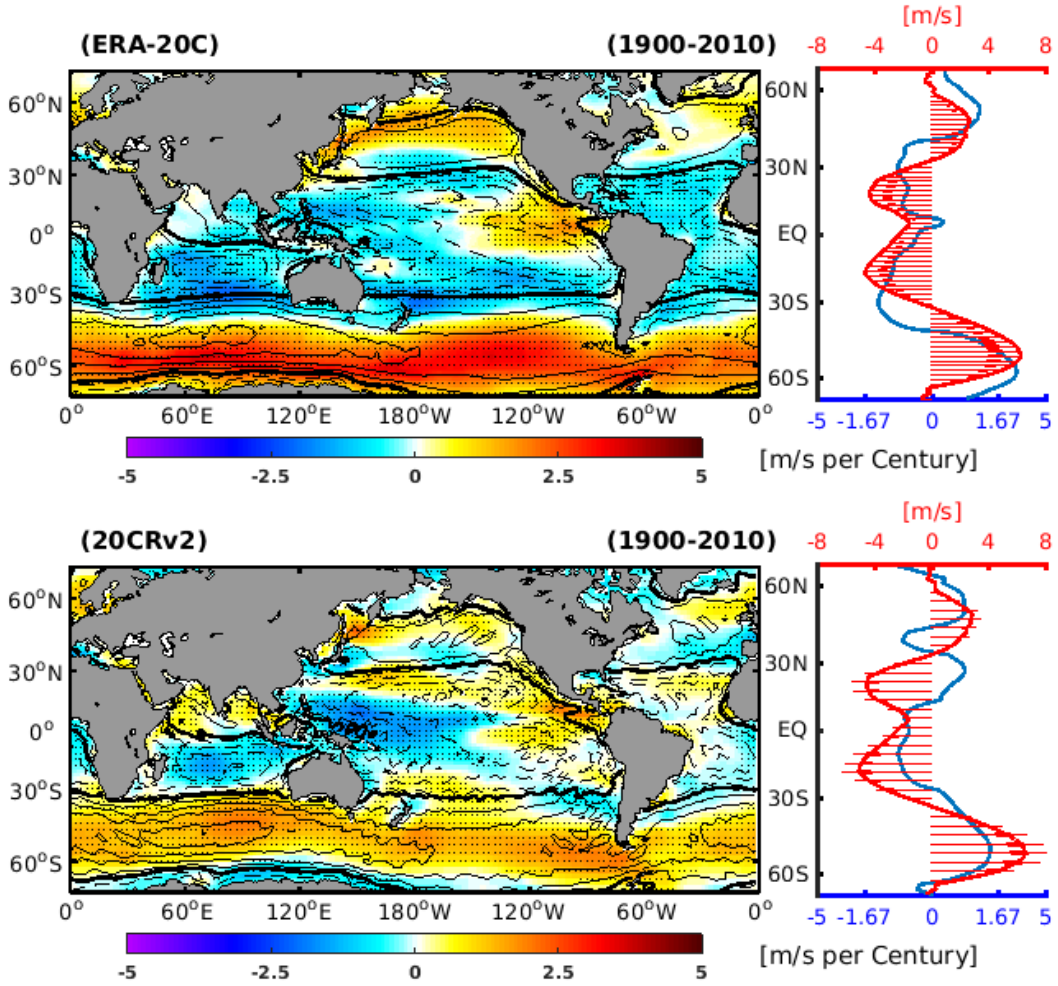

Fig. 3.20: *Left: Trends (shaded) and climatology (contours) near-surface ocean zonal wind. Easterly winds are in solid lines; westerly winds are in dashed lines; zero zonal winds are bold. Stippling indicates regions where the trends pass the 95% confidence level (Student's t-test). Right: Zonally averaged trend (blue) and climatology (red with arrow) of near-surface ocean zonal winds. Results are based on the ERA20c and 20CRv2 atmospheric reanalyses.*

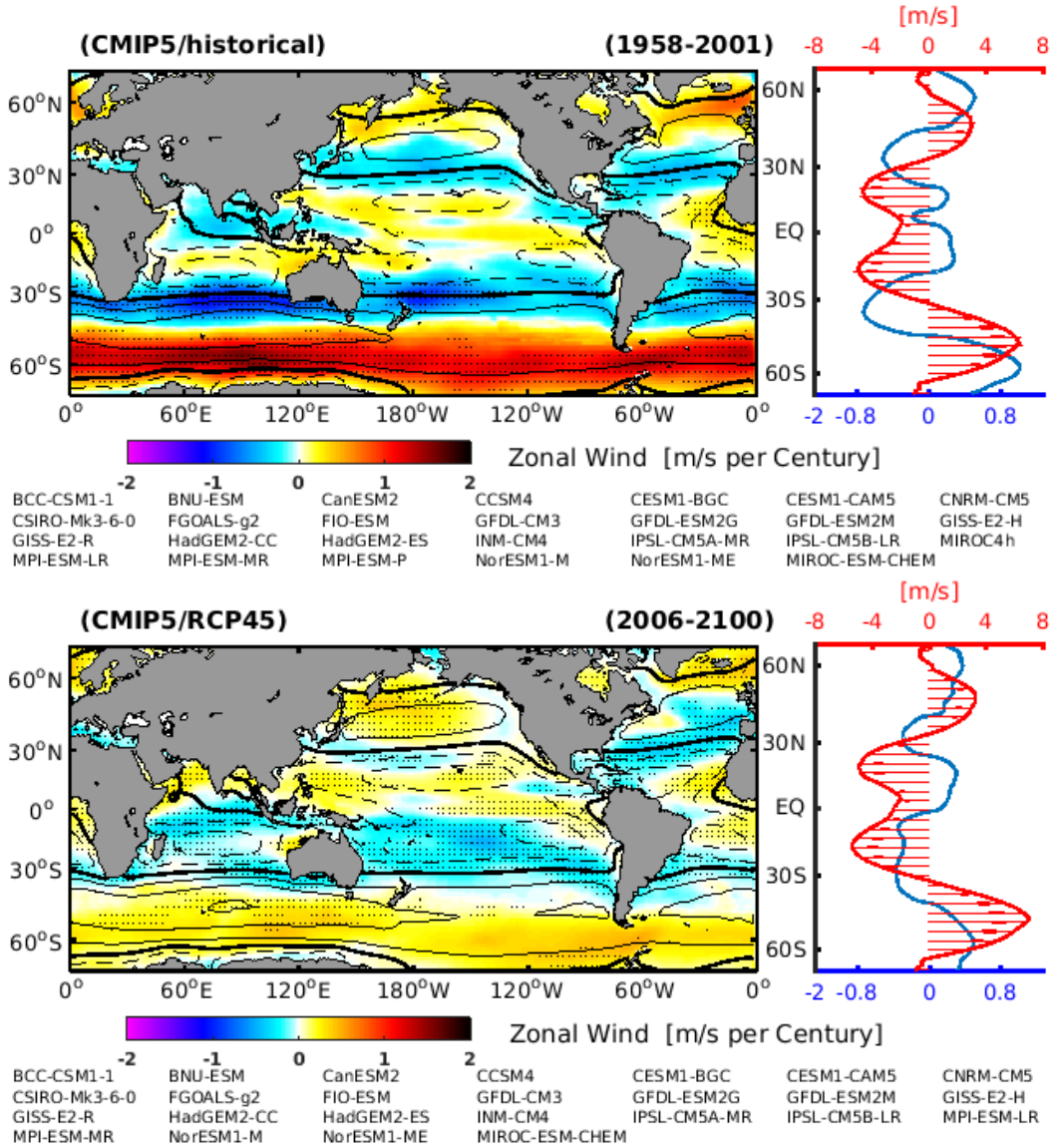

Fig. 3.21: *Left: Multi-model ensemble trends (shaded) and climatology (contours) near-surface ocean zonal wind. Easterly winds are in solid lines; westerly winds are in dashed lines; zero zonal winds are bold. Stippling indicates areas where at least 2/3 of the models agree on the sign of the trends. Right: Zonally averaged trend (blue) and climatology (red with arrow) of near-surface ocean zonal winds. Results are based on the CMIP5/historical and CMIP5/RCP4.5 simulations. The models used to estimate the ensemble values are listed below each panel.*

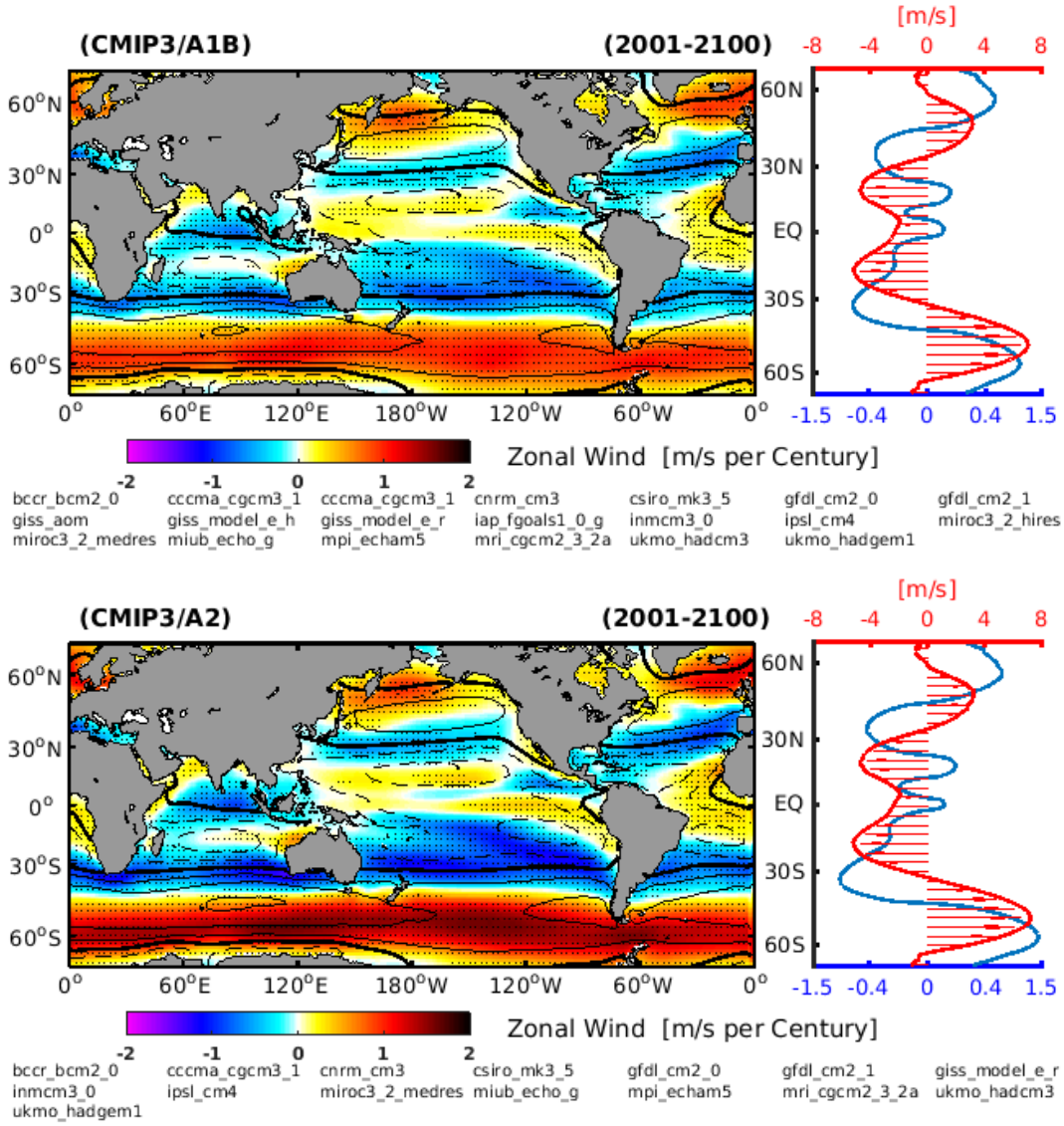

Fig. 3.22: *Left: Multi-model ensemble trends (shaded) and climatology (contours) near-surface ocean zonal wind. Easterly winds are in solid lines; westerly winds are in dashed lines; zero zonal winds are bold. Stippling indicates areas where at least 2/3 of the models agree on the sign of the trends. Right: Zonally averaged trend (blue) and climatology (red with arrow) of near-surface ocean zonal winds. Results are based on the CMIP3/A1B and CMIP3/A2 simulations. The models used to estimate the ensemble values are listed below each panel.*

SLP over mid latitudes of both Hemispheres.

The near-surface ocean zonal wind and SLP show similar features as the positive phase of the annular modes (Northern Annular Mode and Southern Annular Mode), which are characterized by stronger and poleward shifts of the westerly winds, associated with negative SLP anomalies over high latitudes and positive SLP anomalies over mid latitudes. We propose that the positive annular mode-like trends contribute to the intensification of the near-surface ocean zonal winds and to shift them poleward. The changing winds force a strengthening and poleward displacement of the WBCs. As a result, more heat is transported from the tropics to the mid and high latitudes, which could significantly increase the SST and ocean heat loss (Q_{net}) there. Moreover, as the routes of the WBCs are shifting poleward, the position of the high Q_{net} over the WBCs will also shift poleward.

3.4 Discussion

We explore the dynamic changes of WBCs by utilization of multi-type data resources. Over the Southern Hemisphere, observational data and climate models consistently reveal strengthening and poleward shift of the Southern Hemisphere WBCs in a warming climate.

Over the Northern Pacific Ocean, observations (climate models) record an equatorward (poleward) shift of the Kuroshio Current over the period 1958-2001. *Seager et al.* [2001]; *Taguchi et al.* [2007]; *Sasaki and Schneider* [2011] demonstrated that the 1976/77 equatorward shift in basin-scale winds contributed to the decadal equatorward shift of the Kuroshio Current. Similarly, we have also identified that the equatorward shift of Kuroshio Current is consistent with the wind shift over the same time frame. However, from a long term perspective (1900-2010), both 20CRv2 and ERA-20C present a poleward shift of surface wind over the Pacific Ocean, indicating the observed equatorward shift of Kuroshio Current over the period 1958-2001 is likely to be due to natural climate variations.

Over the North Atlantic Ocean, the observations during 1958-2001 present a stronger and poleward shift of the Gulf Stream (consistent with the surface wind), while the climate models show a weakening of the Gulf Stream in response to global warming.

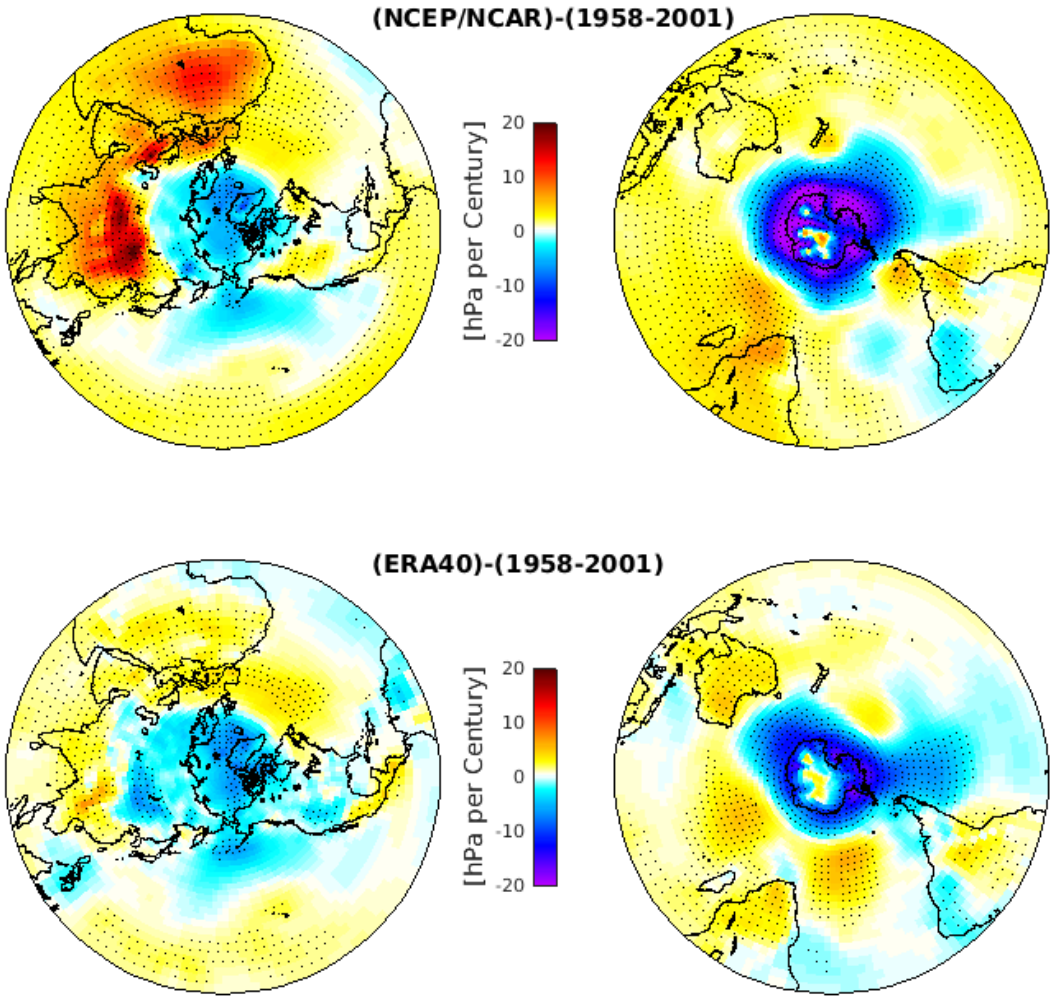

Fig. 3.23: *Trends in SLP based on the NCEP/NCAR and ERA40 data sets, respectively. Stippling indicates regions where the trends pass the 95% confidence level (Student's t-test).*

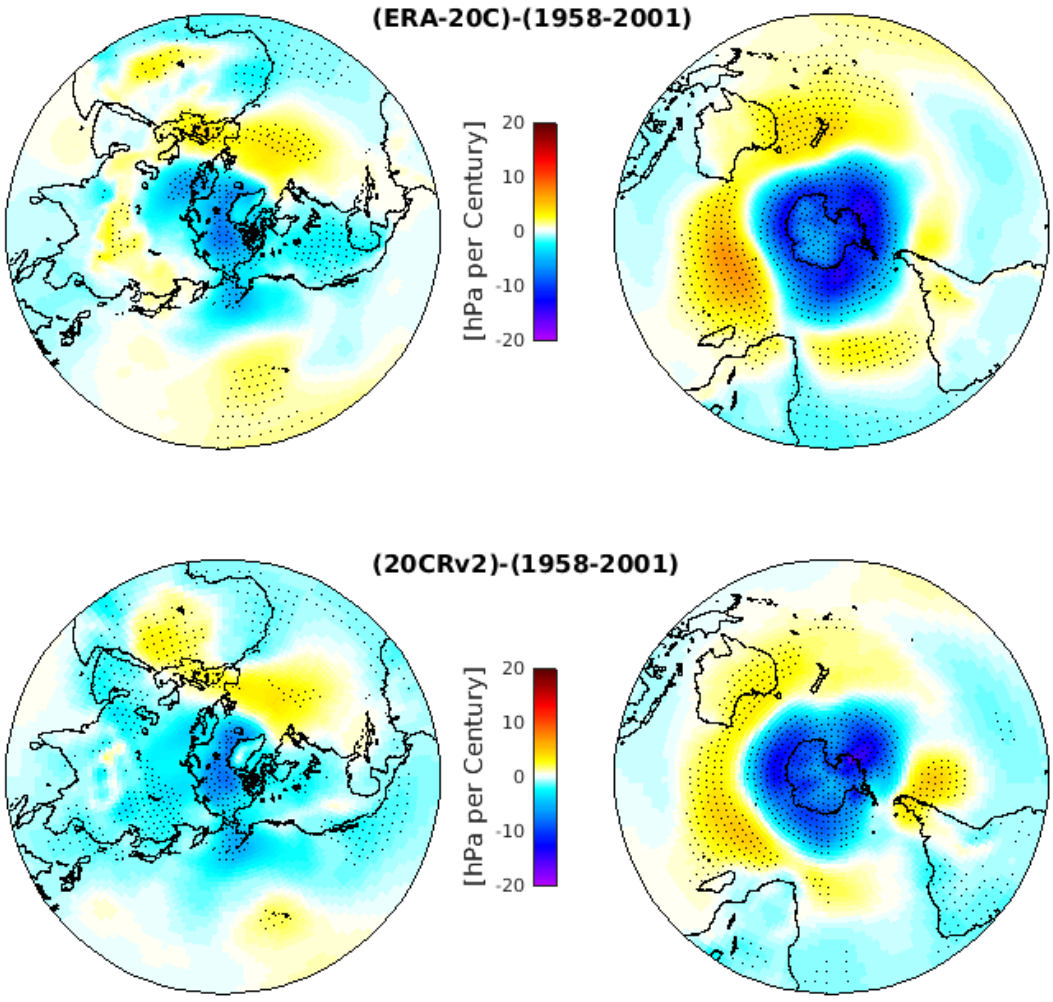

Fig. 3.24: *Trends in SLP based on the ERA20C and 20CRv2 data sets, respectively. Stippling indicates regions where the trends pass the 95% confidence level (Student's t-test).*

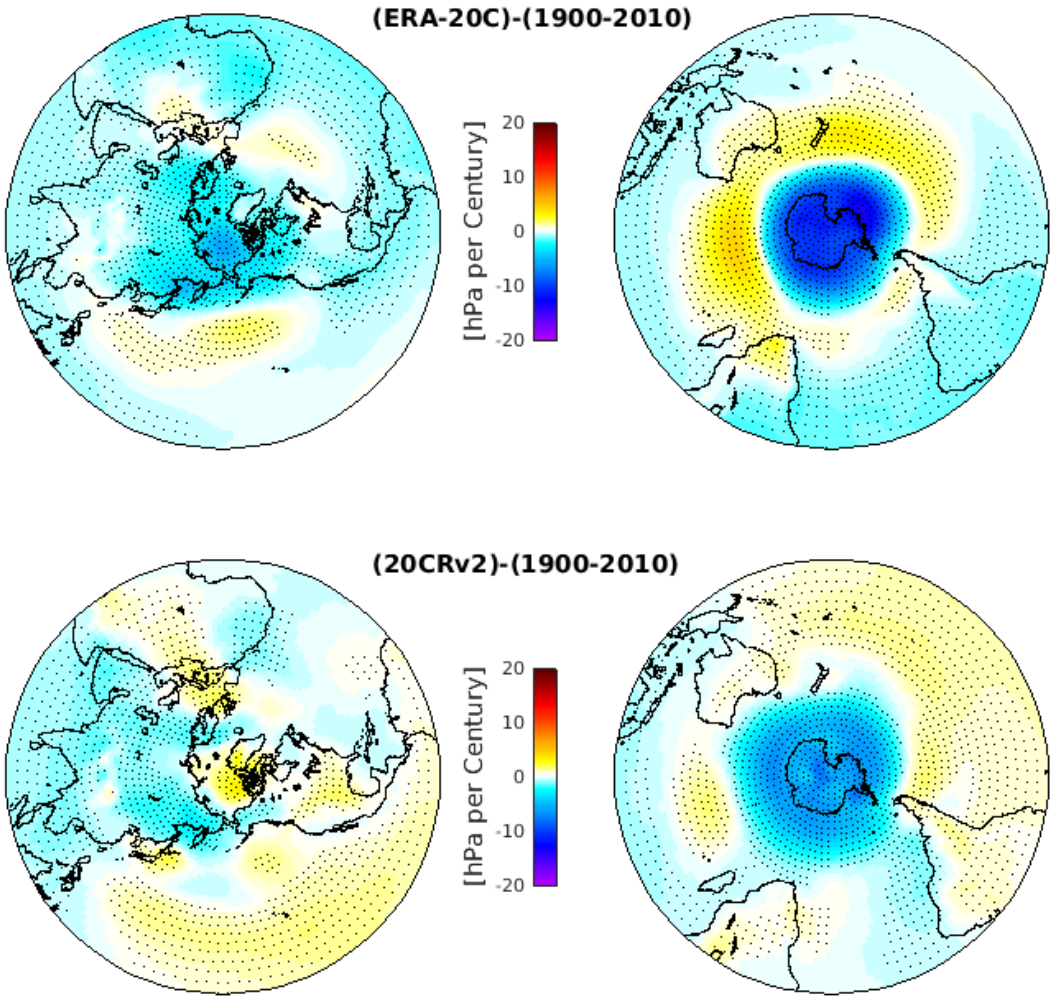

Fig. 3.25: *Trends in SLP based on the ERA20C and 20CRv2 data sets, respectively. Stippling indicates regions where the trends pass the 95% confidence level (Student's t-test).*

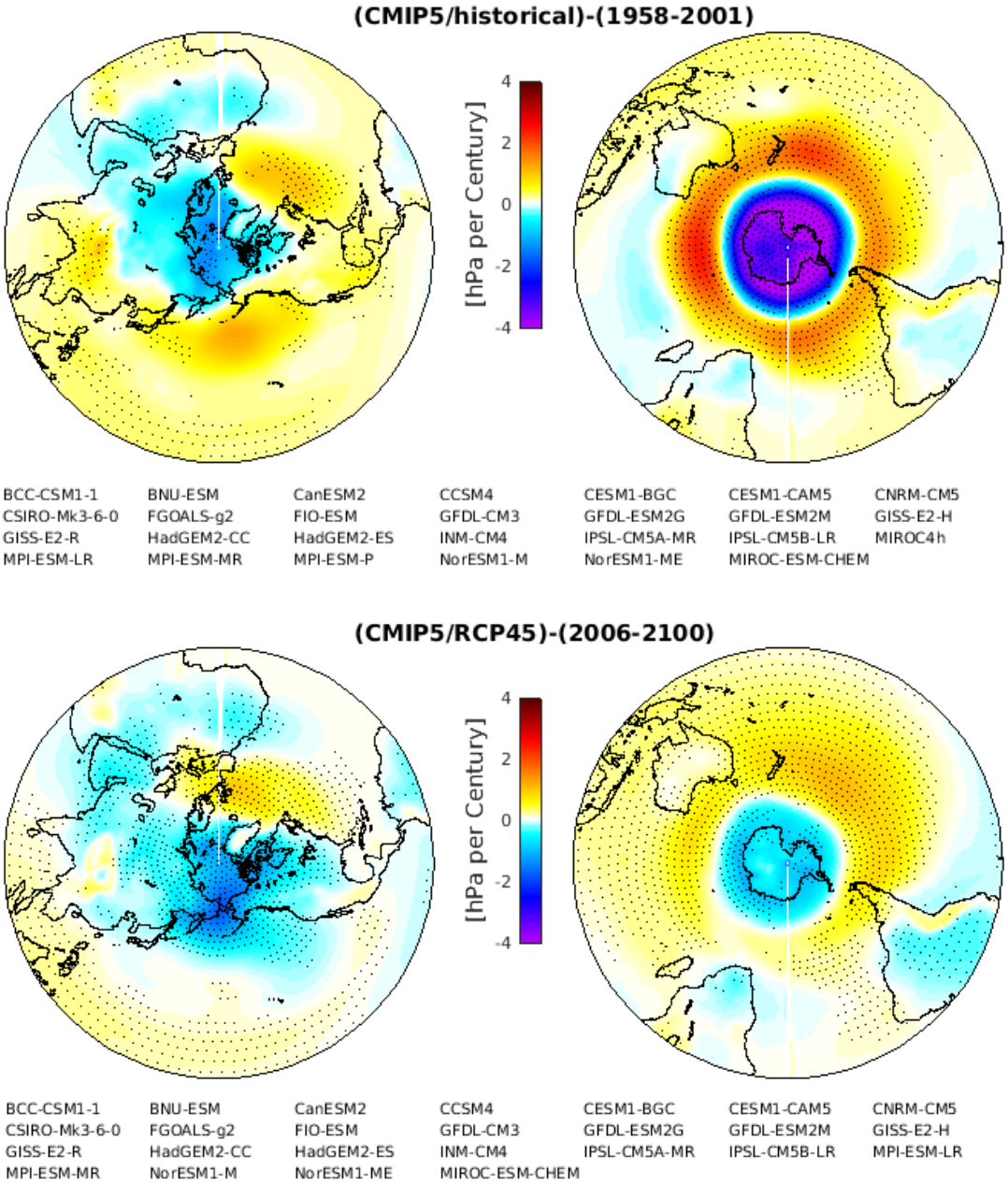

Fig. 3.26: *Multi-model ensemble trends in SLP based on the CMIP5/historical and CMIP5/RCP4.5 simulations. The models used to estimate the ensemble values are listed below each panel. Stippling indicates areas where at least 2/3 of the models agree on the sign of the trends.*

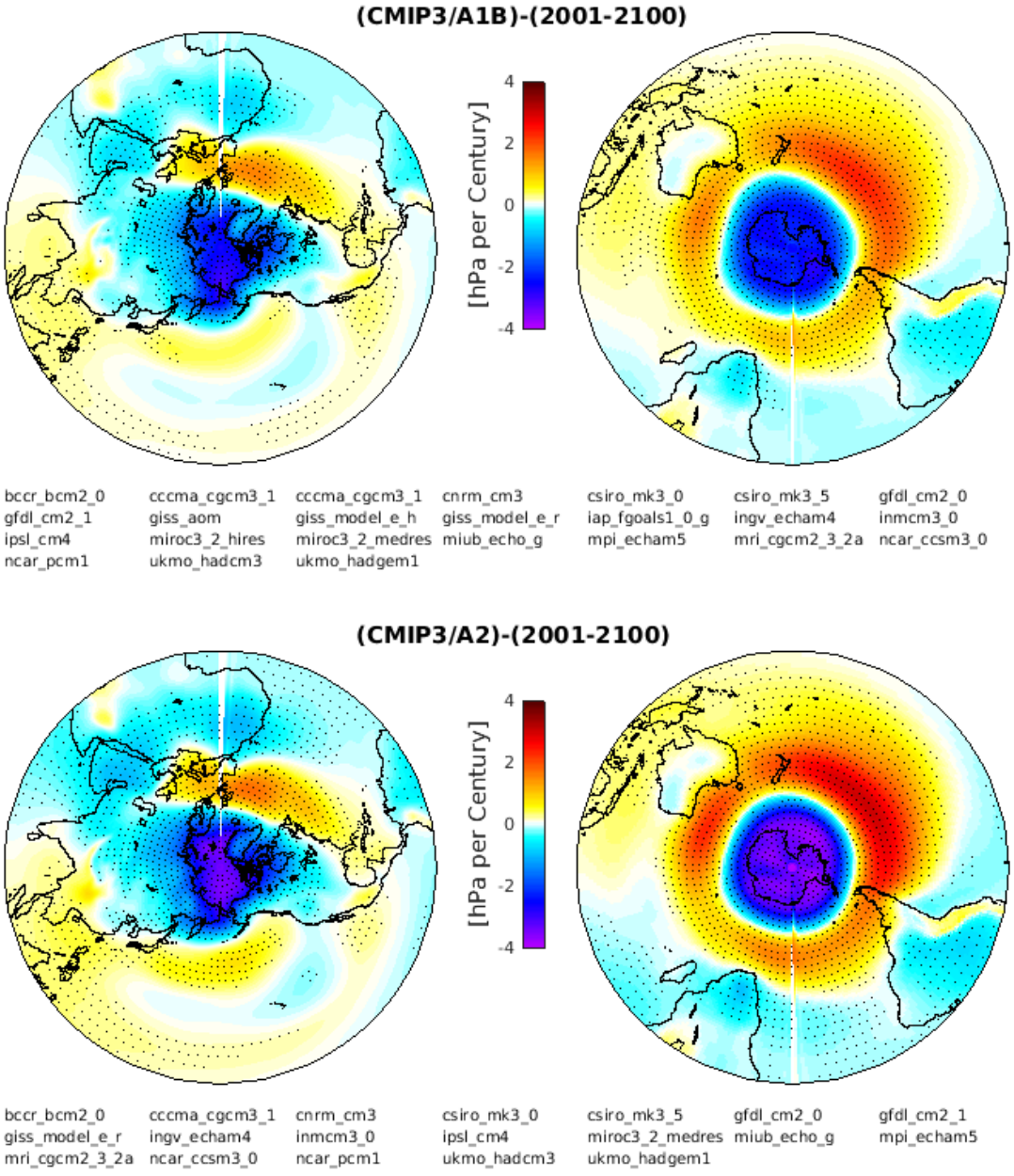

Fig. 3.27: *Multi-model ensemble trends in SLP based on the CMIP5/A1B and CMIP3/A2 simulations. The models used to estimate the ensemble values are listed below each panel. Stippling indicates areas where at least 2/3 of the models agree on the sign of the trends.*

The Gulf Stream is part of the upper branch of the Atlantic Meridional Overturning Circulation (AMOC). Strength of the Gulf Stream is determined not only by the near-surface ocean wind, but also by the AMOC, particularly on multi-decadal and centennial time scales. The simulated weakening of AMOC [e.g., *Lohmann et al.*, 2008; *Cheng et al.*, 2013] is linked to the weakening Gulf Stream.

It is a common problem to distinguish the natural climate variability and the climate trend if the observational record is too short. As shown in Fig. 3.2, both SST indices of the Gulf Stream and the Kuroshio Currents have strong decadal variations. The trend estimations in this period are most likely to capture the phase changes of their decadal natural variability. Continuous long term observations are required to further validate our hypothesis.

Regarding the potential driving mechanism, several previous studies have focused on the climate change over individual WBCs. *Sakamoto et al.* [2005] have investigated the responses of the Kuroshio Current to global warming and suggested that a strengthening of the Kuroshio Current is caused by an El Niño-like mode. Indeed, the climate phenomenon over the Pacific Ocean (i.e., ENSO, PDO) plays a vital role in the variability of the Kuroshio Current, particularly on interannual to decadal time scales [*Qiu*, 2003; *Qiu and Chen*, 2005; *Taguchi et al.*, 2007; *Andres et al.*, 2009; *Sasaki and Schneider*, 2011]. However, we found that the common features of WBCs changes are characterized by an intensification and a poleward shift. Such changes are not an isolated phenomenon over individual ocean basins, but a global effect. Thus, the dynamic changes of the WBCs should be caused by a factor that can influence all ocean basins, such as we proposed, the positive annular mode-like trends over both hemispheres. *Sato et al.* [2006] demonstrated that the Arctic Oscillation-like trends are responses to a northward shift of the subtropical wind-driven gyre in the North Pacific Ocean. *Curry and McCartney* [2001] proved that the transport of the Gulf Stream has intensified due to a stronger North Atlantic Oscillation after the 1960s. Their conclusions are in agreement with our study, because the North Atlantic Oscillation and the Arctic Oscillation (or Northern Annular Mode) show very similar evolutions [*Deser*, 2000; *Rogers and McHugh*, 2002; *Feldstein and Franzke*, 2006]. Modelling studies have also confirmed that the Southern Annular Mode has an impact on the Southern Hemisphere subtropical gyres [*Hall and Visbeck*, 2002; *Cai et al.*, 2005; *Sen Gupta and England*, 2006; *Cai*, 2006; *Fyfe and*

Saenko, 2006; *Sen Gupta et al.*, 2009].

The typical features of the annular modes in the wind field are characterized by an intensification and poleward shift of the westerly winds [*Thompson and Wallace*, 2000]. Here, we suggest that both the easterly winds over the low latitudes and the westerly winds over the mid and high latitudes have strengthened. Meanwhile, the profile of the zonal winds is shifting poleward over both hemispheres. The systematic changes in zonal winds are consistent with several other climate trends, such as the poleward shift of the Hadley Cell [*Hu and Fu*, 2007; *Lu et al.*, 2007; *Johanson and Fu*, 2009], the expansion of the tropical belt [*Santer et al.*, 2003; *Seidel and Randel*, 2007; *Seidel et al.*, 2007; *Fu and Lin*, 2011], and the poleward shift of the subtropical dry zones [*Previdi and Liepert*, 2007].

Over the Southern Hemisphere, both observations [*Thompson and Wallace*, 2000; *Marshall*, 2003] and CGCM simulations [*Fyfe et al.*, 1999; *Stone et al.*, 2001; *Kushner et al.*, 2001; *Cai et al.*, 2003; *Gillett and Thompson*, 2003; *Rauthe et al.*, 2004; *Arblaster and Meehl*, 2006; *Gillett and Fyfe*, 2013] show that the Southern Annular Mode is entering a positive phase. The ozone depletion was suggested to be the main driver for the observed positive trend of SAM [*Thompson and Solomon*, 2002; *Kindem and Christiansen*, 2001; *Sexton*, 2001; *Gillett and Thompson*, 2003; *Thompson et al.*, 2011; *Polvani et al.*, 2011]. However, increasing greenhouse gases were also suggested to have a contribution on it [*Fyfe et al.*, 1999; *Kushner et al.*, 2001; *Cai et al.*, 2003; *Rauthe et al.*, 2004]. As it is shown in Fig. 3.19 and 3.20, stronger SAM trend is presented during 1958-2001 when both the ozone depletion and the increasing green house gas force the SAM. However, in the near future, as ozone levels recover, it will play an oppose role as increasing green house gas. The positive trend in SAM might be weaker or reverse sign over the coming decades [*Arblaster et al.*, 2011].

Over the Northern Hemisphere, observations show a stronger Northern Annular Mode during the past several decades. However, a weaker Northern Annular Mode from the late 1990s is observed [*Thompson and Wallace*, 2000] simultaneously with the global warming hiatus [*Easterling and Wehner*, 2009]. Also, the positive trend of the Northern Annular Mode is not as robust as the Southern Annular Mode in the model simulations (Fig. 3.21), suggesting that the Northern Annular Mode have strong natural variations. Several factors are suggested having impact on the variations of NAM. For example,

the greenhouse gases, the stratosphere-troposphere interaction, local sea ice variability and remote tropical influence [*Fyfe et al.*, 1999; *Wang and Chen*, 2010; *Gillett and Fyfe*, 2013; *Cattiaux and Cassou*, 2013]. The trend in Northern Annular Mode during 1958-2001 is most likely dominated by its natural variations. However, for a longer time period, both the century-long atmosphere reanalysis (i.e., 20CRv2 and ERA-20C) and the CMIP3/CMIP5 climate models illustrate that the Northern Annular Mode is propagating to a positive phase under global warming.

Wu et al. [2012] investigated the WBCs dynamic changes based on two century-long reanalysis data sets, the 20CRv2 and the Simple Ocean Data Assimilation (SODA) [*Giese and Ray*, 2011]. However, the detection of the WBCs dynamics changes is challenging due to limited observations and the uncertainties in the data sets [*Wu et al.*, 2012; *Stocker et al.*, 2013]. To further explore this, we use more independent data sets and more metrics to identify and explain the dynamic changes of WBCs. The common features among these broad ranges of data resources indicate that the WBCs (except the Gulf Stream) are strengthening and shifting towards the poles in a warming climate. We note that the strengthening of the WBCs occurs at the same time as the poleward shifting if the surface wind do not have severe shift to the poles. Correspondingly, if the winds have strong shift to the poles, the primary feature of WBCs dynamic changes is characterized by a poleward shift. The original equatorial flanks of WBCs will experience a weakening. Such effect is notable for the Agulhas Current (Fig. 3.14, 3.15, 3.16 and 3.17).

3.5 Conclusions for this chapter

We find observational and model support for an intensification and poleward movement of WBCs in response to anthropogenic climate change. The one exception to this is the Gulf Stream where a weakening of the AMOC tends to reduce the strength of the Gulf Stream. Elsewhere the poleward shift is postulated to be driven by a poleward shift of the extratropical westerlies and expansion of the Hadley Cell. In the Southern Hemisphere the observed record indicates this intensification and southward shift is already occurring perhaps because ozone depletion and rising greenhouse gas have worked in the same direction in forcing a positive SAM. In the Northern Hemisphere

natural variability appears to be temporarily interrupting the poleward shift of the Kuroshio and have driven a poleward shift of the Gulf Stream via the upward trend in the Arctic Oscillation over the analyzed period (1958-2001). As the 21st century progresses, we expect the poleward shift in the Northern Hemisphere to become clearer as the response to radiative forcing grows in size relative to the natural variability. In the Southern Hemisphere changes in intensity and latitude of the WBCs will depend on the opposing impacts of ozone recovery, rising greenhouse gas and the varying influence of natural variability. In all cases, the dynamic changes of the WBCs impact poleward ocean heat transport, regional climate, storm tracks and ocean ecosystems. So, improved understanding and projection of how they will evolve is an important area of research to which the current work hopefully provides a useful impetus.

4

On the positive trend of Southern Annular Mode

Both observations and climate models have proved that the Southern Hemisphere (SH) is experiencing significant climate changes in a warming climate. These changes include a strengthening and poleward shifting of the southern westerlies, increasing sea level pressure (SLP) over the mid-latitudes and decreasing SLP over the South Pole, which can be summarized as a positive trend of Southern Annular Mode (SAM) [*Thompson and Wallace*, 2000; *Marshall*, 2003; *Cai et al.*, 2003]. However, the surface temperature increase over the SH is relatively low, raising the questions about why the SH experience little temperature increase but significant climate changes.

Previous work proposed that the ozone depletion and increasing greenhouse gas are the major drivers for the positive trend of SAM [*Thompson and Solomon*, 2002; *Kindem and Christiansen*, 2001; *Sexton*, 2001; *Gillett and Thompson*, 2003; *Fyfe et al.*, 1999; *Kushner et al.*, 2001; *Cai et al.*, 2003; *Rauthe et al.*, 2004; *Arblaster and Meehl*, 2006]. While, some research pointed out that the ocean has the potential to influence the SAM [*Mo*, 2000; *Cai et al.*, 2003; *Zhou and Yu*, 2004; *Grassi et al.*, 2005; *Marshall and Connolley*, 2006]. *Mo* [2000] proved that warmer sea surface temperature (SST) over the southern extratropical regions is associated with a positive phase in the SAM. Climate model simulation indicates that if global SSTs are prescribed, there would be some predictability to the SAM [*Zhou and Yu*, 2004].

Based on observations and climate model sensitivity simulation, in this chapter, we propose that the global warming induced meridional SST gradient may be the primary forcing for the significant upward trend of SAM.

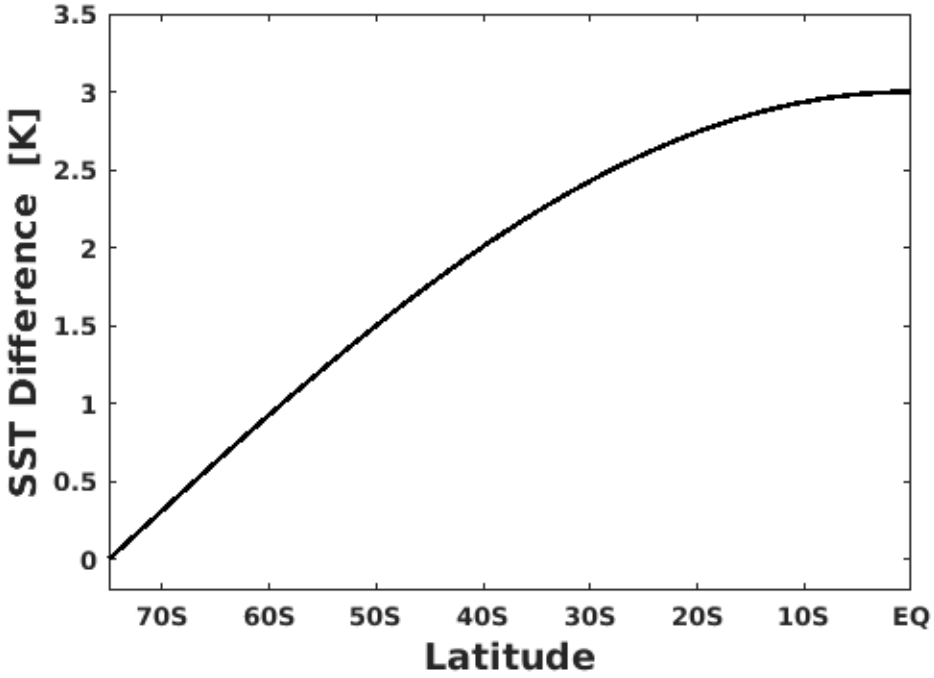

Fig. 4.1: *The SST anomaly added in the sensitivity simulation by ECHAM6.*

4.1 Data and Model

Two atmospheric reanalysis data sets are used to present the observational climate trends over the Southern Hemisphere, namely the National Centers for Environmental Prediction / National Center for Atmospheric Research reanalysis (NCEP/NCAR, 1948-2013) [*Kalnay et al.*, 1996], the European Centre for Medium-Range Weather Forecasts 40-year Reanalysis (ERA40, 1958-2001) [*Uppala et al.*, 2005]. Besides, the $RCP4.5$ simulations from the fifth phase of the Climate Model Intercomparison Project (CMIP5) [*Taylor et al.*, 2012] to present the simulated climate changes over the SH.

Moreover, we carry out two simulations using the atmospheric general circulation model ECHAM6 [*Stevens et al.*, 2013]. The control simulation is forced by a climatological SST (1979-2008). While, an increased meridional SST gradient is added on the forcing of the sensitivity simulation (Fig. 4.1). Both simulations run for 30 years. And the last 10 years' results are used to compare.

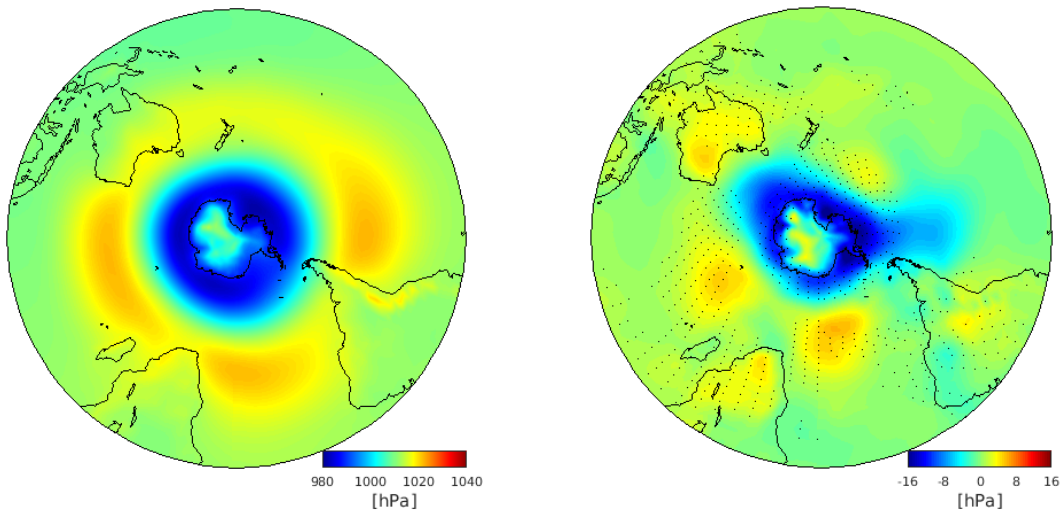

Fig. 4.2: *Left: Spatial distribution of climatological SLP over the Southern Hemisphere. Right: Trend in SLP. Stippling indicates regions where the trends pass the 95% confidence level (Student's t-test). Results based on ERA40 reanalysis.*

4.2 Results and discussion

Figs 4.2- 4.4 present the climatology and trends of SLP based on different data sets. The background climatological SLP pattern is characterized by a high pressure system over the mid-latitude and low pressure systems over the low-latitude and the South Pole. The pattern of SLP trend shares similarity with the climatology values. Besides, the trends in wind also resemble the background circulation, with trend of westerly wind over mid-latitude and easterly wind over the low-latitude (Figs 4.6- 4.8).

The similarity between the background circulation and the trends proves that the SH's background atmosphere circulation is stronger in a warming climate. Since the heat imbalance is the original driver for the atmosphere circulation, these features suggest that the heat imbalance between the tropical and the high-latitudes may be enhanced.

Fig. 4.10 and 4.11 gives the trend in SST based on observation and climate model, respectively. We find that the major feature of global warming induced SST pattern over the SH are characterized by a stronger equator-to-pole gradient. Due to the internal

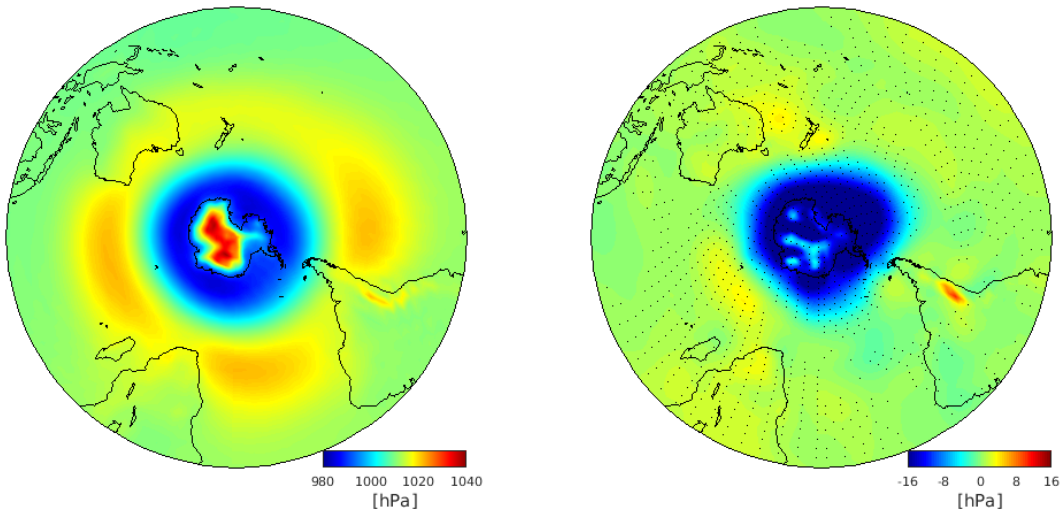

Fig. 4.3: *Left: Spatial distribution of climatological SLP over the Southern Hemisphere. Right: Trend in SLP. Stippling indicates regions where the trends pass the 95% confidence level (Student's t-test). Results based on NCEP/NCAR reanalysis.*

oceanic feedback, the ocean surface warming is not uniform over the SH. Over the South Pole, the existence of sea ice and ice sheet restrict the ocean water temperature close to the freezing point. Meanwhile, the Ekman transport, induced by the southern westerlies, moving the Antarctic cold water northwards, keeping the Southern Ocean cool. Moreover, the wind-driven upwelling in the Southern Ocean also limits the surface temperature increase. As a consequence, the surface warming over the Southern Ocean is much slower than that over the low-latitudes regions, resulting in an enhancing SST gradient between the Tropics and the high-latitudes over the Southern Hemisphere (Fig. 4.11).

In order the isolate the impact of SST gradient on SH's climate change, we carried out two model sensitivity simulations with different forcing merely in SST (as introduced in the Section 4.1). With increasing meridional SST forcing, the climate model can well reproduce the primarily pattern of SH's climate change (as shown in Figs. 4.5 and 4.9), demonstrating that the increasing SST gradient is potential to be the driver for the SH climate changes.

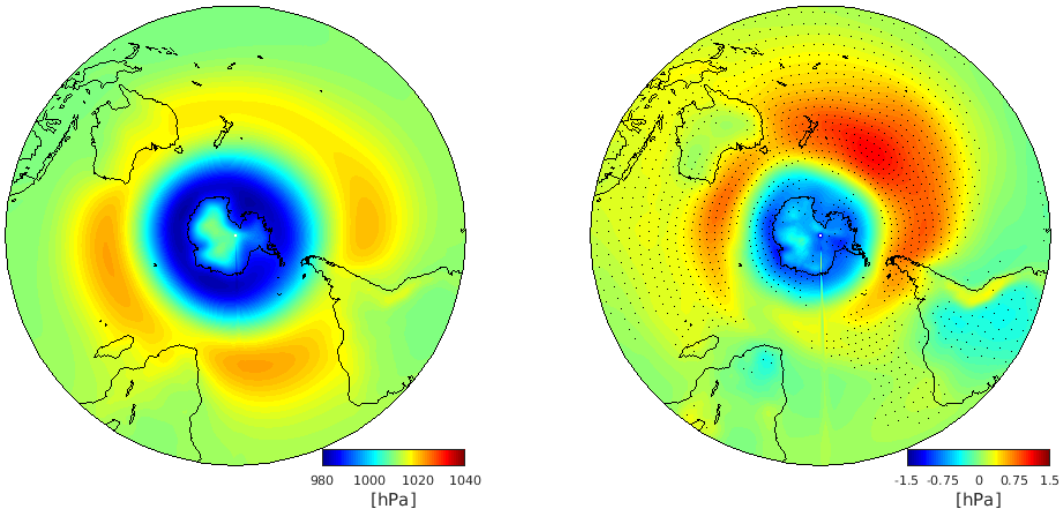

Fig. 4.4: *Multi-model ensemble climatological (left) and trends (right) in SLP (shading) based on the $CMIP5/RCP4.5$ simulations. The models used to estimate the ensemble values are listed below each panel. Stippling indicates areas where at least 2/3 of the models agree on the sign of the trends.*

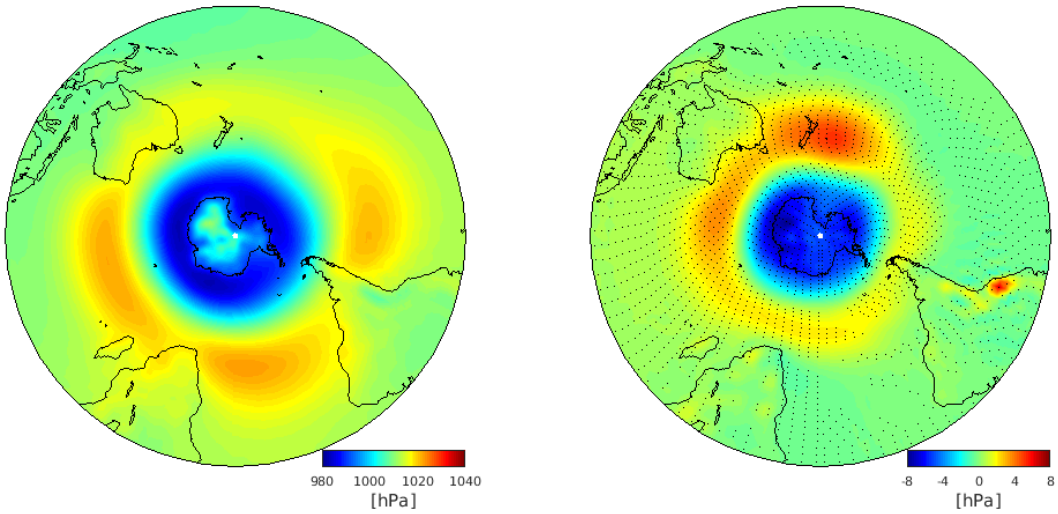

Fig. 4.5: *Left: climatological SLP in the ECHAM6 control run. Right: SLP difference between the two simulations. Stippling indicates regions where the SLP differences pass the 95% confidence level (Student's t-test).*

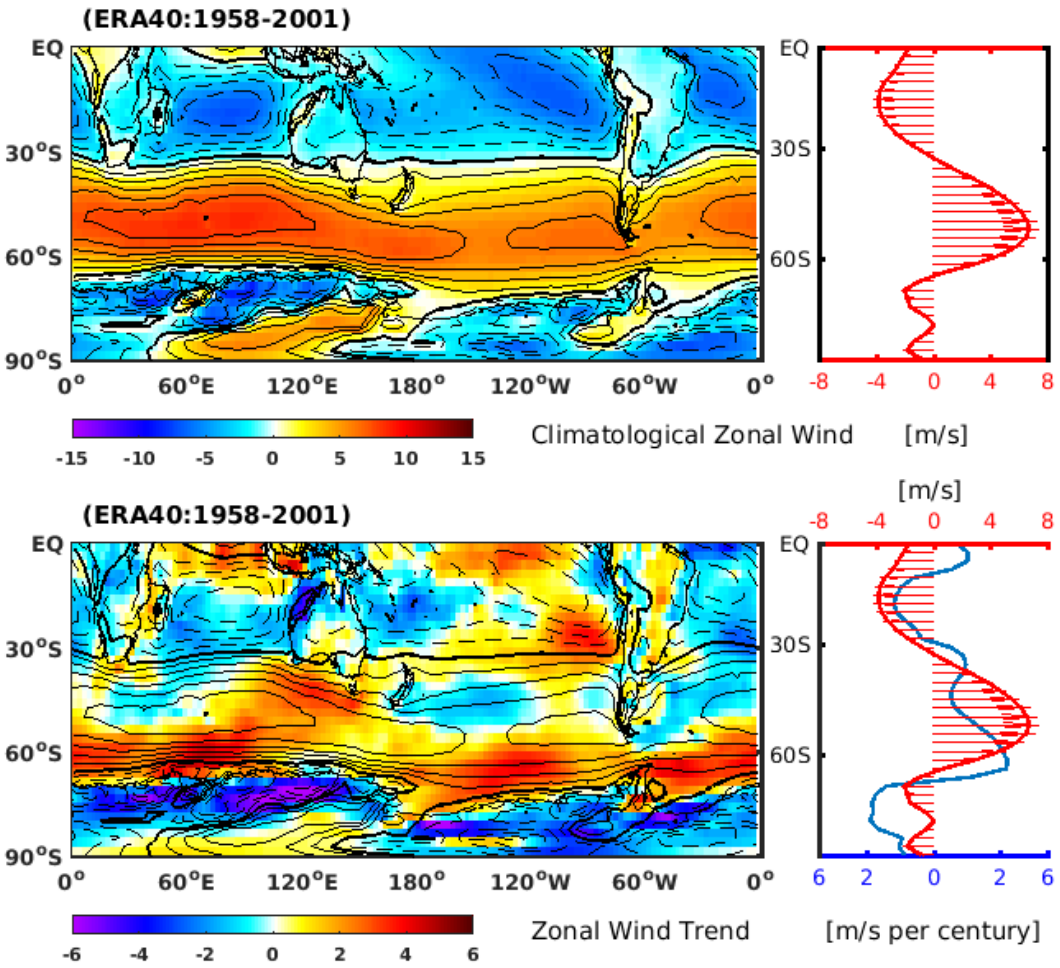

Fig. 4.6: *Left: Spatial distribution of climatological near-surface zonal wind over the Southern Hemisphere. Right: Trend in near-surface zonal wind. Stippling indicates regions where the trends pass the 95% confidence level (Student's t-test). Results based on ERA40 reanalysis.*

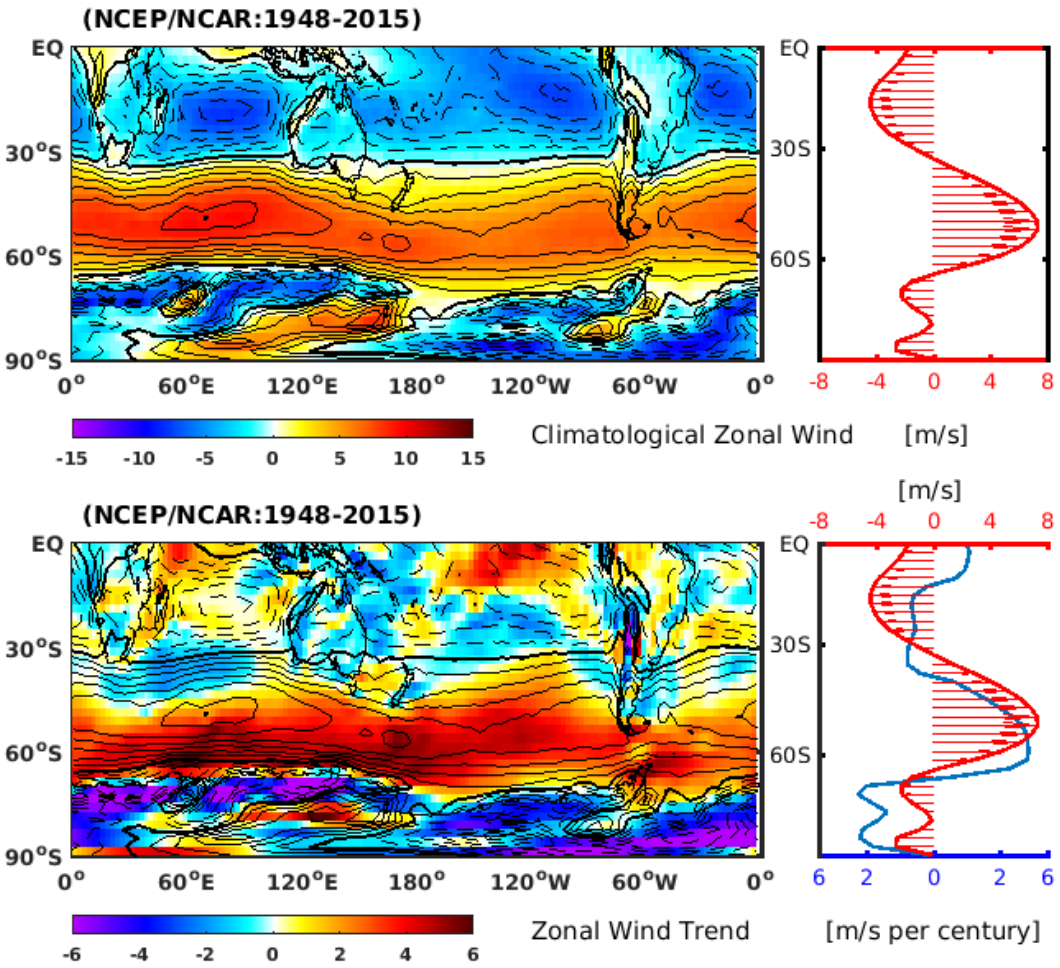

Fig. 4.7: *Left: Spatial distribution of climatological near-surface zonal wind over the Southern Hemisphere. Right: Trend in near-surface zonal wind. Stippling indicates regions where the trends pass the 95% confidence level (Student's t-test). Results based on NCEP/NCAR reanalysis.*

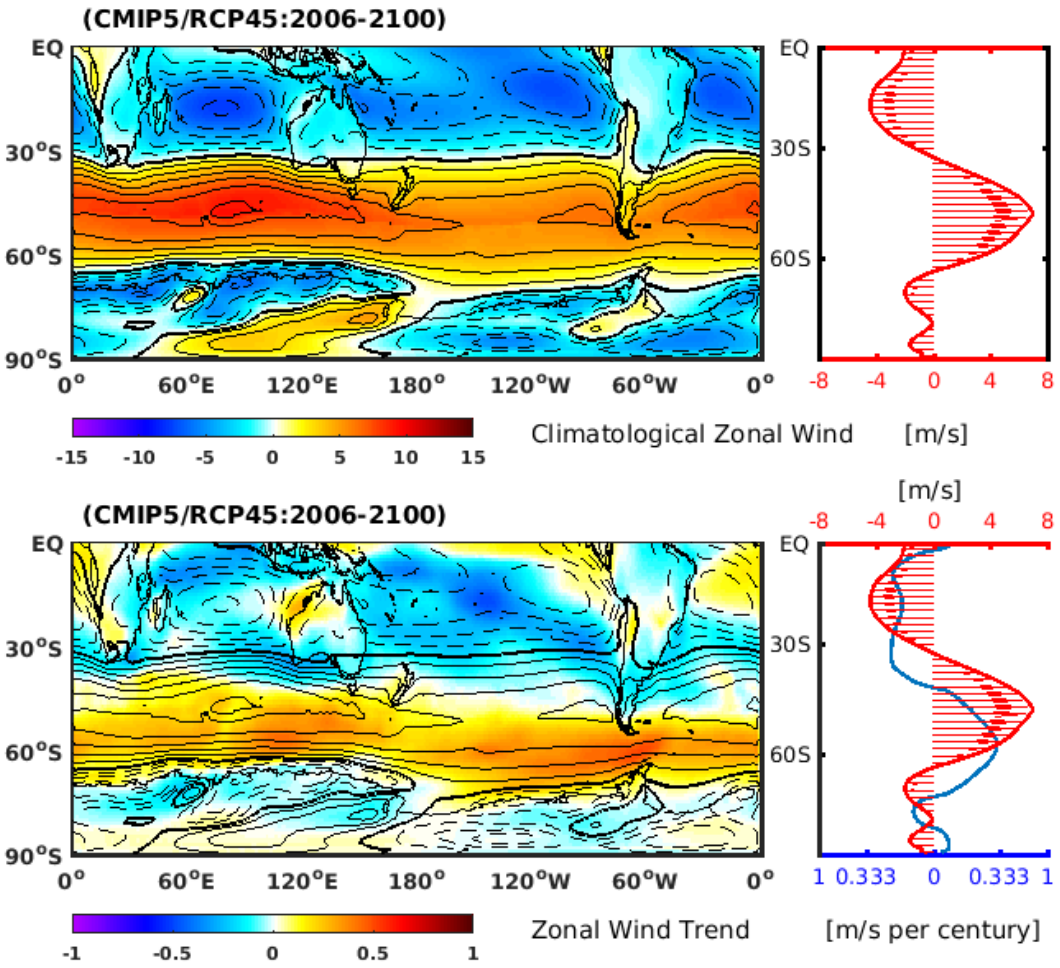

Fig. 4.8: *Multi-model ensemble climatological (left) and trends (right) in near-surface zonal wind based on the $CMIP5/RCP4.5$ simulations. The models used to estimate the ensemble values are listed below each panel. Stippling indicates areas where at least 2/3 of the models agree on the sign of the trends.*

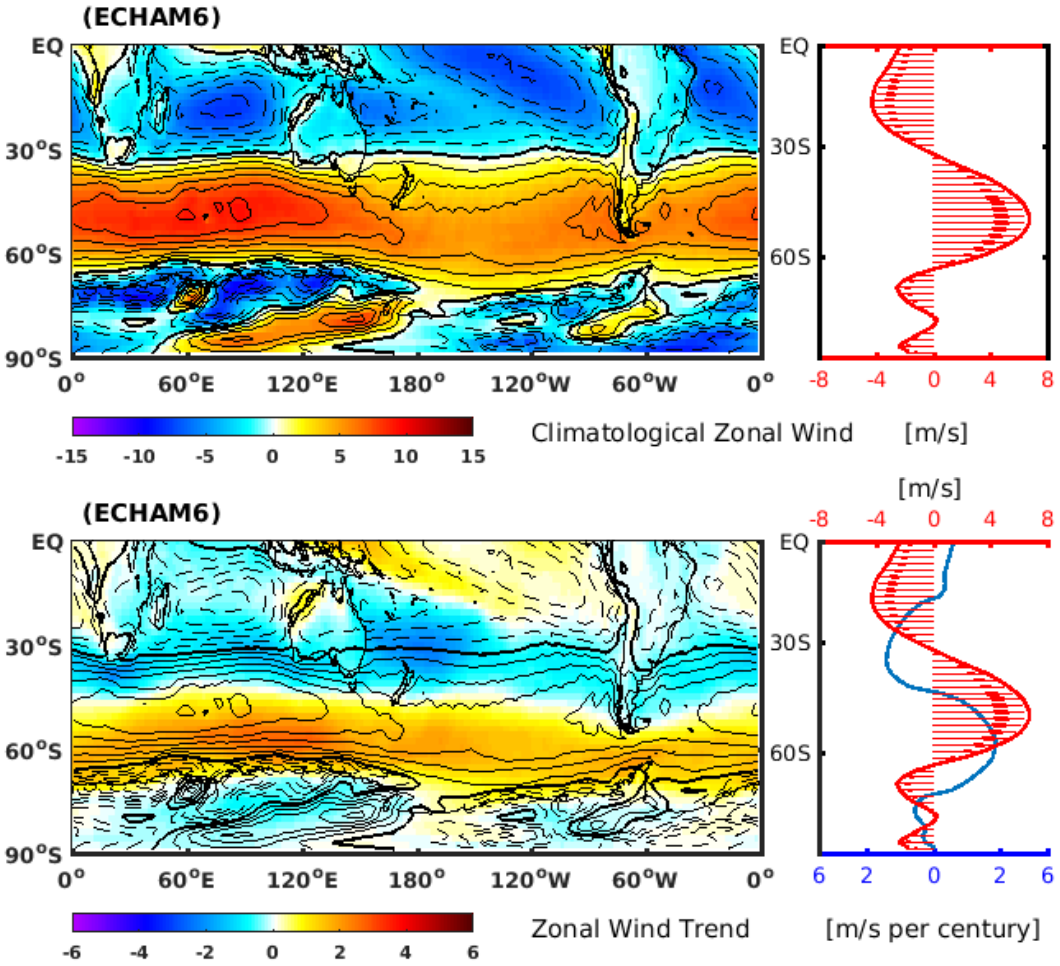

Fig. 4.9: *Left: climatological near-surface zonal wind in the ECHAM6 control run. Right: near-surface zonal wind difference between the two simulations. Stippling indicates regions where the near-surface zonal wind differences pass the 95% confidence level (Student's t-test).*

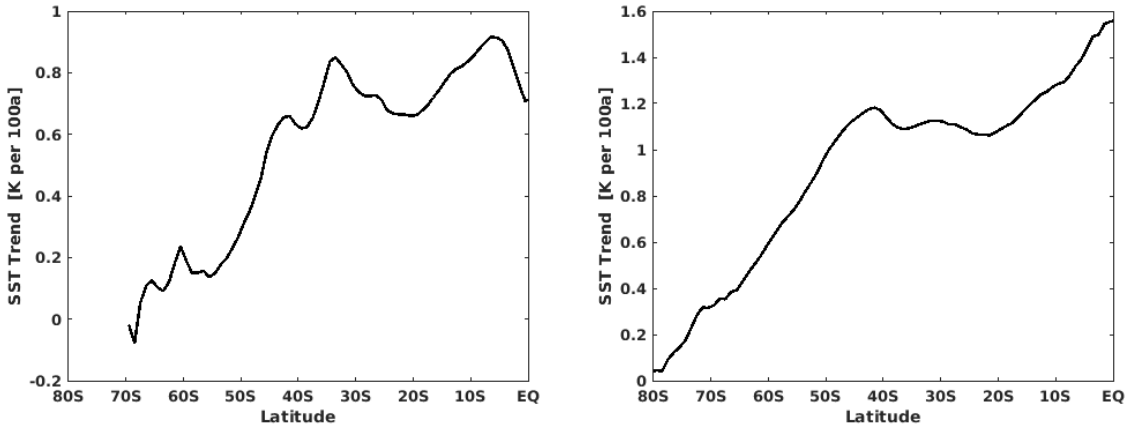

Fig. 4.10: *Left: Observational zonal mean SST trend based on NCEP/NCAR during 1948-2014. Right: Multi-model ensemble zonal mean SST trend based on CMIP/RCP4.5 simulation during 2006-2100. Both trends are scaled to 100 years.*

4.3 Conclusions for this chapter

The ocean response to global warming varies in different regions. Under global warming, the Southern Ocean have less surface temperature increase due to larger thermal interior and the temperature restriction from sea ice. Such effect will result in an increasing meridional SST different over the SH. We demonstrated that the increased meridional SST gradient can enhance the heat imbalance within the atmosphere, forcing a stronger SAM.

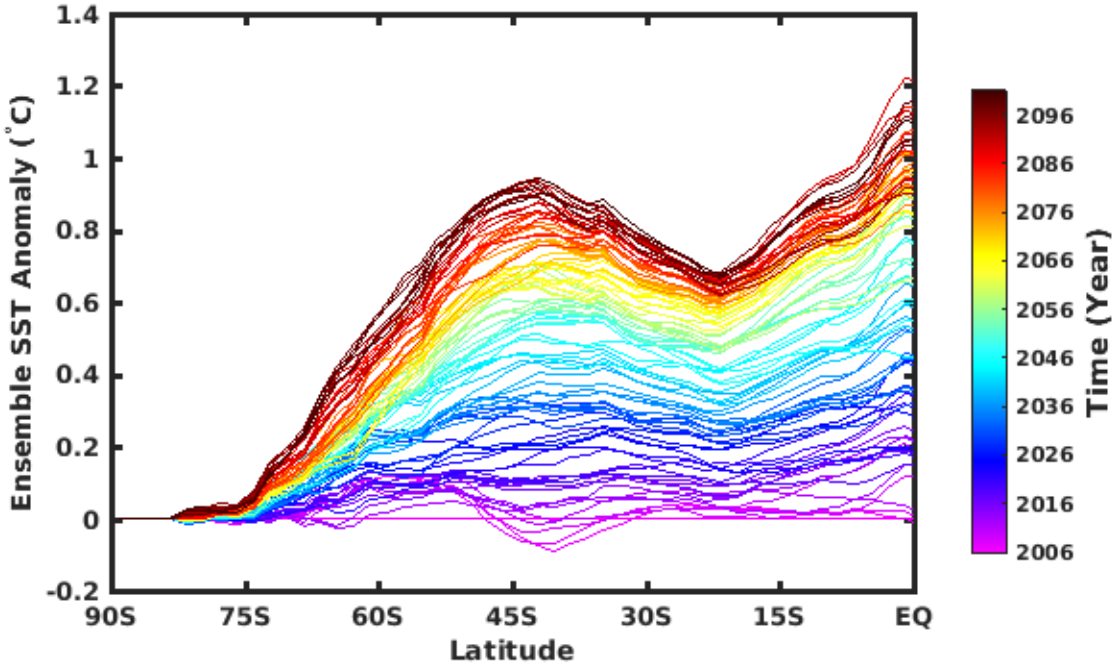

Fig. 4.11: *Multi-model (27 models) ensemble zonal mean SST anomalies relative to the period between 2006 and 2010. Each line with different color represents a individual year indicated by the color bar. Results based on CMIP/RCP4.5 simulation.*

5 Conclusions

The subtropical western boundary currents (WBCs) have a broad impact on the climate and economy over the adjacent mainland, e.g., the temperature, fishing, storms, precipitation and extreme climate events [*Seager et al.*, 2002; *Cai et al.*, 2005; *Minobe et al.*, 2008]. On the basis of studying the trend in ocean surface heat flux during 1958-2013, a prominent increase of ocean heat loss is found over all the subtropical western boundary currents, including the Gulf Stream, the Kuroshio Current, the Brazil Current, the Eastern Australia Current and the Agulhas Current, suggesting significant dynamic changes of these currents. To understand the mechanism, a large range of independent data sources are used to investigate this case. We find that the WBCs (except the Gulf Stream) are intensifying and moving poleward under global warming, helping to transport more heat from the tropical regions to the mid- and high-latitudes. Since the sharp sea surface temperature gradient and extensive ocean heat release along the path of WBCs are the primary driver for the storms [*Hoskins and Valdes*, 1990], stronger WBCs suggest that there will be more severe storm in the future. As *Shaman et al.* [2010] have demonstrated, the storm frequency over the WBCs has increased during the past half century. Moreover, the adjacent regions of the WBCs suffer more warming than other regions, due to the increased heat transport by the WBCs, especially over Eastern Asian, where the Kuroshio Current transports much more heat [*Tang et al.*, 2009]. Distinct from other WBCs, the Gulf Stream is likely to be weaker in the future, mainly attributed to the weakening of the Atlantic Meridional Overturning Circulation under global warming. A weakening of the Gulf Stream can reduce the heat release

from the ocean, and contribute to a relative cooling over Europe and Eastern America, a feature suggested by *Dima and Lohmann* [2010] and *Rahmstorf et al.* [2015].

In a warming climate, both observations and climate models have recorded a poleward-intensifying of ocean surface winds, which are proposed to be the driver for the intensification and poleward shift of WBCs. The trends in ocean surface winds are related to several other global warming phenomena, for instant, the stronger Arctic and Antarctic Oscillations [*Thompson and Wallace*, 2000; *Marshall*, 2003; *Cai et al.*, 2003], the poleward shift of the Hadley Cell [*Hu and Fu*, 2007; *Lu et al.*, 2007; *Johanson and Fu*, 2009], the expansion of the tropical belt [*Santer et al.*, 2003; *Seidel and Randel*, 2007; *Seidel et al.*, 2007; *Fu and Lin*, 2011], and the poleward shift of the subtropical dry zones [*Previdi and Liepert*, 2007]. The above study in the atmosphere have already welled known for a decade. However, the related research in ocean is detailed for several years, mostly due to the limitation in observations. Besides, the influences of the WBCs' dynamic changes to the regional oceanography, ecosystems, and climate is not well investigated [*Seager and Simpson*, 2016]. In the future, we believe that more research based on long-term continues ocean observations and high resolution coupled model will significantly improve our ability to understand climate change. As several studies have already proved that the application of high resolution coupled model can improve climate predictions [*Ma et al.*, 2016; *Roberts et al.*, 2016; *Renault et al.*, 2016].

Focus on the Southern Hemisphere, we find that due to the oceanic feedback, the surface warming over the Southern Ocean is much slower than that over the low-latitudes regions. The uneven temperature increase results in an enhancing sea surface temperature gradient between the Tropics and the high-latitudes. We highlight that such gradient contributes to enhance the thermal heat imbalance within the atmosphere, and is potential to drive a stronger Southern Hemisphere atmosphere circulation. Our model sensitivity simulations have also demonstrated that increasing meridional sea surface temperature gradients can force a poleward-intensifying of ocean surface wind and positive trend of Antarctic Oscillation with equivalent magnitude. The climate changes over the Northern Hemisphere shares some similarity with the Southern Hemisphere from the perspective of positive trend of Arctic Oscillation. However, the mechanism seems to be more complicated owing to the land-sea mask. Further investigation effort is required to get a better understanding.

Bibliography

Andersson, A., K. Fennig, C. Klepp, S. Bakan, H. Graßl, and J. Schulz, The Hamburg Ocean Atmosphere Parameters and Fluxes from Satellite Data-HOAPS-3, *Earth System Science Data Discussions*, *3*, 143–194, 2010.

Andres, M., J.-H. Park, M. Wimbush, X.-H. Zhu, H. Nakamura, K. Kim, and K.-I. Chang, Manifestation of the Pacific decadal oscillation in the Kuroshio, *Geophysical Research Letters*, *36*(16), 2009.

Arblaster, J., G. Meehl, and D. Karoly, Future climate change in the southern hemisphere: Competing effects of ozone and greenhouse gases, *Geophysical Research Letters*, *38*(2), 2011.

Arblaster, J. M., and G. A. Meehl, Contributions of external forcings to southern annular mode trends, *Journal of Climate*, *19*(12), 2896–2905, 2006.

Balmaseda, M. A., K. Mogensen, and A. T. Weaver, Evaluation of the ECMWF ocean reanalysis system ORAS4, *Quarterly Journal of the Royal Meteorological Society*, *139*(674), 1132–1161, 2013.

Bellucci, A., et al., An assessment of a multi-model ensemble of decadal climate predictions, *Climate Dynamics*, *44*(9-10), 2787–2806, 2014.

Biastoch, A., C. W. Böning, F. U. Schwarzkopf, and J. Lutjeharms, Increase in Agulhas leakage due to poleward shift of Southern Hemisphere westerlies, *Nature*, *462*(7272), 495–498, 2009.

Bourassa, M. A., et al., High-latitude ocean and sea ice surface fluxes: Challenges for climate research, *Bulletin of the American Meteorological Society*, *94*(3), 403–423, 2013.

Brunke, M. A., X. Zeng, and S. Anderson, Uncertainties in sea surface turbulent flux algorithms and data sets, *Journal of Geophysical Research: Oceans (1978–2012)*, *107*(C10), 5–1, 2002.

Brunke, M. A., Z. Wang, X. Zeng, M. Bosilovich, and C.-L. Shie, An assessment of the uncertainties in ocean surface turbulent fluxes in 11 reanalysis, satellite-derived, and combined global datasets, *Journal of Climate*, *24*(21), 5469–5493, 2011.

Cai, W., Antarctic ozone depletion causes an intensification of the Southern Ocean super-gyre circulation, *Geophysical Research Letters*, *33*(3), L03,712, 2006.

Cai, W., P. H. Whetton, and D. J. Karoly, The response of the Antarctic Oscillation to increasing and stabilized atmospheric CO2, *Journal of Climate*, *16*(10), 1525–1538, 2003.

Cai, W., G. Shi, T. Cowan, D. Bi, and J. Ribbe, The response of the Southern Annular Mode, the East Australian Current, and the southern mid-latitude ocean circulation to global warming, *Geophysical Research Letters*, *32*(23), L23,706, 2005.

Cane, M., A. Clement, A. Kaplan, Y. Kushnir, D. Pozdnyakov, R. Seager, S. Zebiak, and R. Murtugudde, Twentieth-century sea surface temperature trends, *Science*, *275*(5302), 957–960, 1997.

Carton, J. A., and B. S. Giese, A reanalysis of ocean climate using Simple Ocean Data Assimilation (SODA), *Monthly Weather Review*, *136*(8), 2999–3017, 2008.

Cattiaux, J., and C. Cassou, Opposite CMIP3/CMIP5 trends in the wintertime Northern Annular Mode explained by combined local sea ice and remote tropical influences, *Geophysical Research Letters*, *40*(14), 3682–3687, 2013.

Cayan, D. R., Latent and sensible heat flux anomalies over the northern oceans: Driving the sea surface temperature, *Journal of Physical Oceanography*, *22*(8), 859–881, 1992.

Cheng, W., J. C. Chiang, and D. Zhang, Atlantic Meridional Overturning Circulation (AMOC) in CMIP5 Models: RCP and Historical Simulations, *Journal of Climate*, *26*(18), 2013.

Chou, S.-H., E. Nelkin, J. Ardizzone, R. M. Atlas, and C.-L. Shie, Surface turbulent heat and momentum fluxes over global oceans based on the Goddard satellite retrievals, version 2 (GSSTF2), *Journal of Climate*, *16*(20), 3256–3273, 2003.

Chou, S.-H., E. Nelkin, J. Ardizzone, and R. M. Atlas, A comparison of latent heat fluxes over global oceans for four flux products, *Journal of climate*, *17*(20), 3973–3989, 2004.

Clayson, C. A., and A. S. Bogdanoff, The effect of diurnal sea surface temperature warming on climatological air–sea fluxes, *Journal of Climate*, *26*(8), 2546–2556, 2013.

Colling, A., *Ocean circulation*, vol. 3, Butterworth-Heinemann, 2001.

Compo, G. P., J. S. Whitaker, and P. D. Sardeshmukh, Feasibility of a 100-year reanalysis using only surface pressure data, *Bulletin of the American Meteorological Society*, *87*(2), 175, 2006.

Compo, G. P., et al., The twentieth century reanalysis project, *Quarterly Journal of the Royal Meteorological Society*, *137*(654), 1–28, 2011.

Cronin, M. F., et al., Monitoring ocean-atmosphere interactions in western boundary current extensions, in *Proceedings of the" OceanObs̆2019 09: Sustained Ocean Observations and Information for Society" Conference*, vol. 2, 2010.

Curry, J., et al., Seaflux, *Bulletin of the American Meteorological Society*, *85*(3), 409–424, 2004.

Curry, R. G., and M. S. McCartney, Ocean gyre circulation changes associated with the North Atlantic Oscillation, *Journal of Physical Oceanography*, *31*(12), 3374–3400, 2001.

Da Silva, A., C. Young, and S. Levitus, Atlas of Surface Marine Data 1994, vol. 1, Algorithms and Procedures, NOAA Atlas NESDIS 6, *US Dep. of Commer., Washington, DC*, 1994.

Dee, D., M. Balmaseda, G. Balsamo, R. Engelen, A. Simmons, and J.-N. Thépaut, Toward a consistent reanalysis of the climate system, *Bulletin of the American Meteorological Society*, *95*(8), 1235–1248, 2014.

Deser, C., On the teleconnectivity of the "Arctic Oscillation", *Geophysical Research Letters*, *27*(6), 779–782, 2000.

Deser, C., M. Alexander, and M. Timlin, Evidence for a wind-driven intensification of the Kuroshio Current Extension from the 1970s to the 1980s, *Journal of Climate*, *12*(6), 1697–1706, 1999.

Dima, M., and G. Lohmann, Evidence for two distinct modes of large-scale ocean circulation changes over the last century, *Journal of Climate*, *23*(1), 5–16, 2010.

DiNezio, P. N., L. J. Gramer, W. E. Johns, C. S. Meinen, and M. O. Baringer, Observed interannual variability of the florida current: Wind forcing and the north atlantic oscillation, *Journal of Physical Oceanography*, *39*(3), 721–736, 2009.

Easterling, D. R., and M. F. Wehner, Is the climate warming or cooling?, *Geophysical Research Letters*, *36*(8), 2009.

Fairall, C., E. F. Bradley, J. Hare, A. Grachev, and J. Edson, Bulk parameterization of air-sea fluxes: Updates and verification for the COARE algorithm, *Journal of climate*, *16*(4), 571–591, 2003.

Feldstein, S. B., and C. Franzke, Are the North Atlantic Oscillation and the northern annular mode distinguishable?, *Journal of the Atmospheric Sciences*, *63*(11), 2915–2930, 2006.

Frankignoul, C., and E. Kestenare, The surface heat flux feedback. Part I: Estimates from observations in the Atlantic and the North Pacific, *Climate Dynamics*, *19*(8), 633–647, doi:10.1007/s00382-002-0252-x, 2002.

Fu, Q., and P. Lin, Poleward shift of subtropical jets inferred from satellite-observed lower-stratospheric temperatures, *Journal of Climate*, *24*(21), 5597–5603, 2011.

Fyfe, J., G. Boer, and G. Flato, The Arctic and Antarctic Oscillations and their projected changes under global warming, *Geophysical Research Letters*, *26*(11), 1601–1604, 1999.

Fyfe, J. C., and O. A. Saenko, Simulated changes in the extratropical Southern Hemisphere winds and currents, *Geophysical Research Letters*, *33*(6), 2006.

Gao, S., L. S. Chiu, and C.-L. Shie, Trends and variations of ocean surface latent heat flux: Results from GSSTF2c data set, *Geophysical Research Letters*, 2013.

Giese, B. S., and S. Ray, El Niño variability in simple ocean data assimilation (SODA), 1871–2008, *Journal of Geophysical Research: Oceans (1978–2012)*, *116*(C2), 2011.

Gillett, N., and J. Fyfe, Annular mode changes in the CMIP5 simulations, *Geophysical Research Letters*, *40*(6), 1189–1193, 2013.

Gillett, N. P., and D. W. Thompson, Simulation of recent Southern Hemisphere climate change, *Science*, *302*(5643), 273–275, 2003.

Goni, G. J., F. Bringas, and P. N. DiNezio, Observed low frequency variability of the Brazil Current front, *Journal of Geophysical Research: Oceans (1978–2012)*, *116*(C10), 2011.

Grassi, B., G. Redaelli, and G. Visconti, Simulation of Polar Antarctic trends: Influence of tropical SST, *Geophysical research letters*, *32*(23), 2005.

Gulev, S., T. Jung, and E. Ruprecht, Estimation of the impact of sampling errors in the VOS observations on air-sea fluxes. Part I: Uncertainties in climate means, *Journal of Climate*, *20*(2), 279–301, 2007a.

Gulev, S., T. Jung, and E. Ruprecht, Estimation of the impact of sampling errors in the VOS observations on air-sea fluxes. Part II: Impact on trends and interannual variability, *Journal of Climate*, *20*(2), 302–315, 2007b.

Gulev, S. K., and K. Belyaev, Probability Distribution Characteristics for Surface Air-Sea Turbulent Heat Fluxes over the Global Ocean, *Journal of Climate*, *25*(1), 184–206, 2012.

Gulev, S. K., L. Mojib, K. Noel, P. Wonsun, and K. Klaus Peter, North Atlantic Ocean control on surface heat flux on multidecadal timescales, *Nature*, *499*, 464–467, 2013.

Hall, A., and M. Visbeck, Synchronous Variability in the Southern Hemisphere Atmosphere, Sea Ice, and Ocean Resulting from the Annular Mode, *Journal of Climate*, *15*(21), 3043–3057, 2002.

Hoskins, B. J., and P. J. Valdes, On the existence of storm-tracks, *Journal of the atmospheric sciences*, *47*(15), 1854–1864, 1990.

Hu, Y., and Q. Fu, Observed poleward expansion of the Hadley circulation since 1979, *Atmospheric Chemistry and Physics*, *7*(19), 5229–5236, 2007.

Inatsu, M., H. Mukougawa, and S. Xie, Tropical and extratropical SST effects on the midlatitude storm track, *Journal of the Meteorological Society of Japan*, *80*(4B), 1069–1076, 2002.

Iwasaki, S., and M. Kubota, Increasing trends for the surface heat flux and fresh water flux in the North Pacific eastern subtropical region, *Geophysical Research Letters*, *38*(10), L10,604, 2011.

Johanson, C. M., and Q. Fu, Hadley cell widening: Model simulations versus observations, *Journal of Climate*, *22*(10), 2713–2725, 2009.

Kalnay, E., et al., The NCEP/NCAR 40-year reanalysis project, *Bulletin of the American Meteorological Society*, *77*(3), 437–471, 1996.

Kelly, K. A., M. J. Caruso, S. Singh, and B. Qiu, Observations of atmosphere-ocean coupling in midlatitude western boundary currents, *Journal of Geophysical Research: Oceans (1978–2012)*, *101*(C3), 6295–6312, 1996.

Kelly, K. A., R. J. Small, R. Samelson, B. Qiu, T. M. Joyce, Y. O. Kwon, and M. F. Cronin, Western boundary currents and frontal air-sea interaction: Gulf Stream and Kuroshio Extension, *Journal of Climate*, *23*(21), 5644–5667, doi: 10.1175/2010JCLI3346.1, 2010.

Kindem, I. T., and B. Christiansen, Tropospheric response to stratospheric ozone loss, *Geophysical Research Letters*, *28*(8), 1547–1550, 2001.

Köhl, A., Evaluation of the GECCO2 ocean synthesis: transports of volume, heat and freshwater in the Atlantic, *Quarterly Journal of the Royal Meteorological Society*, *141*(686), 166–181, 2015.

Köhl, A., and D. Stammer, Variability of the meridional overturning in the North Atlantic from the 50-year GECCO state estimation, *Journal of Physical Oceanography*, *38*(9), 1913–1930, 2008.

Kosaka, Y., and S.-P. Xie, Recent global-warming hiatus tied to equatorial Pacific surface cooling, *Nature*, *501*(7467), 403–407, 2013.

Krueger, O., F. Schenk, F. Feser, and R. Weisse, Inconsistencies between long-term trends in storminess derived from the 20cr reanalysis and observations, *Journal of Climate*, *26*(3), 868–874, 2013.

Kubota, M., N. Iwasaka, S. Kizu, M. Konda, and K. Kutsuwada, Japanese ocean flux data sets with use of remote sensing observations (J-OFURO), *Journal of Oceanography*, *58*(1), 213–225, 2002.

Kushner, P. J., I. M. Held, and T. L. Delworth, Southern Hemisphere atmospheric circulation response to global warming, *Journal of Climate*, *14*(10), 2238–2249, 2001.

L'Ecuyer, T. S., and G. L. Stephens, The tropical oceanic energy budget from the TRMM perspective. Part I: Algorithm and uncertainties, *Journal of climate*, *16*(12), 1967–1985, 2003.

Liu, J., and J. Curry, Variability of the tropical and subtropical ocean surface latent heat flux during 1989–2000, *Geophys. Res. Lett*, *33*, L05,706, 2006.

Liu, J., J. A. Curry, C. A. Clayson, and M. A. Bourassa, High-resolution satellite surface latent heat fluxes in North Atlantic hurricanes, *Monthly Weather Review*, *139*(9), 2735–2747, 2011.

Liu, W. T., K. B. Katsaros, and J. A. Businger, Bulk parameterization of air-sea exchanges of heat and water vapor including the molecular constraints at the interface, *Journal of the Atmospheric Sciences*, *36*(9), 1722–1735, 1979.

Lohmann, G., H. Haak, and J. H. Jungclaus, Estimating trends of Atlantic meridional overturning circulation from long-term hydrographic data and model simulations, *Ocean Dynamics*, *58*(2), 127–138, 2008.

Lu, J., G. A. Vecchi, and T. Reichler, Expansion of the Hadley cell under global warming, *Geophysical Research Letters*, *34*(6), 2007.

Ma, X., et al., Western boundary currents regulated by interaction between ocean eddies and the atmosphere, *Nature*, *535*(7613), 533–537, 2016.

Mantua, N. J., S. R. Hare, Y. Zhang, J. M. Wallace, and R. C. Francis, A Pacific interdecadal climate oscillation with impacts on salmon production, *Bulletin of the american Meteorological Society*, *78*(6), 1069–1079, 1997.

Marshall, G. J., Trends in the Southern Annular Mode from observations and reanalyses, *Journal of Climate*, *16*(24), 4134–4143, 2003.

Marshall, G. J., and W. M. Connolley, Effect of changing Southern Hemisphere winter sea surface temperatures on Southern Annular Mode strength, *Geophysical Research Letters*, *33*, L17,717, 2006.

Meehl, G. A., C. Covey, K. E. Taylor, T. Delworth, R. J. Stouffer, M. Latif, B. McAvaney, and J. F. Mitchell, The WCRP CMIP3 multimodel dataset: A new era in climate change research, *Bulletin of the American Meteorological Society*, *88*(9), 1383–1394, 2007.

Meehl, G. A., J. M. Arblaster, J. T. Fasullo, A. Hu, and K. E. Trenberth, Model-based evidence of deep-ocean heat uptake during surface-temperature hiatus periods, *Nature Climate Change*, *1*(7), 360–364, 2011.

Minobe, S., A. Kuwano-Yoshida, N. Komori, S. P. Xie, and R. J. Small, Influence of the Gulf Stream on the troposphere, *Nature*, *452*(7184), 206–209, 2008.

Mo, K. C., Relationships between low-frequency variability in the Southern Hemisphere and sea surface temperature anomalies, *Journal of Climate*, *13*(20), 2000.

Moore, G., and I. Renfrew, An assessment of the surface turbulent heat fluxes from the NCEP-NCAR reanalysis over the western boundary currents, *Journal of Climate*, *15*(15), 2020–2037, 2002.

Morice, C. P., J. J. Kennedy, N. A. Rayner, and P. D. Jones, Quantifying uncertainties in global and regional temperature change using an ensemble of observational estimates: The HadCRUT4 data set, *Journal of Geophysical Research: Atmospheres (1984–2012)*, *117*(D8), 2012.

Pedlosky, J., *Ocean circulation theory*, Springer Science & Business Media, 1996.

Poli, P., et al., Era-20c: An atmospheric reanalysis of the 20th century, *Journal of Climate*, *0*(2016), 2016.

Polvani, L. M., D. W. Waugh, G. J. Correa, and S.-W. Son, Stratospheric ozone depletion: The main driver of twentieth-century atmospheric circulation changes in the southern hemisphere, *Journal of Climate*, *24*(3), 795–812, 2011.

Previdi, M., and B. G. Liepert, Annular modes and Hadley cell expansion under global warming, *Geophysical Research Letters*, *34*(22), 2007.

Qiu, B., Kuroshio Extension variability and forcing of the Pacific decadal oscillations: Responses and potential feedback, *Journal of Physical Oceanography*, *33*(12), 2465–2482, 2003.

Qiu, B., and S. Chen, Variability of the Kuroshio Extension jet, recirculation gyre, and mesoscale eddies on decadal time scales, *Journal of Physical Oceanography*, *35*(11), 2090–2103, 2005.

Qiu, B., and S. Chen, Decadal variability in the large-scale sea surface height field of the South Pacific Ocean: Observations and causes, *Journal of Physical Oceanography*, *36*(9), 1751–1762, 2006.

Qiu, B., and T. M. Joyce, Interannual variability in the mid-and low-latitude western North Pacific, *J. Phys. Oceanogr*, *22*(9), 1062–1079, 1992.

Rahmstorf, S., G. Feulner, M. E. Mann, A. Robinson, S. Rutherford, and E. J. Schaffernicht, Exceptional twentieth-century slowdown in Atlantic Ocean overturning circulation, *Nature Climate Change*, 2015.

Rauthe, M., A. Hense, and H. Paeth, A model intercomparison study of climate change-signals in extratropical circulation, *International Journal of Climatology*, *24*(5), 643–662, 2004.

Rayner, N., D. Parker, E. Horton, C. Folland, L. Alexander, D. Rowell, E. Kent, and A. Kaplan, Global analyses of sea surface temperature, sea ice, and night marine air temperature since the late nineteenth century, *Journal of Geophysical Research: Atmospheres (1984–2012)*, *108*(D14), 2003.

Refsgaard, J. C., et al., A framework for testing the ability of models to project climate change and its impacts, *Climatic Change*, *122*(1-2), 271–282, 2014.

Renault, L., M. J. Molemaker, J. Gula, S. Masson, and J. C. McWilliams, Control and stabilization of the gulf stream by oceanic current interaction with the atmosphere, *Journal of Physical Oceanography*, *46*(11), 3439–3453, 2016.

Reynolds, R. W., N. A. Rayner, T. M. Smith, D. C. Stokes, and W. Wang, An improved in situ and satellite SST analysis for climate, *Journal of Climate*, *15*(13), 1609–1625, 2002.

Ridgway, K., Long-term trend and decadal variability of the southward penetration of the East Australian Current, *Geophysical Research Letters*, *34*(13), 2007.

Ridgway, K., R. Coleman, R. Bailey, and P. Sutton, Decadal variability of East Australian Current transport inferred from repeated high-density XBT transects, a CTD survey and satellite altimetry, *Journal of Geophysical Research: Oceans (1978–2012)*, *113*(C8), 2008.

Roberts, M. J., H. T. Hewitt, P. Hyder, D. Ferreira, S. A. Josey, M. Mizielinski, and A. Shelly, Impact of ocean resolution on coupled air-sea fluxes and large-scale climate, *Geophysical Research Letters*, *43*(19), 2016.

Roemmich, D., J. Gilson, R. Davis, P. Sutton, S. Wijffels, and S. Riser, Decadal spinup of the South Pacific subtropical gyre, *Journal of Physical Oceanography*, *37*(2), 162–173, 2007.

Rogers, J., and M. McHugh, On the separability of the North Atlantic Oscillation and Arctic Oscillation, *Climate Dynamics*, *19*(7), 599–608, 2002.

Rossow, W. B., and R. A. Schiffer, ISCCP cloud data products, *Bulletin of the American Meteorological Society*, *72*(1), 2–20, 1991.

Sakamoto, T. T., H. Hasumi, M. Ishii, S. Emori, T. Suzuki, T. Nishimura, and A. Sumi, Responses of the Kuroshio and the Kuroshio Extension to global warming in a high-resolution climate model, *Geophysical Research Letters*, *32*(14), 2005.

Santer, B. D., et al., Contributions of anthropogenic and natural forcing to recent tropopause height changes, *Science*, *301*(5632), 479–483, 2003.

Santorelli, A., R. Pinker, A. Bentamy, K. Katsaros, W. Drennan, A. Mestas-Nuñez, and J. Carton, Differences between two estimates of air-sea turbulent heat fluxes over the Atlantic Ocean, *Journal of Geophysical Research: Oceans (1978–2012)*, *116*(C9), 2011.

Sasaki, Y. N., and N. Schneider, Decadal Shifts of the Kuroshio Extension Jet: Application of Thin-Jet Theory, *Journal of Physical Oceanography*, *41*(5), 979–993, 2011.

Sato, Y., S. Yukimoto, H. Tsujino, H. Ishizaki, and A. Noda, Response of North Pacific ocean circulation in a Kuroshio-resolving ocean model to an Arctic Oscillation (AO)-like change in Northern Hemisphere atmospheric circulation due to greenhouse-gas forcing, *Journal of the Meteorological Society of Japan*, *84*(2), 295–309, 2006.

Schlesinger, M. E., and N. Ramankutty, An oscillation in the global climate system of period 65-70 years, *Nature*, *367*(6465), 723–726, 1994.

Seager, R., and I. R. Simpson, Western boundary currents and climate change, *Journal of Geophysical Research: Oceans*, *121*(9), 7212–7214, 2016.

Seager, R., Y. Kushnir, N. H. Naik, M. A. Cane, and J. Miller, Wind-Driven Shifts in the Latitude of the Kuroshio-Oyashio Extension and Generation of SST Anomalies on Decadal Timescales, *Journal of Climate*, *14*(22), 4249–4265, 2001.

Seager, R., D. S. Battisti, J. Yin, N. Gordon, N. Naik, A. C. Clement, and M. A. Cane, Is the Gulf Stream responsible for Europe's mild winters?, *Quarterly Journal of the Royal Meteorological Society*, *128*(586), 2563–2586, 2002.

Seidel, D. J., and W. J. Randel, Recent widening of the tropical belt: Evidence from tropopause observations, *Journal of Geophysical Research: Atmospheres (1984–2012)*, *112*(D20), 2007.

Seidel, D. J., Q. Fu, W. J. Randel, and T. J. Reichler, Widening of the tropical belt in a changing climate, *Nature Geoscience*, *1*(1), 21–24, 2007.

Sen Gupta, A., and M. H. England, Coupled ocean-atmosphere-ice response to variations in the Southern Annular Mode, *Journal of Climate*, *19*(18), 4457–4486, 2006.

Sen Gupta, A., A. Santoso, A. S. Taschetto, C. C. Ummenhofer, J. Trevena, and M. H. England, Projected changes to the Southern Hemisphere ocean and sea ice in the IPCC AR4 climate models, *Journal of Climate*, *22*(11), 3047–3078, 2009.

Sexton, D., The effect of stratospheric ozone depletion on the phase of the Antarctic Oscillation, *Geophysical Research Letters*, *28*(19), 3697–3700, 2001.

Shaman, J., R. Samelson, and E. Skyllingstad, Air-sea fluxes over the Gulf Stream region: atmospheric controls and trends, *Journal of Climate*, *23*(10), 2651–2670, 2010.

Stevens, B., et al., Atmospheric component of the MPI-M Earth System Model: ECHAM6, *Journal of Advances in Modeling Earth Systems*, *5*(2), 146–172, 2013.

Stocker, T. F., et al., Climate Change 2013. The Physical Science Basis. Working Group I Contribution to the Fifth Assessment Report of the Intergovernmental Panel on

Climate Change-Abstract for decision-makers, *Tech. rep.*, Groupe d'experts intergouvernemental sur l'evolution du climat/Intergovernmental Panel on Climate Change-IPCC, C/O World Meteorological Organization, 7bis Avenue de la Paix, CP 2300 CH-1211 Geneva 2 (Switzerland), 2013.

Stone, D., A. J. Weaver, and R. J. Stouffer, Projection of climate change onto modes of atmospheric variability, *Journal of Climate*, *14*(17), 3551–3565, 2001.

Taguchi, B., S.-P. Xie, N. Schneider, M. Nonaka, H. Sasaki, and Y. Sasai, Decadal Variability of the Kuroshio Extension: Observations and an Eddy-Resolving Model Hindcast, *Journal of Climate*, *20*(11), 2357–2377, 2007.

Taguchi, B., H. Nakamura, M. Nonaka, and S. Xie, Influences of the Kuroshio/Oyashio Extensions on Air-Sea Heat Exchanges and Storm-Track Activity as Revealed in Regional Atmospheric Model Simulations for the 2003/04 Cold Season, *Journal of Climate*, *22*(24), 6536–6560, 2009.

Tang, X., F. Wang, Y. Chen, and M. Li, Warming trend in northern East China Sea in recent four decades, *Chinese Journal of Oceanology and Limnology*, *27*, 185–191, 2009.

Tanimoto, Y., H. Nakamura, T. Kagimoto, and S. Yamane, An active role of extratropical sea surface temperature anomalies in determining anomalous turbulent heat flux, *Journal of Geophysical Research*, *108*(c10), 3304, doi:10.1029/2002JC001750, 2003.

Taylor, K. E., V. Balaji, S. Hankin, M. Juckes, B. Lawrence, and S. Pascoe, CMIP5 Data Reference SyntaxF (DRS) and Controlled Vocabularies, 2010.

Taylor, K. E., R. J. Stouffer, and G. A. Meehl, An overview of CMIP5 and the experiment design, *Bulletin of the American Meteorological Society*, *93*(4), 485–498, 2012.

Thompson, D. W., and S. Solomon, Interpretation of recent Southern Hemisphere climate change, *Science*, *296*(5569), 895–899, 2002.

Thompson, D. W., and J. M. Wallace, Annular modes in the extratropical circulation. Part I: month-to-month variability, *Journal of Climate*, *13*(5), 1000–1016, 2000.

Thompson, D. W., S. Solomon, P. J. Kushner, M. H. England, K. M. Grise, and D. J. Karoly, Signatures of the antarctic ozone hole in southern hemisphere surface climate change, *Nature Geoscience*, *4*(11), 741–749, 2011.

Tomita, H., and M. Kubota, Increase in turbulent heat flux during the 1990s over the Kuroshio/Oyashio extension region, *Geophysical Research Letters*, *32*(9), L09,705, 2005.

Uppala, S. M., et al., The ERA-40 re-analysis, *Quarterly Journal of the Royal Meteorological Society*, *131*(612), 2961–3012, 2005.

Van de Poll, H., H. Grubb, and I. Astin, Sampling uncertainty properties of cloud fraction estimates from random transect observations, *Journal of Geophysical Research: Atmospheres (1984–2012)*, *111*(D22), 2006.

Wang, L., and W. Chen, Downward Arctic Oscillation signal associated with moderate weak stratospheric polar vortex and the cold December 2009, *Geophysical Research Letters*, *37*(9), 2010.

Woodruff, S. D., et al., ICOADS Release 2.5: Extensions and enhancements to the surface marine meteorological archive, *International Journal of Climatology*, *31*(7), 951–967, 2011.

Wu, L., et al., Enhanced warming over the global subtropical western boundary currents, *Nature Climate Change*, *2*(3), 161–166, 2012.

Yu, L., and R. A. Weller, Objectively Analyzed Air–Sea Heat Fluxes for the Global Ice-Free Oceans (1981–2005), *Bulletin of the American Meteorological Society*, *88*(4), 2007.

Yu, L., X. Jin, and R. A. Weller, Multidecade Global Flux Datasets from the Objectively analyzed Air-sea Fluxes (OAFlux) Project: Latent and Sensible Heat Fluxes, Ocean Evaporation, and Related Surface Meteorological Variables, *Tech. rep.*, OAFlux Project Tech. Rep. OA-2008-01, 2008.

Zeng, X., M. Zhao, and R. E. Dickinson, Intercomparison of bulk aerodynamic algorithms for the computation of sea surface fluxes using TOGA COARE and TAO data, *Journal of Climate*, *11*(10), 2628–2644, 1998.

Zhang, G. J., and M. J. Mcphaden, The relationship between sea surface temperature and latent heat flux in the equatorial Pacific, *Journal of Climate*, *8*(3), 589–605, 1995.

Zhang, L., L. Wu, X. Lin, and D. Wu, Modes and mechanisms of sea surface temperature low-frequency variations over the coastal China seas, *Journal of Geophysical Research*, *115*(C8), C08,031, 2010a.

Zhang, W., J. Li, and X. Zhao, Sea surface temperature cooling mode in the Pacific cold tongue, *Journal of Geophysical Research: Oceans (1978–2012)*, *115*(C12), 2010b.

Zhou, T., and R. Yu, Sea-surface temperature induced variability of the Southern Annular Mode in an atmospheric general circulation model, *Geophysical research letters*, *31*(24), 2004.

Acknowledgements

Firstly, I would like to express my deepest gratitude to my supervisor Prof. Gerrit Lohmann, for the continuous support of my PhD study and related research, and for his patience, motivation, and immense knowledge. He also gave me great support during the hardest time when my daughter was born. I could not have imagined having a better advisor and mentor for my Ph.D study.

Besides, I would like to thank Prof. Rüdiger Gerde for agreeing to be my reviewer. I truly appreciate for his time and assistance as I navigated this process!

Additionally, thanks for Prof. Jiping Liu, for his support and encouragement during my Ph.D research. I want to thank Dr. Wei Wei, Mihai Dima, Monica Ionita, Xun Gong, Xu Zhang, Qinghua Yang and Sebastian Hinck for their helpful discussions, and Stefanie Klebe for her friendly review. I also want to thank all my colleagues from the Paleoclimate Dynamic group, for the inspiring working environment.

I thank my master thesis adviser Prof. Dr. Xueen Chen and Dr. Thomas Pohlmann, for giving me the opportunity to start my research in Germany.

A very special thanks is due to my wife Xiaoxu Shi for her patience, assistance, support and faith in me. Without her continuous moral support, encouragement and love I could have never completed this dissertation. I am also grateful to my little daughter Coco, who motivated me with her enduring smile and love. You are my

Further acknowledgement and thanks is due to my parents for their encouragement and continued support over the years and their enthusiasm as I neared my goal.

This work is funded by China Scholarship Council (CSC).